

EXPERIMENTAL TRANSITION PROBABILITIES

FOR LINES OF Fe I

Thesis by

Mario Martinez-Garcia

In Partial Fulfillment of the Requirements

For the Degree of

Doctor of Philosophy

California Institute of Technology

Pasadena, California

1971

Submitted December 8, 1970

ACKNOWLEDGMENTS

I wish to thank the faculty and staff of the Kellogg Radiation Laboratory for the assistance and encouragement provided during the course of this work. Special thanks go to Professor Ward Whaling for allowing me to work with him in this laboratory. He directed and actively participated in this project. His time and patience devoted to me are gratefully acknowledged. I also thank Professor C. A. Barnes for his interest and concern in my research situation at the early stages of my graduate training. Dr. George M. Lawrence, Dr. Donald L. Mickey, and Mr. Peter L. Smith provided valuable aid in the form of illuminating discussions and in the construction and operation of apparatus. The calibration of the instruments was carried out in collaboration with Dr. Mickey. Mr. Valdar Oinas assisted me in the abundance determination, and Mr. John E. Ross at UCLA ran his abundance determination program using some of my transition probabilities.

I thank all my coauthors for allowing me to use the lifetime measurement paper in this thesis. Professor Robert B. King shared his secrets and knowledge with us.

The Douglas Advanced Research Laboratories loaned some of the equipment used in this project. This research was supported in part by the National Science Foundation and the Office of Naval Research. I was partially supported by the Instituto Nacional de la Investigacion Cientifica in Mexico City, and by a one year scholarship from the Department of State.

Finally, I wish to dedicate this thesis to my parents and my wife.

ABSTRACT

The transition probabilities of twenty-nine lines of Fe I have been determined by combining (1) the measurement of the branching ratio for all the known transitions which depopulate a level with (2) the measurement of its lifetime.

The lifetime was obtained by the beam-foil time-of-flight method. Iron atoms accelerated to an energy of 500 kev were excited by letting them traverse a thin carbon foil. The variation of the light emitted in a particular transition was measured as a function of the downstream distance from the foil to determine the lifetime of the upper level of the transition. The levels studied were restricted to energies higher than 6 ev. to avoid cascading repopulation.

For the branching ratio measurements, the iron levels were excited in a hollow-cathode discharge. Two monochromators were used to measure simultaneously (1) the intensity of each known transition from the level under investigation, and (2) the intensity of a reference line to monitor the population of that level.

The transition probabilities obtained are compared with other recent measurements by different techniques. As far as the limited overlap permits comparison, agreement is found among these results.

Comparison with the Corliss and Tech compilation indicates:

1. The CT tables are in error by an amount that increases

with the excitation energy of the upper level.

2. The CT tables yield reliable branching ratio for the strongest lines. However, deviations up to a factor of three may occur for the weakest branches.

The new transition probabilities are used to determine a photospheric solar iron abundance. The result obtained supports the high iron abundance determined by Garz et al. in agreement with the corona values.

TABLE OF CONTENTS

<u>PART</u>	<u>TITLE</u>	<u>PAGE</u>
1	BRIEF OUTLINE OF THE THESIS	1
2	INTRODUCTION	3
3	THEORY	10
4	THE BEAM-FOIL METHOD	15
5	REMARKS ABOUT THE CONCLUSIONS REACHED IN THE LIFETIME EXPERIMENT, SECTION 11	19
6	MEASUREMENT OF THE BRANCHING RATIOS	21
	6.1 Experimental Equipment	21
	A. The Source	21
	B. The Optical System	23
	C. The Detector: The Rowland System	25
	D. The Monitor	26
	6.2 Experimental Procedure	27
	A. Line Identification	27
	B. Measurement of the Photon Intensities	29
	C. Example of Experimental Procedure	33
	6.3 Self-Absorption	35
	6.4 Data Reduction	37
	6.5 Experimental Uncertainties	38
7	TRANSITION PROBABILITIES	43
	7.1 Obtaining Transition Probabilities	43
	7.2 Uncertainties in the Transition Probabilities	43

<u>PART</u>	<u>TITLE</u>	<u>PAGE</u>
8	COMPARISONS AND CONCLUSIONS	45
	8.1 Comparison with Recent Experiments	45
	8.2 Comparison with the Corliss and Tech Compilation	47
	8.3 Examination of the Error Present in the CT Compilation	51
9	ABUNDANCE OF Fe IN THE SUN	56
10	CALIBRATION OF THE INSTRUMENTS	61
	10.1 Introduction	61
	10.2 The McPherson System	62
	A. Calibration in the Region $\lambda > 2800\text{\AA}$	63
	1) The Source	63
	2) Experimental Setup	64
	3) Relations	64
	4) Experimental Procedure	67
	(a) Linearity of the Slits	67
	(b) Calibration of the Filters	68
	(c) Counting Losses	71
	5) Results	72
	B. Calibration in the Middle Ultraviolet	72
	1) Method and Equipment	72
	2) Experimental Setup	74
	3) Experimental Procedure	75
	4) Results	76
	C. Conclusions	77

<u>PART</u>	<u>TITLE</u>	<u>PAGE</u>
	10.3 Calibration of the Rowland System	78
REFERENCES		81
TABLES		85
FIGURES		107
11	LIFETIMES OF SOME Fe I STATES BY BEAM-FOIL SPECTROSCOPY (COAUTHORED BY W. WHALING AND R. B. KING; PUBLISHED IN ASTROPHYSICAL JOURNAL, <u>158</u> , 389 (1969)).	151

1. BRIEF OUTLINE OF THE THESIS

This thesis deals with the determination of transition probabilities for lines emitted from highly excited ($E > 6$ ev.) states in Fe I. The introduction, Section 2, reviews the concept of transition probability and its usefulness, especially in astrophysics where it is necessary for abundance determinations of elements from stellar spectra. The motivation of this experiment is then presented, including a short history of the events behind the iron transition probabilities compiled by the NBS and their absolute scale.

In Section 3 a short theory relating the concepts of transition probability, lifetime of a level and oscillator strength or "f" value is given. The transition probabilities are absolutely determined if the lifetime of the level and the branching ratio of the transitions originating in that level are known. These two quantities are to be determined experimentally in this work. In Section 4 and as introduction to the lifetime measurement the principles of the beam-foil method are outlined, with some computations related to the conditions existing in the experimental setup used for the measurements. The actual measurement of the lifetimes is reported in Section 11, at the end of the thesis. Because it is felt that the conclusions reached in the paper in Section 11, even when accurate at the time the paper was written, now seem incomplete and inconclusive under the light of results recently published, in Section 5 special remarks dealing with the conclusions of the lifetime paper are included.

Section 6 is devoted to the determination of the branching

ratio of the transitions from the levels whose lifetime was measured. To transform the photon intensity measurements into branching ratios, the relative efficiency of the detecting equipment as a function of wavelength is needed. This efficiency was obtained separately. The method used is described and the results reported in Section 10. This section is not a part of the main text, so it play the role of an appendix. In Section 6 the experimental uncertainties present in the branching ratios and the possible presence of self-absorption in the source are studied. In Section 7 the results and uncertainties of the lifetimes and the branching ratios are combined, and transition probabilities are obtained.

In Section 8 the transition probabilities obtained in this experiment are compared first to results available from recent experiments and then to the data in the Corliss and Tech (1968) compilation (hereafter referred to as CT). In the same section several possible explanations of the errors present in the CT compilation are then proposed and examined. Section 9 is an application of the measured transition probabilities to obtain the abundance of iron in the sun. Comparison with recently published values is there made.

2. INTRODUCTION

An atom in an excited state has a certain probability of making a transition to a lower state and simultaneously emitting radiation. The transition probability A_n^m is defined as the probability per unit time that an atom initially in the excited state m will spontaneously (without external influence) jump to the lower state n , with emission of radiation.

Transition probabilities are very useful to determine temperatures and densities of radiating atoms in hot gases and plasmas. They have an important application in astrophysics where they are used to determine the abundance of elements in solar and stellar atmospheres.

It would be possible to obtain theoretically the transition probabilities for permitted lines if the electric dipole matrix element could be calculated accurately. Because the matrix element depends strongly on small changes of approximate wave functions, for the complex atoms, where the wave functions are poorly known, it is preferred to obtain the transition probabilities experimentally.

A bibliography on the available atomic transition probabilities has been published by the National Bureau of Standards (Miles and Wiese, 1970). A good summary of the most common experimental methods used to obtain transition probabilities is given by Wiese (1968a) and Foster (1964).

This experiment, designed to yield values of transition probabilities for lines in Fe I, has not been undertaken due to the lack of transition probabilities for this element. The importance of the spectrum of neutral iron in astrophysics has been recognized for a long time and many man-hours have been devoted to obtain, evaluate and compile those transition probabilities.

The motivation for this experiment came indirectly from the long standing disagreement of the solar iron abundance obtained from measurements in the solar corona and in the photosphere, the determinations disagreeing by factors of 10 to 20. This difference could not be explained easily by the normal uncertainties that accompany the experimental and observational parameters required in an abundance determination. So, it was not unreasonable to assume that the difference was a real phenomenon that had to be explained in terms of physical processes taking place in the sun. However, to believe that this was the actual situation required full confidence in the methods and auxiliary quantities employed in the abundance calculation. Unfortunately, the setting was far from perfect. The available iron transition probabilities were surrounded by a cloud of skepticism. In order to understand why the transition probabilities could be a source of disbelief, it is necessary to review briefly how the widely used NBS compilation originated and developed.

During more than thirty years a very extensive program of intensity measurements was carried at the National Bureau of

Standards that ended with the publication (Meggers et al, 1961) of intensity measurements on 39,000 lines of 70 elements in the wavelength range between 2000 Å and 9000 Å. As a light source they used a low current (10 A.) free burning arc between copper electrodes to which the element under study was added in a ratio of 1:1000. They determined peak intensities (wide slits were used so that the total intensity was proportional to the flat peak intensity) by standard photographic photometry.

To convert these line intensities into transition probabilities, Corliss and Bozman (1962) (hereafter referred to as CB) determined "effective" arc temperature by comparing the line intensity measurements to relative transition probabilities available in the literature. Then, assuming thermodynamical equilibrium, they obtained relative transition probabilities.

By comparing line intensities of neutral and ionized spectra to already known absolute transition probabilities and invoking the Saha equation, they determined the degree of ionization of eleven elements, and determined an electron density in the arc of $\sim 10^{14}/\text{cm}^3$. Then, they compared their relative transition probabilities to known absolute values and determined an absolute scale. However, they noticed that lines from highly excited states appeared stronger than what was expected if the upper level was populated accordingly to the Boltzmann distribution function. Because Meggers et al. (1961) had obtained the intensities by admitting into the spectrograph light from all the regions of the arc, Corliss and Bozman (1962) reasoned that the overpopulation of the high energy states was due

to an abnormal excitation near the arc electrodes. To correct this problem they folded into their absolute scale a normalization function. This CB normalization function is equal to one in the range $2.25 \text{ ev.} < E < 6 \text{ ev.}$ and decreases for $E > 6 \text{ ev.}$ It decreases also for $E < 2.25 \text{ ev.}$ because levels with these low energies are excited in the low temperature regions which occupy a larger volume of the radiating gas. The good agreement found between this absolute scale and the scale determined theoretically by normalizing relative f values in order to obey the f -sum rule (Allen and Corliss, 1963) gave confidence in the use of the CB normalization function.

Corliss and Warner (1964, 1966) reported new measurements for many more (fainter) lines using arc and spark sources with pure iron electrodes. In this work only light from a very small region between the electrodes was admitted into the spectrograph. However, they also noticed an overpopulation of the highly excited states, and in order to obey the f -sum rule they had to use the same CB normalization function, but in this occasion they did not find an explanation for the departure of the population of these states from the Boltzmann distribution. Besides their own measurements, they reduced and incorporated into their publications all the "reliable" published data, intensities and relative gf values. All these data were normalized to the modified absolute scale employed by Corliss and Bozman. By doing this they obtained many absolute gf determinations, often more than one for a transition, and recommended a "best" value, usually the unweighted mean of the

different determination. These values were the basis for most of the iron abundance determinations published in the period between 1966 and 1969.

However, in 1964 Warner, and after him Withbroe (1967), calculated solar curves of growth for Fe I using oscillator strength reduced to the CB modified absolute scale. The results showed an anomalous behavior for lines originating in levels with energy greater than 6 eV.

Dr. Robert B. King, who for a long time had been measuring f -values at Caltech using the atomic beam method and was responsible for some of the absolute measurements used by Corliss and Bozmann to determine the absolute scale, recognized the problems involved in determining the concentration of atoms from his absorption furnace, and suggested the use of the beam-foil method developed by Bashkin (1964) to measure the lifetime or total transition probability of the Fe I levels and in this way determine the absolute scale and test the validity of the CB normalization function.

Huber and Tobey (1968) measured some oscillator strengths of Fe I, Cr I and Cr II lines using absorption spectroscopy on a pressure-driven shock tube. Comparing their results to the values published by the NBS (Corliss and Warner, 1964, 1966) they found (1) a difference in the absolute scale of approximately a factor of 8, and (2) that the highly excited states in the CB and CW arc and spark followed a Boltzmann distribution (no deviation from TE) and so there was no need for the use of the CB normalization function.

This experimental evidence and the findings of Warner and Cowley (1967) from a theoretical study of a model arc, led to the publication by Corliss and Tech (CT) (1968) of a compilation of transition probabilities for Fe I line normalized to the CB absolute scale but with the normalization function removed for $E > 6$ ev. However, CT disregarded the discrepancy in the absolute scale found by Huber and Tobey because they did not have confidence in the determination of the density of atoms in the shock tube. So, by comparing the CT compilation to the results of Huber and Tobey one finds the ratio $\frac{A_{CT}}{A_{HT}} \sim 8$ independent of excitation energy.

The results of the lifetime measurements from the present experiment were presented in 1968 (Martinez et al, 1968) and appeared in the literature in 1969 (Whaling et al, 1969). (A copy of this article appears as Section 11 at the end of this thesis.) These results disagree with Huber and Tobey (1968) and also with Corliss and Tech (1968). The discrepancy strongly depends on the energy of the upper level and raises questions about the population distribution implicitly assumed in the CT compilation.

Since then other measurements (Garz and Kock, 1969a; Bridges and Wiese, 1970) have confirmed that the findings reported in this thesis are correct. Garz et al (1969b) also showed that the measured transition probabilities are indeed in the right direction to solve the solar iron abundance discrepancy.

If the relative transition probabilities for lines of different upper levels obtained from the CT compilation are in error, it is of

interest to know how reliable are their relative transition probabilities for lines with a common upper level. Corliss and Warner (1964, 1966) had recommended for each transition a "best" gf value that came from a mixture of different results obtained from different experiments, each with its own uncertainties and systematic errors. Furthermore, several investigations (Withbroe, 1967; Grasdalen et al, 1969) had reported a wavelength dependent error in the Corliss and Bozman absolute scale. So, as part of this program it was felt worthwhile to measure the branching ratios for all the transitions coming from those levels whose lifetime had been measured by the beam-foil method. This phase of the experiment would then a) test the reliability of the Corliss and Tech relative transition probabilities, and b) yield reliable absolute transition probabilities for each individual line, independent of any other work.

3. THEORY

It is possible to obtain, using time dependent perturbation theory, a theoretical expression for the spontaneous transition probability A_n^m (see Wiese, 1968a)

$$A_n^m = \frac{64\pi^4 \nu_{mn}^3}{3hc^3} \frac{1}{g_m} \sum_{k,\ell} | \langle M_k | Q | N_\ell \rangle |^2 \quad (1)$$

where $g_m = 2J_m + 1$, $h\nu_{mn} = E_m - E_n$ is the energy of the transition and Q is an operator. The sum indices run over the $2J + 1$ substates of both levels. For "allowed" transitions, Q represents the electric dipole operator $e\vec{r}$ with e being the charge of the electron and \vec{r} refers to the atomic coordinates. Because of the nature of the operator, in order to calculate the matrix element it is necessary to know accurately the wave function of both states m and n . Here is where the uncertainties arise in complex atoms, approximate methods not yielding useful results.

When the electric dipole matrix vanishes, i.e. both wave functions have the same parity, higher order transitions can occur. Because they are rather slow, the magnetic dipole and electric quadrupole transitions being respectively 10^5 and 10^8 times slower than electric dipole transitions, they are called "forbidden" transitions. These transitions are important in tenuous gases, such as the solar corona where the de-excitation collision rate is slower than the rate of radiation from forbidden transitions. Because in

the corona one finds highly ionized atoms of iron, which reduces the complexity of their electronic structure, and because of the nature of the magnetic dipole operator, which does not change the radial part of the wave function, it is then relatively simple and accurate to calculate transition probabilities for forbidden lines of the solar corona. Thus the iron abundance derived from the solar corona is not subject to the uncertain transition probabilities that plague the photospheric abundance determination.

From the experimental point of view, the interest lies in how the transition probability is related to the observed spectral intensity of a transition from a source. For an optically thin (emitted intensity proportional to the source thickness) source of depth ℓ , the observed radiation intensity I_o (energy emitted per unit area, time and solid angle) due to transitions of atoms from excited state m to lower state n is given by

$$I_o = \int_{\text{line profile}} I_{\nu} d\nu = \frac{1}{4\pi} N_m A_n^m h\nu_{mn} \ell \quad (2)$$

where N_m is the number of atoms per unit volume in level m .

When one measures not the energy emitted but the number of photons of a given energy being emitted, then one talks about the photon intensity

$$I_{p_n} = \frac{I_o}{h\nu} \propto N_m A_n^m$$

The measurement of the photon intensity I_{p_i} of each of the transitions down from a common level m , when done while the population of the level m is maintained constant by collisional excitation, is equivalent to the knowledge of the relative transition probabilities or branching ratios

$$\frac{A_i^m}{\sum_k A_k^m} = \frac{I_{p_i}}{\sum_k I_{p_k}}$$

for those transitions.

To normalize these relative transition probabilities into an absolute scale one can use the lifetime of the upper level. How can these two quantities be connected? Suppose that initially there are N_m undisturbed atoms in an excited state m which is unable to repopulate itself, and there are several lower states n to which a transition can occur. If the radiative mode is considered as the only important mode of depopulation (both particle and photon collision processes considered negligible) then the decay is governed by

$$\frac{dN_m}{dt} = -N_m \sum_n A_n^m \quad (3)$$

or

$$N_m(t) = N_m(0) \exp \left[-t \sum_n A_n^m \right]$$

If τ_m or the lifetime of level m is defined as the time required for the level to decay to e^{-1} its initial population, then

$$\tau_m = \left(\sum_n A_n^m \right)^{-1} \quad (4)$$

and then

$$A_i^m = \frac{1}{\tau_m} \frac{I_{p_i}}{\sum_k I_{p_k}} \quad (5)$$

So it is possible, by using the lifetime of the level, to normalize the photon intensity measurements of the transitions from that level and obtain absolute transition probabilities.

Because of the common usage in absorption experiments of the Ladenburg oscillator strength or f-value more than the transition probabilities, the concept of oscillator strength is introduced now. The absorption oscillator strength f_{nm} represents the number of classical oscillators per atom in state n, necessary to absorb the same amount of energy actually absorbed by the atoms in their transition from lower state n to higher state m.

Any textbook on the subject gives the derivation of the relation between the emission A's and the absorption f's (e.g. Wiese, 1968a). The final relation is:

$$g_m A_n^m = \frac{8\pi^2 e^2 v_{mn}^2}{mc^2} g_n f_{nm} \quad (6)$$

or, inserting numerical values:

$$g_m A_n^m = 1.499 \times 10^{-8} \lambda^2 g_n f_{nm} \quad (7)$$

with λ expressed in microns ($1\mu = 10^4 \text{ \AA}$).

As a summary, it is important to remember that usually the quoted f 's are absorption oscillator strengths and the g with them refers to the lower level statistical weight, while the g with the transition probability is the statistical weight of the upper level.

4. THE BEAM-FOIL METHOD

A good review of the beam-foil source and its application to the measurement of atomic lifetimes is available in the literature (Bashkin, 1968; Whaling, 1968). What follows will give a summary of the principles and relevant features of the method.

Ions of the element under study are accelerated to a known energy and admitted to an evacuated target chamber where they are made to traverse a thin foil, usually made of carbon because of its ruggedness and low Z which reduces scattering. While traversing the foil the ions suffer a large number of collisions and reach equilibrium in excited and ionized states. They emerge from the foil traveling in vacuum at a constant and almost uniform velocity and decaying spontaneously from those excited levels with the consequent emission of radiation. A measurement of the intensity of a particular transition as a function of the distance from the exciting foil is equivalent to a measurement of the population of the decaying level as a function of time. From this decay curve the lifetime of the level can be inferred (time of flight technique). The method is applicable to highly excited and/or highly ionized species not attainable in any other source.

For this experiment a 0.1μ amp Fe^+ beam ($\sim 6 \times 10^{11}$ part/sec) was accelerated to an energy of 500 keV, or to a velocity of 1.28×10^8 cm/sec ($\sim 0.004c$) and was made to strike a carbon foil that had a nominal thickness of $10 \mu\text{gr}/\text{cm}^2$ ($\sim 400 \text{ \AA}$). It takes

about 10^{-14} sec. for the particles to traverse the foil. So, the position and time of the excitation of all the particles is well defined.

The beam used had a cross sectional area of 0.02 cm^2 (1 x 2mm), so the beam density amounted to $\sim 2.5 \times 10^5 \text{ part/cm}^3$ at any point in the beam. The target chamber evacuated to $2 \times 10^{-6} \text{ mm Hg}$ had a residual gas particle density of around $7 \times 10^{10} \text{ part/cm}^3$ (mean free path of $\sim 1.5 \text{ Km}$). Due to the low particle density and low radiation density, stimulated emission, both radiation induced and collision induced, including excitation of beam particles by collision with residual gas molecules, followed by spontaneous emission, are completely negligible and the light radiated from the beam is entirely due to spontaneous transitions from the levels to which the atoms were excited while crossing the foil (Bickel, 1967).

It is possible, by adjusting the energy of the ions, to maximize the ionic species under study emerging from the foil (Smith et al., 1969). It is not possible, however, to control the degree of electronic excitation of a given ion. So, when measuring lifetimes of low excited levels, frequently it is found that the level under study is being repopulated from upper states (cascading), resulting in an enhancement of intensity and a complication of the decay curve. The strongest iron line identified in the 500 keV beam-foil spectrum as shown in Table 1 of Section 11 is $\lambda 4045.82$. The experimental decay curve obtained for this transition is complex, which indicates that its upper level, $y^3 F_4^0 (36686 \text{ cm}^{-1})$ is being

repopulated by transitions from higher levels. It is possible, in principle, to adjust a sum of exponentials to the experimental decay curve and obtain the sought lifetime. However, for this particular transition the decay curve was obtained for bombarding energies of 200, 400 and 500 kev; and for carbon foil thicknesses of 5, 10 and $20 \mu\text{gr}/\text{cm}^2$. The analysis of the decay curves obtained did not yield a value for the sought lifetime which was independent of these experimental parameters. Because of this problem, the lifetime measurements were limited to levels with excitation energies greater than 6 ev. For all the levels presented in Section 11 the decay curves were simple and no ambiguities were detected when the experimental parameters were changed.

In addition to cascading, there is another problem which has its origin in the nature of the experimental method (see Fig. 1). The intensity of a particular transition is detected looking at the beam perpendicular to its direction of motion. The finite angle subtended at the beam by the collecting lens introduces a Doppler width in the observed line. This broadening sets a limit on the possible spectral resolution that can be attained.

The description of the lifetime measurements and the results obtained were published in 1969 (Whaling et al.). A copy of that paper has been printed at the end of this thesis and is referred to as Section 11. Because in the paper there is no schematic of the experimental setup used to perform the lifetime measurements, one has been included as Fig. 1. Now it is felt that the analysis

carried in Section 11 is incomplete under the light of new information, so some remarks about those conclusions are made in Section 5. Since the publication of this paper, new measurements of the lifetime of the same levels have been performed at Aarhus by T. Andersen (1969). His unpublished results are listed in Table 1.

5. REMARKS ABOUT GOAL AND CONCLUSIONS REACHED
IN THE LIFETIME EXPERIMENT (Section 11)

Initially the lifetime experiment was undertaken with the idea of finding the right absolute scale for the Fe I transition probabilities. After the lifetimes were obtained, it was found that the ratio of a lifetime measured experimentally to the lifetime computed from the transition probabilities from the CT compilation depended strongly on the excitation energy of the level as shown in Table 2 of Section 11. But still in the lifetime paper, the idea that the only adjustment necessary to fix the CT data was a simple change of the absolute scale was still alive, especially after the results published by Huber and Tobey (1968) which did not show any energy dependent disagreement with the CT compilation. So, an average of the ratios $\tau^{\text{exp}}/\tau_{\text{CT}}$ was obtained from all the six levels measured, concluding then that the transition probabilities listed in the CT compilation were too high by about a factor of 9, in close agreement with the Huber and Tobey results. However, it was stated there that due to the different ratios found for the lifetimes, far from constant, it was possible that the population distribution assumed by Corliss and co-workers in transforming intensities into transition probabilities could be in error. At the time it was not possible to derive any other conclusion because the data available were limited to a narrow range of energies. New recent determinations of transition probabilities of lines with a wider range of upper level energies which will be discussed in

Section 8, have shown that the CT compilation cannot be corrected applying a constant factor: the factor by which each transition probability in their compilation is in error is a function of the energy of the level from which the transition originated. So in Section 11, the talk about the search for a constant factor should be disregarded.

6. MEASUREMENT OF THE BRANCHING RATIOS

6.1 Experimental Equipment

A. The Source

Figure 2 shows a diagram of the hollow cathode discharge tube used in this experiment. The cathode was a cylinder of Armco iron 75 mm long and 12.5 mm diameter with a canal 3 mm in diameter along its axis. The anode, a stainless steel sleeve 25 mm wide and 50 mm in diameter, was concentric with the cathode. The quartz end windows were kept 15 cm away from the discharge to avoid any iron deposit on them through sputtering. The aluminum water-cooled body was very effective on keeping the temperature of the cathode down (no red glow was seen in the cathode during operation). Because of the low temperature, it is believed (Tolansky, 1947) that the iron atoms were detached from the cathode and then excited through ion bombardment rather than thermal evaporation. So the iron atoms were an impurity compared to the atoms of the carrier gas. To carry the discharge several gases were tried. Using a cathode with a hole 11 mm in diameter He and Ar were tested. He produced a strong Fe II spectrum but few and relatively weak Fe I lines (because of its low mass it has a low sputtering action). With Ar the iron spectrum showed many strong transitions from the neutral species, and few and weak Fe II lines.

Using this gas it was possible to see the strongest branches from the high levels measured in this experiment, but not yet the weakest ones. A mixture of He and Ar did not prove successful in

increasing the population of these high levels. But by reducing the diameter of the canal and increasing the gas pressure both by a factor of 4 (to a 3 mm diameter cathode and ≈ 0.5 mm Hg pressure) holding the current in the discharge constant at 200 ma, the population of these high levels was increased by a factor of 80. Pressure of the gas, diameter of the canal and current of the discharge were inter-related parameters and it was not possible to reduce, for the 11 mm canal, the gas pressure below 0.2 mm Hg at a constant current of 200 ma without quenching the discharge in the cathode. To go below that threshold pressure, the discharge current had to be increased. It is interesting to notice that for maximum brilliance of the lines from these high levels, the gas pressure had to be the lowest possible before the discharge came out of the canal into a dim glow between the cathode and the anode.

The 3 mm diameter cathode was used permanently in the source for the measurement of the branches. Typically, the pressure of the Argon, measured by a thermocouple gauge and by an oil manometer (oil with specific gravity of 0.9), was of the order of 1 mm Hg. The Argon flowed through the source at a rate of $3 \text{ cm}^3(\text{NPT})/\text{minute}$ and the discharge was run at $V \sim 280\text{V}$ and $I \sim 350 \text{ ma}$. At a power of ~ 100 watts it was possible to observe lines with $A \geq 10^5 \text{ sec}^{-1}$. The hollow cathode was powered by a motor generator set (1500 V max) with ballast resistors included in the circuit for stability. Traps cooled to dry ice temperature were included in the gas input line to remove water vapor from the gas, and in the fore-pump line to

stop oil coming into the discharge.

Even when the discharge current and pressure were held constant within a few percent it was observed that the population of an Fe I upper level, measured by the photon intensity of one of the transitions from it, would vary slowly by as much as a factor of 2 during the period of a few hours required to perform the photon intensity measurements on all the decay channels. This variation could be due to changes in the amount or composition of the impurities on the gas flowing in the discharge, or changes in the temperature of it. In order to correct for this variation it was decided to monitor continuously the population of the upper level.

B. Optical System

Figure 3 shows a schematic of the optical system. A 4.7 cm diameter, 16.6 cm focal length quartz lens was placed between the source and the beam splitter. It magnified the source canal by approximately a factor of 3.5 at the entrance slit of the spectrometers. It was positioned to maximize the counting rate observed in the Rowland spectrometer.

The light beam splitter consisted of a 5 cm diameter GE-151 quartz wedge with a refracting angle of .009 rad. and a thickness at the center of 4.5 mm, turned at an angle of $\sim 45^\circ$ to the light beam. About $10\% \pm 1\%$, depending on wavelength (GE fused quartz catalog) of the light traversing the splitter, was reflected from the front surface of the wedge and a similar amount from its back surface. The light reflected from the front surface was directed

to the entrance slit of a McPherson monochromator used to monitor the population of an Fe I upper level by observing continuously one of the transitions from it. The distance from the front surface of the wedge to the entrance slit of the McPherson monochromator was made equal to 50 cm, equal to the distance from the front surface of the wedge to the entrance slit of the Rowland spectrometer. Light from the back surface of the wedge diverged from light from the front surface of it and it was possible to discriminate against it at the entrance slit of the monitor.

Being a thin prism, the wedge deflected and dispersed the light beam that crossed it. Light of $\lambda 5460$ suffered a deflection of 2 mm at the entrance slit of the Rowland spectrometer. For all the transitions with a common upper level the change in the index of refraction between extreme wavelengths was not greater than 0.02 (data from the GE catalog). With a refracting angle of 0.009 rad. and a distance of 500 mm, one obtains a separation of extreme wavelengths at the entrance slit of 90μ . Has this separation any effect on the branching-ratio measurements? It could be argued no, because due to the finite depth of the source, the radial dependence of the emission intensity at the source gets washed out at the plane of the entrance slit. However, to be certain without speculating, the following check was made: Using as a source the Fe-Ne commercial hollow cathode (Westinghouse, 20 ma max) and no monitor, the ratio of the photon intensity of two lines, $\lambda 3789.18$ and $\lambda 5242.5$ of similar strength and common upper level but different in wavelength, was

obtained with the quartz wedge in and out of the light path (see Fig. 3) being careful on each occasion to realign the optics so that the light beam going into the spectrometer would be perpendicular to the entrance slit of it. The ratios obtained in each case agreed within the experimental uncertainty.

C. The Detector

The light through the wedge was analyzed by a Rowland spectrometer. A summary of the characteristics of this instrument is given in Table 2. The entrance slit width of the instrument was varied between 40_{μ} and 100_{μ} . Line profiles with $50 \text{ m}\overset{\circ}{\text{A}}$ at the half width were easily obtained at the lowest entrance slit widths used.

The exit slit and photomultiplier tube assembly can be driven back and forth along a line tangent to the focal curve of the spectrometer. Ashenfelter (1967), on page 38 of his thesis, describes the way this carriage is driven. Because of its variable scanning speeds one can accurately scan a small section of a spectrum and look for fine detail.

The light through the exit slit of the spectrometer was detected by an EMI 9526B photomultiplier tube which has a quartz window and an S-13 photocathode. The tube was wrapped in magnetic shielding material and placed in its dry-ice cooled refrigerator. Light from the exit slit was piped through the thermal insulation to the photocathode in an arrangement similar to the one described in Section 10.2 for the McPherson system. The particular photomultiplier tube used here (serial number 5916) has a dark current

fifty times lower than the average specified by the manufacturer.

The signal from the photomultiplier was handled using conventional electronics. A schematic of the electronics used is shown in Fig. 4. The preamplifier-discriminator used here was designed by Mickey et al (1970). The gate generator originally in the design had been disconnected in the present unit. The instrument was designed to accept counting rates up to 1 MHz without significant losses.

D. The Monitor

The small portion of light reflected from the front surface of the beam splitter was allowed to enter through the entrance slit of a $f/5.3$ Model 218 Czerny-Turner type McPherson monochromator (loaned to this lab by Douglas Adv. Research Laboratories) with similar characteristics to the one described in Section 10.2 as part of the McPherson system. The light that would emerge through its exit slit was collected by the photocathode of an EMI 6256S photomultiplier tube. The signal from it was then amplified and detected through conventional electronics. A diagram of the electronics used is shown in Fig. 4.

If the same transition was observed simultaneously by both systems, the Rowland spectrometer and the McPherson monochromator, it was found that in order for the ratio of the counting rates detected by the systems to remain constant as the conditions of the discharge were varied, it was necessary to reduce the aperture of

the McPherson monochromator to $f/48$, equivalent to that existing in the Rowland instrument, so that both systems would detect photons coming from the same region in the discharge. The reduction was performed by placing, in front of the entrance collimator mirror, a black mask with a 6.25 mm x 2.50 mm rectangular hole on its center. After that, even when both instruments had similar apertures, the equivalence was not perfect because the height of the entrance slit of both instruments was set to 5 mm.

The effectiveness of this scheme was tested by changing drastically the conditions of the discharge. Even when the line brightness was changed by a factor of 3, differences smaller than five percent were observed in the counting rate ratios.

6.2 Experimental Procedure

A. Line Identification

The CT compilation was used to find the classified transitions out of each of the levels from Table 1. A transition not listed there is probably so weak that its omission will not affect the lifetime. Table 3 gives a list of the transition classified with upper and lower level configuration, level designation and energy. The multiplet number is shown as found in Moore's Multiplet Tables (1945). The level energies, designations and configurations are taken from Moore's Atomic Energy Levels (1952).

For each of the transitions the Rowland spectrometer was set in the wavelength region of interest, within $\pm 10\text{\AA}$ of the sought

transition's wavelength. Then the exit slit assembly was driven back and forth for 15 or 20Å and the spectrum was recorded on paper by the chart plotter, using the counting rate meter in the log scale. This spectrum was obtained with a narrow entrance slit width ($\sim 50\mu$) and discriminating against radiation of unwanted orders by the use of filters. The filters used in this context were either the Schott WG-320 or the Corning 7-54. For a description of these filters the reader is referred to Section 10.2-A.4. Direct comparison of the spectrum obtained to an Fe arc spectrum for the same region, or to the published Fe spectrum from an Fe-Ne hollow cathode source (Crosswhite, 1958), "usually" gave a one to one identification for the strong lines. This was a useful start, to then interpolate the wavelengths and identify all the Fe I lines listed by Corliss and Tech, and the Fe II, Ar I and Ar II listed elsewhere (Moore, 1945; MIT Tables, 1939; Striganov and Sventitskii, 1968). By then the transition of interest had been identified without any doubt. A second scan of a narrow region of the spectra, including the transition to be measured, was then obtained but on this occasion using no discriminating filter to determine the need for it. Either the presence of transitions from another order blending the transition of interest, or an increase in background that would reduce the signal to background ratio were reasons to use the filters.

All the transitions of this study were identified following the described method. The only transition not seen at all was

$\lambda 2411.56$ from level $z^1H_5^0$ to a 5F_5 , classified by Kiess et al, (1960). On Fig. 5 a spectrum in the region of this wavelength is included. Perhaps the transition is there but due to the inefficiency of the spectrometer at that wavelength it cannot be clearly detected. However, if the background present at $\lambda 2411.56$ is measured, and one assumes that the signal from the transition is comparable to this background, so that this number is used to obtain a transition probability (Table 5), the resulting value is already smaller than the one given by CT (1966) in their compilation.

Because of being blended with Ar lines, two of the transitions had to be measured using He as the carrier gas in the hollow cathode. The transition $\lambda 4309.04$ from level $y^3I_6^0$ (52514 cm^{-1}) was blended with Ar II $\lambda 4309.11$, and transition $\lambda 4537.68$ from level $z^1H_5^0$ (48383 cm^{-1}) was blended with Ar II $\lambda 4537.67$.

B. Measurement of the Photon Intensities

Knowing the spectrum for a group of transitions with common upper level it was then possible to decide which line could be used as the monitor and what kind of slit widths and filters were to be used for both instruments. For each group, the transition with the best signal to noise ratio and best separation from its neighbors was chosen to serve as the monitoring line, always choosing a medium size line, avoiding the strongest ones. The region was then scanned with the McPherson and the instrument was set at the peak of the monitor line with as wide a pass band as

possible. These settings in the monitor remained fixed during the measurements of all the lines of the group.

To measure the photon intensities, the Rowland spectrometer entrance slit was set as wide as possible avoiding blends, usually 90μ . If one of the transitions would not tolerate the slit width because of contributions from a neighboring line, then that line and another one of the same group which had already been measured with the wide slit setting, would be remeasured using narrower slits.

To be sure that changing the entrance slit width of the Rowland spectrometer did not affect the ratio of measurements of two branches, the ratio of two lines, 5242.5\AA and 3789.18\AA , similar in strength but different in wavelength, both from the same upper level $z^1\text{H}_5^0$ were obtained with respect to a monitor line, in this case 5242.5\AA . For different settings of the entrance slit width of the Rowland spectrometer -- 40μ , 80μ , and 120μ -- the ratio of the two lines agreed within the experimental error.

The actual procedure for the measurement went as follows: The particular transition under study was first scanned and recorded at low speed (usually $32\frac{\text{mA}}{\text{inch}}$ of paper in the plotter). With this detailed spectrum at hand it was then possible to rescan the same transition and stop the exit slit at the center wavelength in the flat top of the transition to measure it, or at the wavelength where the background was to be measured. So, with the monitor set at the peak wavelength of the monitoring line, and the Rowland spectrometer

at either peak or background wavelength of a particular transition, photons reaching the detectors were counted simultaneously during 20 sec., and repeated three or four times. Because the positioning of the Rowland spectrometer at the peak or background wavelengths was delicate and critical, the instrument was repositioned at those wavelengths several times, and on each occasion the photons were counted. Agreement among the different measurements within the experimental error was always required. By this procedure first the monitor line was measured, then after two or three transitions were measured, the monitor line would be remeasured; and at the end the last line measured in a run would be, once more, the monitor line. This would give a recorded check on the performance and alignment of the monitoring scheme along that particular run. At least two complete independent measurements were made for all the transitions with a common upper level.

For the transitions that had to be measured using He instead of Ar in the discharge, the following procedure was followed, for example, when the line $\lambda 4309.04$ was going to be measured the monitor was set at $\lambda 4219.36$ transition which had also been used as a monitor when measuring the other branches from the same level with Ar in the discharge. Then with the Rowland spectrometer both lines, $\lambda 4219.36$ and $\lambda 4309.04$, were measured against the monitor line. So the relative branching ratio between the two lines was known independently of monitor line, always watching for self-absorption effects, as will be seen later. The knowledge of this relative branching ratio

made it simple to incorporate this line to the group already measured using completely different conditions. The spectrum obtained in the region $\lambda 4219.36$ using He as the carrier gas in the discharge is shown in Fig. 6.

Because three of the transitions studied had $\lambda < 2900\text{\AA}$ ($\lambda 2411.56$, $\lambda 2656.15$ and $\lambda 2669.49$) and the Rowland system had been calibrated only down to 2900\AA , to carry on the measurement of the photon intensities for these transitions the Rowland system was substituted by the McPherson system. (See Section 10.2 and Fig. 17 for details.) Each instrument had one of the LiF_2 lenses in front of it, 24.5 cm away from the entrance slits. With this new setting the following measurements were made: For the level $x^3I_6^0$ (57070 cm^{-1}) the transitions $\lambda 3254.36$ and $\lambda 2669.49$ were measured against the monitor transition $\lambda 3254.36$ in the second McPherson, and for the upper level $x^3I_7^0$ at 57028 cm^{-1} the transitions $\lambda 3233.05$ and $\lambda 2656.15$ were measured against the monitor $\lambda 3233.05$. In this way the relative branching ratio of two transitions from a same upper level was determined. For the level $x^3I_7^0$ both of its branches were measured using this system, but for the level $x^3I_6^0$ where the relative branching ratio of $\lambda 3538.79$ to $\lambda 3254.36$ had already been obtained with the Rowland system, it was necessary to incorporate the new measurement to the other two.

C. Example of Experimental Procedure

The left side of Fig. 7 depicts a schematic diagram of level $x^3I_7^0$ (52655 cm^{-1}) and the two transitions coming out of it, $\lambda 3005.3$ to level a^3H_6 at 19390 cm^{-1} and $\lambda 3765.54$ to level b^3H_6 at 26106 cm^{-1} . The right side shows the spectrum obtained at the wavelengths of the transitions, using the hollow cathode discharge as a source. Both transitions were obtained using the Rowland spectrometer in second order and there was no need to use discriminating filters in either case. The transition $\lambda 3005.3$ was recorded using an entrance slit width of 80μ , and the $\lambda 3765.54$ transition with an entrance slit width of 40μ trying to resolve the $\lambda 3765.70$ Fe I transition. As seen from the spectrum, the strength of this last transition is so small that it can be considered negligible. The feature shown at $\lambda 3765.41$ has not been identified as any known transition. However, its strength makes a negligible contribution to the strength of $\lambda 3765.54$ and so it will be considered non-existent. The peak strength of the $\lambda 3765.27$ ArII transition is $\sim 5\%$ the strength of the $\lambda 3765.54$ and is 0.27\AA away. A 90μ entrance slit width in the Rowland spectrometer would produce lines with full half widths of $\sim .11\text{\AA}$ and flat tops. With this type of resolution the Ar II line will not be seen while sitting at $\lambda 3765.54$, so this was the setting used.

In this case, the transition chosen to be detected by the McPherson monochromator for monitoring the population of the level was $\lambda 3765.54$, mainly because of its strength, and even when it has several neighbors nearby all of them can be considered negligible. The

entrance and exit slits of the McPherson were set at 30μ and 10μ respectively. This arrangement gave to the lines a flat top and half widths of ~ 400 mÅ. At this width the ArII neighbor line would not be resolved, but as said before, its contribution to the total intensity seen is negligible. For both lines the positioning for taking the background was simple: For the $\lambda 3765.54$ transition, the background was measured at point a, and for the $\lambda 3005.3$ transition at point b. Sometimes deciding where the background should be taken was not so simple. One example at hand in the same Fig. 6 is the position of the ArII $\lambda 3765.27$ transition with respect to the Fe $\lambda 3765.54$ transition. This situation was observed several times in this experiment, i.e., $\lambda 3475.87$ riding on the wing of $\lambda 3475.54$ (Fig. 10), or $\lambda 3785.71$ riding on the wing of $\lambda 3785.95$. In these cases the background was determined in the following way: A measurement was first taken by setting the spectrometer at the wavelength corresponding to the point of lowest strength in the region c, and then in the wavelength of the point of breaking slope in region d. The background for the transition was computed as the mean average of these two measurements. For each individual case, how satisfactory was the procedure was reflected on the uncertainty assigned to each background determination.

The only case where a correction was applied due to a blending contribution was to the transition $\lambda 4595.36$ from level $z^1H_5^0$ (48383 cm^{-1}) which was not completely resolved from $\lambda 4595.21$. This last transition was approximately one fifth the strength of $\lambda 4595.36$, and in this case the spectrograph had to be used in first order. So an 8% correction was effected in the $\lambda 4595.36$ measurement to correct for contributions

from $\lambda 4595.21$.

6.3 Self-absorption

The hollow cathode discharge used in the present experiment is an extended light source of finite depth. Light which originates at some point in the interior of the canal is subject to be re-absorbed on its way to the outside. This process will then weaken the intensity of the light observed from the source.

A good study of the problem of self-absorption of spectrum lines has been made by Cowan and Dieke (1948). In general, the extent to which self-absorption will be present on a given transition depends, among other parameters, on the number of atoms per unit volume found in the line of sight capable of absorbing that particular transition, and on the strength of the line proportional to the transition probability A proportional to the Einstein absorption coefficient B . So, if the ratio of the density of atoms capable of absorbing the transition to the density of atoms capable of emitting it can be considered constant, then the effects of self-absorption are proportional to the emission intensity of a line, and its unnoticed presence will seriously affect the measurement of the branching ratios. It is then necessary to determine to what extent it is present in these measurements.

If one assumes that the level population in a source is governed by the Boltzmann distribution function one may easily argue that the higher the energy of the lower level of a given transition, the lower the density of atoms in that level and so the lower the chance to have self-absorption on the measurement of the intensity of

the transition. However, in the present source the level population distribution is not known. So, even when all the transitions seen have their low level higher than 2.3 ev., this argument is not sufficient to rule out the presence of self-absorption.

In order to check for self-absorption in the present study, the following experiment was performed. For the transitions with upper level at 48383 cm^{-1} , the transition at 4199.1\AA has a transition probability (Table 6) approximately twenty times stronger than the corresponding one for the transition at 4120.21\AA , 5242.5\AA and 3789.18\AA , the latter three having similar strength. Besides these last three transitions have their low level respectively (see Table 3) similar to, slightly higher and slightly lower than the lower level of $\lambda 4199.10$. If self-absorption is present, its effect will be stronger in $\lambda 4199.1$ than in any of the other transitions. If the ratio of photon intensities of $\lambda 4199.1$ to each of the other of the three transitions is computed for different conditions of the discharge (changing the number of atoms capable of absorbing the transitions) the presence of self-absorption will be manifest if the ratios are not constant as a function of discharge conditions. Here the ratios were obtained, using as a monitor line $\lambda 5242.5$, for changes in the current of the discharge from 180 ma to 600 ma, the pressure of the Ar gas from 0.5 mm Hg to 3.0 mm of Hg, and changing the nature of the gas from Ar to He. In every case the ratios were constant within the experimental uncertainties. It was noticed, however, that with the current fixed at 550 ma, pressures of the gas higher than

3.5 mm Hg would yield unreliable ratios. But for the standard conditions used in this experiment no self-absorption effect is present. As a precaution, because sometimes when measuring a group of lines with the same upper level in order to detect the weak transitions, it was necessary to raise the current to 350 ma or 400 ma, if in the group one or two of the transitions were stronger than the rest; then the branching ratio of these transitions, obtained with respect to the monitor line, would be remeasured using 180 ma as the discharge current. In no case was a disagreement found between the measurements at different discharge conditions.

Besides, by comparing the results obtained by Bridges and Wiese (1970) with the results obtained in this experiment for the overlapping transitions, Table 6 and Fig. 8, it can be concluded that the excellent agreement found rules out the presence of self-absorption in these measurements.

6.4 Data Reduction

With the measurements of photon intensities for peak and background wavelengths of each transition recorded on paper and all the intensities normalized to their monitor, the next step was to obtain a corrected photon intensity rate M_{cn}^i for each transition λ_n with a common upper level i

$$M_{cn}^i = \frac{1}{F_n \epsilon_n} (M_{pn} - M_{Bn}) \quad (8)$$

where M_{pn} and M_{Bn} represent respectively the measurements at peak and background for the transition λ_n , normalized to constant monitor counting rate. F_n stands for the discriminating filter transmission when used, equal to one if not present; and ϵ_n is the wavelength efficiency for the Rowland system, read directly from Fig. 22. For an account of how this efficiency was obtained, the reader is referred to Section 10.3. A list of λ_n , ϵ_n , M_{pn} , M_{Bn} and M_{cn}^i for each of the transitions λ_n studied in this experiment is shown on Table 4.

For a transition λ_n define the branching ratio R_n^i as:

$$R_n^i = \frac{M_{cn}^i}{\sum_j M_{cj}^i} \quad (9)$$

where the index j runs over all transitions with common upper level i . So we have by definition

$$\sum_j R_j^i = 1. \quad (10)$$

The branching ratios for the lines of this experiment are listed in Table 5.

6.5 Experimental Uncertainties in the Branching Ratios

It is difficult to assess the accuracy of the branching ratios obtained in this experiment, mainly because of the possible presence of unsuspected systematic errors which have not been taken into account.

In the following analysis the difference between systematic and statistical uncertainties has not been kept clear because of the subjective nature of the assessment of many of the uncertainties quoted.

The different sources that contribute to the experimental uncertainty in the stated values of M_{cn}^i , the photon intensity measurements (see eq. 8 in Section 6.4) are: a) estimated accuracy of the efficiency calibration; b) uncertainty in the transmission of the filters used; c) uncertainty in the ratio of the measurements of peak wavelength versus monitor and background versus monitor; and, in an indirect way, d) the ratio of signal to background for a given transition.

The calibration of the instrument is discussed in full detail in Section 10.3. For the Rowland system an uncertainty of 4% was assigned to the detection efficiency of this system in the region with $\lambda > 3100\text{\AA}$ and 12% for $2800\text{\AA} < \lambda < 3100\text{\AA}$. As noted in the same section, these estimates are due to the spread obtained when plotting together several sets of measurements.

The transitions with $\lambda < 2900\text{\AA}$ were measured using the McPherson monochromator instead of the Rowland spectrometer. The experimental changes that were effected for these measurements were already discussed in Section 6.2-B. One source of uncertainty in this region originates from the fact that the efficiency of the McPherson system did not include the effects of the quartz window of the source and the quartz wedge of the splitter. The error intro-

duced in the efficiency calibration due to this omission is of 3%, negligible compared to the 20% uncertainty assigned to the efficiency calibration in this wavelength range $2500\text{\AA} < \lambda < 2800\text{\AA}$.

The transmission characteristics for the filters were known with an uncertainty of 2% for the UV cutoff Schott WG-320 filter, and 5% for the UV transmitting Corning 7-54 filter.

The uncertainty assigned to the peak to monitor and background to monitor ratios, more than representing counting statistics which for the present purpose are negligible, gives an estimate of the performance of the monitoring scheme. The estimate was deduced after runs of several hours where the ratio of the counting rates obtained with both systems detecting the same transition was obtained as a function of time and as a function of the discharge conditions. As mentioned in Section 6.1-D, deviations from the average not larger than 5% were observed for this ratio while the pressure of the gas was changed from 0.5 mm Hg to 2.5 mm Hg and the current was varied from 180 ma to 500 ma. Similar changes in the ratio were obtained when the discharge was let to run with fixed conditions and the ratio was recorded as a function of time.

The sequence followed when measuring the lines with common upper level was designed to check regularly the performance of the monitoring system. Mainly, the monitor line was remeasured in the Rowland spectrometer at regular intervals while effecting the measurement of the group of transitions, including the beginning and the end of the run.

For some of the transitions the background has been charged with a higher uncertainty, reflecting the difficulty of deciding where the real background lay.

The uncertainty in M_{cn}^i can be found from expression 8:

$$\left(\frac{\Delta M_{cn}^i}{M_{cn}^i}\right) = \left[\left(\frac{\Delta F_n}{F_n}\right)^2 + \left(\frac{\Delta \epsilon_n}{\epsilon_n}\right)^2 + \left(\frac{M_{Bn}}{M_{pn} - M_{Bn}}\right)^2 \left(\frac{\Delta M_{Bn}}{M_{Bn}}\right)^2 + \left(\frac{M_{pn}}{M_{pn} - M_{Bn}}\right)^2 \left(\frac{\Delta M_{pn}}{M_{pn}}\right)^2 \right]^{\frac{1}{2}} \quad (11)$$

from where the importance of the signal to noise ratio for a transition is explicitly obvious. The last column of Table 4 lists the uncertainty in M_{cn}^i for each transition studied.

From expression 9 for the branching ratio R_n^i from the individual M_{cn}^i and by propagation of errors, the following expression for the uncertainty associated with each branch is obtained

$$\left(\frac{\Delta R_n^i}{R_n^i}\right) = \frac{1}{\sum_n M_{cn}^i} \left[\left(\frac{\Delta M_{cn}^i}{M_{cn}^i}\right)^2 \left(\sum_{j \neq n} M_{cj}^i\right)^2 + \sum_{j \neq n} \left(\frac{\Delta M_{cj}^i}{M_{cj}^i}\right)^2 M_{cj}^i \right]^{\frac{1}{2}} \quad (12)$$

In column 3 of Table 5 the uncertainties obtained in the branching ratio determination for each transition is shown. As expected, the strongest branches are almost free of uncertainties while the weak

branches have uncertainties slightly larger than the corresponding uncertainties in M_{cn}^i .

7. TRANSITION PROBABILITIES

7.1 Obtaining Transition Probabilities

If for each transition, one multiplies its branching ratio R_n^i listed in column 2 of Table 5 by the inverse of the lifetime of its upper level, listed in Table 1, one obtains its transition probability:

$$A_n^i = \left[\frac{M_{cn}^i}{\sum M_{cj}^i} \right] \times \frac{1}{\tau^i} \quad (13)$$

A list of the transition probabilities obtained for each of the lines studied is given in column 4 of Table 5. In column 5 of the same table the log gf obtained from A is shown.

7.2 Uncertainties in the Transition Probabilities

The uncertainty in the transition probabilities arise from the uncertainties in the branching ratios and in the lifetimes:

$$\left(\frac{\Delta A_n^i}{A_n^i} \right) = \left[\left(\frac{\Delta R_n^i}{R_n^i} \right)^2 + \left(\frac{\Delta \tau^i}{\tau^i} \right)^2 \right]^{\frac{1}{2}} \quad (14)$$

Before computing expression 14, it is necessary to decide what uncertainty should be assigned to the measured lifetimes. The obvious uncertainties in the lifetime measurements are the uncertainty in the velocity of the beam due to the uncertainty in the

thickness of the carbon foil, and the deviation obtained from statistics in the fitting of the exponentials to the experimental data. These combined errors produce an uncertainty in the quoted lifetimes of the size of 8% to 12%. Besides the lifetime obtained will be influenced by the size of the beam dependent background which is the decay curve obtained at a background wavelength. This background carries much larger statistical fluctuations. Its influence depends on the ratio of the signal of the transition being measured to its background at the sides. For some of the transitions used in Section 11 to measure the lifetime, this ratio was 1.25 or worse. Taking into consideration all the former sources of uncertainty it has been decided to assign an uncertainty of $\pm 20\%$ to all the measured lifetimes.

When this uncertainty is combined with the uncertainties from the branching ratios, through expression 14, the uncertainty in A_n^i is obtained. The uncertainty in the transition probabilities is given in column 4 of Table 5.

8. COMPARISONS AND CONCLUSIONS

8.1 Comparison to Recent Experiments

In Table 6, columns 4 and 5, other measurements are listed for the transitions studied in this experiment. Grasdalen et al, (1969) using the equipment developed by Huber and Tobey (1968) has measured 34 Fe I lines, two of which overlap with the list given in Table 6. They used photographic absorption spectroscopy in Ar + 0.2% Fe(CO)₅ heated to ~8000^oK in a pressure-driven shock tube. By measuring the parameters of the tube including the temperature and knowing the composition of the gas, they were able to determine absolute transition probabilities. Unfortunately, Grasdalen disagrees with Huber and Tobey in the absolute scale by a factor of 2.5. This could reflect the problems involved in the measurement of the number density in a shock tube. For the two transitions in common in column 5, Grasdalen's determinations are a factor of ~2 smaller than this experiment's determinations.

G. L. Wares et al. (1970) have measured photographically emission line strengths from a shock-heated mixture of Ne with Fe(CO)₅ of known composition. They too determined absolute transition probabilities. Of the transitions they have measured, one λ 4219.36 is common to this experiment, and its value in column 5 agrees within the experimental uncertainty.

Garz and Kock (1969) measured photographically relative intensities of lines emitted from a wall-stabilized arc burning in

Ar plus a small but unknown amount of iron chloride at currents between 10 and 80 A. They observed the arc axially and claim that the source was optically thin. The temperature of the arc axis was determined from intensity measurement of Ar lines with known transition probabilities. They converted their relative transition probabilities to an absolute scale by normalizing to the well-measured f value of $\lambda 3720$. They averaged five values obtained from different experiments (see Garz and Kock, 1969) and used $f(3720) = 0.037 \pm .005$ (13%). They published absolute transition probabilities for 50 lines. The ratio of A_{CT}/A_{GK} for these 50 lines as a function of upper level energy is included in Fig. 14. Unfortunately none of these lines overlap with the lines of the present work. Privately, Dr. Garz has informed us that they measured the transition probability for $\lambda 3765.54$. This result in column 5 of Table 6 agrees with this work's result within the experimental uncertainty.

Bridges and Wiese (1970) measured transition probabilities for 80 lines of Fe I chosen to provide maximum overlap with all the recently published experiments. They used essentially the same procedure used by Garz and Kock at Kiel, but have improved the stability of the arc over longer periods of time, reason that enables them to make photoelectric observations which are more precise than the photographic ones. They too normalize their relative transition probabilities using the oscillator strength of $\lambda 3720$, but they chose $f = 0.041$ as an average of the three most recent measurements of this oscillator strength. Sixteen of the lines measured by them are common

to this experiment. Their values are listed in column 4 of Table 6, and Fig. 8 shows a plot of A_{BW}/A_{CT} vs. wavelength. The agreement found is excellent. Because of the different nature of both methods, the agreement found is a strong support for the reliability of these transition probabilities.

8.2 Comparison to the CT Compilation

The transition probabilities listed in the CT compilation for the transitions studied in this experiment are listed in column 6 of Table 6. As stated in Section 5 and Section 11, the lifetime of the level computed from the individual CT transition probabilities is in error by a factor which depends on the energy of the level. This disagreement also appears in a comparison of the transition probabilities, Fig. 14. Still the extensive collection of data involved in the CT compilation is potentially valuable if it can be corrected. For this reason it is very important to compare the transition probabilities of lines with a common upper level, i.e., the branching ratios. This will enable one to decide if the CT branching ratios can be used to compute transition probabilities when the lifetime of the level or the transition probability of one of the lines is known.

Table 7 gives a list of the branching ratios measured in this experiment and the branching ratios $\frac{A_{ij}}{\sum A_{in}}$ computed from the CT A-values. In the last column the ratio of the branching ratios has been computed.

For the first three transitions from level $z^1H_5^O$ (48383 cm^{-1})

the ratio of the branching ratios deviates from the average more than the rest of them. The transition at $\lambda 2411.56$ in Fig. 5 is not obviously present in this experiment and only an upper limit to its transition probability has been given. However, this upper limit is already smaller than the value quoted by CT.

In Fig. 9a the spectrum obtained in this experiment in the neighborhood of $\lambda 3496.19$ is shown, with some of the transitions labelled. The transition probability for $\lambda 3496.19$ in the CT compilation was obtained from the "best" gf value of Corliss and Warner (1966). This best value is the result of an intensity measurement made by Crosswhite in his Fe-Ne hollow cathode. In Fig. 9b a portion of the spectrum in the region of interest published by Crosswhite (1958) has been reproduced. There one notices that the line labelled 3496.19\AA is actually 3495.90\AA . The transition at 3496.19\AA is missing in that spectrum.

In Fig. 10 the spectrum in the neighborhood of $\lambda 3475.87$ is shown. This transition is riding on the wing of the strong $\lambda 3475.45$. If the line is not well resolved one would possibly see contributions from $\lambda 3475.45$ and $\lambda 3475.65$. In Fig. 9b the same line is shown in Crosswhite's spectrum. The way the photon intensity measurement was performed for this line was already discussed in Section 6.2-C. The position of this transition is very similar to $\lambda 3785.71$ riding on the wing of $\lambda 3785.95$, except for no equivalent to $\lambda 3475.65$. However, for the latter case the ratio $R_{CT}/R_{\text{this exp.}}$ is 1.67, while $\lambda 3475.87$ is 12.1. The best gf value listed by CW comes from an averaging of

two measurements, one from Crosswhite and the other from CW arc, the former being a factor of 2.3 larger than the latter. It is interesting to note that CW found a discontinuity in the Crosswhite intensity as a function of wavelength, so they increased the intensity of all the transitions below $\lambda 3750$ by 0.35 in the log scale, equivalent to a factor of 2.2. That could account for the difference found in the CW compilation among the arc and hollow cathode measurements, and reduce slightly the discrepancy with this experiment's measurement. Still more, if one computes the ratio of intensities for $\lambda 5242.5$ and $\lambda 3475.87$ from Crosswhite intensity tables (1958) ($\log I_2 (\lambda 5242.5)=3.20$; $\log I_2 (\lambda 3475.87)=3.40$), the value obtained does not agree with an eye estimate from his spectrum. Some of the disagreement could be due to a different instrumental efficiency at those two wavelengths, but it seems more likely that the intensity tabulated by Crosswhite for $\lambda 3475.87$ is only the peak intensity with no background subtracted.

Because there are reasons to doubt the CT values for these three transitions, they will be excluded from the following discussion. The reader should be made aware that any conclusion reached below will probably not apply for 10% of the lines.

In Fig. 11 the ratio $R_{CT}/R_{\text{this exp.}}$ has been plotted as a function of wavelength. From it one may conclude that there is no wavelength trend present in this ratio. In Fig. 12 the same ratio $R_{CT}/R_{\text{this exp.}}$ has been plotted against the branching ratio obtained in this experiment. From it, it can be concluded that there is some tendency for the CT strongest lines to be diminished relative to their weaker ones.

From the last column of Table 7 and Fig. 12, one finds that for the weak branches ($< 3\%$) the ratio $R_{CT}/R_{\text{this exp.}}$ deviates from unity more than the combined uncertainties of the two sets of data, and a root mean square deviation (with respect to one) of 0.73 for the ratio only reflects this higher spread of the weak branches. If one considers only transitions with branching ratio higher than 3% , then the experimental standard deviation will be only 0.24. So when the lifetime of a level or the transition probability of one of the branches is known, the CT compilation can be used to compute transition probabilities for the stronger branches, the spread in the weakest branches not introducing any significant error. However, transition probabilities for the weak branches computed using the CT compilation will be useful only when making an estimate within a factor of ~ 3 .

Grasdalen et al. (1969) and Withbroe (1967) have suggested the possibility of a wavelength dependent error in the CW compilation. In Fig. 13 a plot of the ratio $A_{CT}/A_{\text{this exp.}}$ versus wavelength is shown. From the figure one would be tempted to conclude that there is a wavelength dependent trend in the ratio. In the present case, the trend is artificially produced by the dependence on the energy of the upper level of the ratio $A_{CT}/A_{\text{this exp.}}$. When this dependence is removed, in Fig. 11, the wavelength dependence also disappears.

8.3 Examination of the Errors Present in the CT Compilation

Figure 14 shows a plot of the ratio $\frac{A_{CT}}{A_{\text{selected experiments}}}$ vs. the energy of the upper level of the transitions. The selected experiments include Garz and Kock (1969a), Bridges and Wiese (1970) and the results of the present experiment. From this figure it can be concluded first that the spread found in the CT branching ratios exists in all the CT data, especially for the high energy levels. This can be accounted for by considering that the CT compilation was integrated from contributions from many different experiments, each with its own problems and uncertainties. Besides, the highly excited states are the ones where the experimental conditions are harder to control, so that the transitions from those levels have a much higher uncertainty in their transition probability. Second, there is indeed an energy dependent error in the Corliss and Tech transition probabilities which cannot be corrected by a simple change of the absolute scale. Several proposals have been offered to explain the discrepancy (Bridges and Wiese, 1970; Garz and Kock, 1969a)

a) Assuming LTE, Corliss (1962) deduced an "effective" temperature of Meggers arc by comparing the intensity of the lines measured by Meggers to their relative gf values known at the time. From the slope of the plot $\log I\lambda^3/gf$ vs. E upper level, the temperature can be deduced. The argument here is that many of the gf's used by Corliss were plagued by errors of their own. Garz and Kock (1969a) have plotted, for lines that overlap with King and King's (1938) work, the ratio A_{KK}/A_{GK} against upper level energy. They

found a slope $\Delta\theta = 0.426$ where

$$\Delta\theta = \frac{\Delta \log A_{KK}/A_{GK}}{\Delta E(\text{ev})} = 5040 \left[\frac{1}{T_{\text{used}}} - \frac{1}{T_{\text{truth}}} \right] \quad (15)$$

This slope is equivalent to $T_{\text{truth}} = 2560^{\circ}\text{K}$, 460°K or 22% hotter than the temperature King measured using an optical pyrometer. Corliss (1962) used not only King's furnace oscillator strengths, but he used 31 sets of data from five different laboratories. Of those sets, seven were obtained using King's furnace. If one assumes that the seven California sets had the 22% temperature error, the mean temperature found by Corliss would be shifted from 5100°K to 5380°K , a 5.7% increase. The slope produced by this change is shown by the lower line in Fig. 14 (assuming the oscillator strength for $\lambda 3720$ is correct). This does not account for the error found in the experimental data. For the sake of argument, suppose one assumes that by some strange mechanism, King's error in temperature was fully transmitted to Corliss' temperature. The temperature should then have obtained as an average 6450°K . This change would produce the slope of the line marked 6450°K as shown in Fig. 14. Not even this correction explains the experimental discrepancy. There is no way to account for the discrepancy found in the Corliss and Tech data solely in terms of an error in King's measurements.

b) The conditions in the arc used by Meggers et al. (1961) were far from those required to produce LTE and permit the use of the Boltzmann's distribution functions. Perfect thermodynamical

equilibrium can only be achieved by a gas in an isolated, isothermal enclosure. There the temperature is the only parameter necessary to describe the spectroscopic state of the gas, completely independent of the excitation mechanisms. When the flux of radiation from the gas is small compared to the total radiative energy content in the gas, it can be assumed that a state of LTE, local TE, exists. This means that the distribution functions characteristic of TE can be applied in this state, but these functions have as a parameter the "local" value of the temperature. To establish LTE in an arc, two conditions are required (Wiese, 1968b): First, that the collision rate between the electrons and the heavy particles is high, for the electrons which receive the energy from the electric field to be able to transfer it to the heavy particles, achieving then a "unique" temperature (gas temperature equal electron temperature) in the plasma. Second, the plasma population should be determined by collision processes rather than radiative ones, to have a high rate of energy exchange processes. In order to achieve these conditions, it has been predicted and proved (Wiese, 1968b) the need to have electron densities of around $10^{16}/\text{cm}^3$ minimum in the low current arcs (< 10 amps) and at large radial distances of the high current ones. Below this density, strong deviations from LTE are expected. As mentioned in the introduction, the MCS arc had a density of $\sim 10^{14}/\text{cm}^3$, two orders of magnitude below the minimum required.

Another arc study (Takens, 1970) suggests that the time required for the atoms to get excited and reach equilibrium is actually larger

than the time the atoms remained in Meggers arc. Another objection is that the Corliss and Bozman (1962) did not resolve spatially the temperature and densities in the arc, but obtained averaged values over its whole inhomogeneous cross section.

It is possible that the discrepancies found in the Corliss and Tech data are due to one or all of the reasons stated above, and probably a detailed study would free the data from all its possible uncertainties. But, if in Fig. 14 a straight line is drawn to best fit the experimental points, and if its slope ($\Delta\theta = 0.28$) is believed to be due to an error in temperature, and a new temperature of 7100°K is used to recompute the transition probabilities for the Fe I lines, then the new data obtained will be free of the energy dependent error but will be loaded with the spread present in Fig. 14. of the data points with respect to the 7100°K line. This spread is comparable to the one obtained for the branching ratios. But unlike the case of the branching ratios, the spread in these transition probabilities is general, for both strong and weak transitions.

Summarizing the possible uses of the CT compilation to recompute new transition probabilities for Fe I lines:

a) If the branching ratios are to be used because the lifetime of the level or the transition probability of one of the branches is known then the strong branches ($R > 0.03$) will yield reliable transition probabilities, but the weak ones will only produce estimates within a factor of 3.

b) If the lifetime or one transitions probability are not

known, then a recomputation of the CT a values using a temperature of 7100^oK will yield estimates for the transition probabilities better than a factor of 3.

9. THE ABUNDANCE OF IRON IN THE SUN

The abundance of iron in the sun, as was mentioned in the introduction, has been for a long time a subject of considerable controversy. The iron abundance derived from coronal observations has been ten to twenty times larger than the iron abundance derived from photospheric observations. This problem was one of the motivations to undertake the present study. It will seem then inconclusive not to discuss the abundance discrepancy under the light of the new values obtained for the transition probabilities.

A new calculation for the photospheric iron abundance was reported by Garz et al. (1969b) utilizing the recently published f -values from Kiel (Garz and Kock, 1969a). In this paper they report an abundance $\log \frac{N_{\text{Fe}}}{N_{\text{H}}} + 12.00 = 7.60 \pm 0.15$ in agreement with the coronal determinations. However, lately Ross (1970) and Cowley (1970) have questioned the damping constants used by Garz et al. in their determination and suggest that 7.2 would probably be an upper limit for the iron abundance in the photosphere.

Due to the nature of the objections raised, there are only two ways to resolve this new discrepancy. Either good reliable damping constants are measured for those transitions with f -values well known, or f -values are measured for weak lines and using them an iron abundance determination is then made. By doing the latter, the analysis will be independent of the choices of damping constants and microturbulence velocity.

Out of the transitions listed in Table 3, Table 8 lists the ones whose observational data have been considered cleaner in the Utrecht Atlas of the Solar Spectrum (1965). Perhaps they are not ideal, but they are better than the ones omitted. Half of the transitions in Table 8 have wavelengths smaller than 4000\AA , where the solar spectrum is very crowded, being difficult to determine the continuum. Besides, the continuous absorption coefficient is not as well known in the UV (for $\lambda < 4500\text{\AA}$) as it is in the visible. Keeping in mind that these uncertainties exist already in the data due to their nature and quality, it is then necessary to decide what is the best use that can be made of these data to help to settle the iron abundance discrepancy.

A fine analysis model atmosphere calculation using these transitions would be worthless because most of the lines are medium to strong, the abundance determination depending then on the choice made for the damping constant Γ and the microturbulence velocity, free parameters fed as an input for the calculations. This will not help to clarify the situation.

However, two of the transitions, $\lambda 4487.75$ and $\lambda 4537.68$, can be considered weak and acceptable and an abundance determination with them will be independent of any other external parameter. The information from these two lines was fed into a direct-integration curve-of-growth program by John E. Ross, using the facilities at UCLA. The solar model used in the calculation is due to Elste. The program chooses an abundance and from it, it computes exactly, by

direct integration, an equivalent width. This is repeated over and over until the computed equivalent width matches the observational one. The iron abundance determined from $\lambda 4487.75$ was $\log \frac{N_{\text{Fe}}}{N_{\text{H}}} + 12.00 = 7.55$, and from $\lambda 4537.68$ was 7.31. If one obtains a mean of these determinations and computes an uncertainty only from the uncertainties existing in the $\log gf$'s from Table 5 aside from any other uncertainties existing in the observational data or in the determination process, one obtains $\log \frac{N_{\text{Fe}}}{N_{\text{H}}} + 12.00 = 7.45 \pm 0.10$.

Before discussing if this result means anything, it is probably worthwhile to make a rough curve of growth analysis using all the transitions from Table 8 and see how the abundance determined from it compares with the result obtained using the accurate analysis. Most important yet, if a similar rough analysis is made to the data used by Garz et al., in their abundance determination, it would then be possible to detect differences among the sets.

For the weak lines, the equivalent width of a line can be related to the abundance of the element producing it by an equation of the form (see, for example, Goldberg and Pierce, 1959).

$$\left(\frac{W_{\lambda}}{\lambda} \right)_{\text{weak}} = \left(\frac{N_{\text{Fe}}}{N_{\text{H}}} \right) gf\lambda 10^{-\theta_0 X_{\lambda}} C_{\lambda} \quad (16)$$

where C_{λ} is a function of the ionization and excitation potentials of the element, wavelength of the transition, solar model used and, if not included in the model, of the depth dependence of the continuous absorption coefficient; $\theta_0 = 5040/T_0$ where T_0 represents the mean temperature at the layers where the lines are formed, g is

the statistical weight of the lower level of the transition and χ_ℓ its excitation energy in electron volts; f is the oscillator strength of the transition and λ its wavelength.

An empirical curve of growth will be obtained by plotting the observed values $\log \frac{W}{\lambda}$ vs. $\log gf\Gamma$ where $\log \Gamma$ is defined as:

$$\log \Gamma = \log \lambda C_\lambda - \theta_0 \chi_\ell \quad .$$

By comparing this empirical curve of growth to a theoretical one, the 45° line corresponding to the unsaturated region can be well defined (the plot of eq. 16). Then if this straight line is extended to the point where $\log gf\Gamma = 0$, then

$$\log \left(\frac{W_\lambda}{\lambda} \right)_{\text{weak}} = \log \frac{N_{\text{Fe}}}{N_{\text{H}}} \quad . \quad (17)$$

To obtain the empirical curve of growth the Γ 's calculated by Cayrel and Jugaku (1963) have been used in this work. They obtained the Γ 's using a model-atmosphere fine-analysis procedure. The Γ 's in their paper are tabulated as a function of λ and χ_ℓ . Figure 15 shows the empirical curve of growth obtained using the data in Table 8, and Fig. 16 shows the curve of growth using the data from Table 1 of Garz et al. (1969b) paper.

A theoretical curve of growth obtained by Hunger (1956) using pure absorption as the line forming mechanism and the Milne-Eddington model atmosphere, has been fitted to both empirical curves of growth,

fitting especially in the weak and flat region. From the fits shown one obtains an iron abundance in the sun $\log \frac{N_{\text{Fe}}}{N_{\text{H}}} + 12.00 \sim 7.60$ for the Garz et al. data, in agreement with their published data, and ~ 7.40 using the data from this experiment.

It should be noticed that the fitting to this experiment curve of growth depends entirely on the positioning of the two weakest transitions. The rest of the points could be fitted for a wide range of positions of the theoretical curve, especially with the uncertainty of the damping constants. So the iron abundance determination from the transitions of this experiment depends entirely on $\lambda 4487.75$ and $\lambda 4537.68$.

Can this slightly lower abundance be reconciled with the Garz et al. published value? ... Yes. In their paper they reported they found different iron abundance depending on the configuration of the upper level of the transitions used. Determinations from transitions with upper level configuration $3d^6 4s 4p$ and $3d^7 4p$ (odd parity) yielded an abundance, on the average, $10^{0.20}$ smaller than determinations from lines with upper level $3d^7 4d$, $3d^7 4s$ and $3d^6 4s 4d$ (even parity). This is significant because the configuration of the upper levels for all the transitions from this experiment listed in Table 3 are of the former type. This fact, together with the existence of some uncertainties in the observational data help to conclude that the iron abundance determined using this thesis' experimental values agrees with and supports the Garz et al. iron determination which yields a value for the photosphere in agreement with that obtained in the corona determinations.

10. CALIBRATION OF THE INSTRUMENTS

10.1 Introduction

In order to determine branching ratios from observed photon intensities, the relative efficiency $\epsilon(\lambda)$ as a function of wavelength for the instruments used to measure these intensities has to be obtained. What follows describes the way in which this efficiency $\epsilon(\lambda)$ was determined for two detection systems referred to as the McPherson system and the Rowland system. The McPherson system was calibrated in the range $1900\text{\AA} < \lambda < 7600\text{\AA}$, and the Rowland system in the range $\lambda > 2900\text{\AA}$. For the region $\lambda > 2900\text{\AA}$ the method used to calibrate both systems was similar. For this reason the calibration of the McPherson system will be analyzed in detail and then a short discussion concerning the calibration of the Rowland system will be given, mentioning mainly details not treated before and of relevance to the photon intensity measurements.

The simplest way to calibrate a detecting system is to observe with it a standard light source of known intensity. The most common sources used in this fashion are a tungsten ribbon lamp or a carbon arc. Unfortunately, for wavelengths below $\lambda 3000$ the emission of the tungsten lamp is very weak and the emission of the carbon arc is dominated by hot arc gases and is not reproducible (Hennes et al. 1966). Because of the lack of an intensity standard for the region $\lambda < 3000\text{\AA}$, another technique for the calibration has to be used. In this experiment the relative efficiency of the system in this wavelength range

was obtained by comparing its response to that of a system of known efficiency. Light from a source with a strong continuum in the middle ultraviolet ($2000\text{\AA} < \lambda < 3000\text{\AA}$) was shone through a monochromator. The output of it at its exit slit constituted then a monochromatic source. In order to measure the flux from of this source, a luminescent wavelength shifter (sodium salicylate) was used, assuming that its excitation spectrum was flat in the region $1900\text{\AA} < \lambda < 3100\text{\AA}$. The blue emission of the sodium salicylate was collected by the cathode of a photomultiplier. Only a relative $\epsilon(\lambda)$ could be obtained because the absolute conversion efficiency for the sodium salicylate is not well known. By renormalizing the obtained efficiency curve in this region to match a section of the efficiency curve for $\lambda > 2800\text{\AA}$ one would obtain the calibration curve for the system in the whole range $1900\text{\AA} < \lambda < 7600\text{\AA}$.

10.2 The McPherson System

The McPherson system shown schematically in Fig. 17, consisted of a 0.3m f/5.3 Czerny-Turner monochromator sold as model 218 by McPherson. It had two interchangeable $5 \times 5 \text{ cm}^2$ gratings: one with $2400\text{\AA}/\text{mm}$ blazed at $\lambda 3000$ coated with MgF_2 for less absorption in the U.V.; the other a $1200\text{\AA}/\text{mm}$ blazed at $\lambda 5000$. To focus the light from the source onto the entrance slit of the monochromator, two achromatic $\text{LiF} - \text{SiO}_2$ lenses were used. They had a 4.8 cm diameter and each had a measured focal length of $17.9 \pm .1\text{cm}$ for white light, and a measured transmission of 85% at $\lambda 3800$. The measured focal length

of the two lenses placed together was 9.0 ± 0.3 cm. At the exit slit of the monochromator the light was piped through the thermal insulation surrounding an EMI 6256S photomultiplier tube operated at dry ice temperature, to its cathode. The light pipe shown in Fig. 17 consisted of a glass cylinder 1 cm in diameter (matching the photocathode area) and 2.5 cm long. Its internal surface was coated with aluminum. The two ends of the cylinder were closed with $1/32''$ thick fused quartz discs. The inside contained dry Argon at atmospheric pressure. The arrangement was designed to avoid water vapor condensation on the cooled windows. Photons detected in the photomultiplier were counted using conventional electronics.

A. Calibration for the Region $\lambda > 2800\text{\AA}$

1) The source

The lamp commonly used as a standard of spectral radiance for the region with $\lambda > 2800\text{\AA}$ is an incandescent tungsten ribbon lamp with a fused silica window. Stair et al. (1960) of the National Bureau of Standards described the calibration of this lamp by comparing its emission to the radiation of a blackbody. The lamp used in the present calibration was a GE-30A/T24/17 calibrated at a current of 35 Amps A.C. by Eppley Labs. They provided with the lamp a calibration table in the range $2500\text{\AA} > \lambda > 7500\text{\AA}$ obtained by comparing this lamp against two working standards which in turn were calibrated against two NBS standards used as shelf standards by them. The power supply for the lamp was designed following the circuit given by Stair et al. (1960) and the ammeter used to set the current of the

lamp was calibrated by Precision Instruments in Pasadena. Eppley Labs provided the calibration table in monochromatic brightness (microwatts/(cm² of source x steradian x nanometer)) versus wavelength at convenient wavelength intervals. For convenience, the monochromatic brightness was changed to photons/(sec x cm² of source x steradian x nm.) (monochromatic photon intensity).

2) Experimental setup

A schematic of the experimental setup used for the calibration of the system in the range $\lambda > 2800\text{\AA}$ is shown in Fig. 18. The geometry was kept simple with just one requirement: to overfill the grating with light. The reasons for this requirement were first to make the variation, as a function of wavelength, of the solid angle subtended by the grating at the entrance slit of the monochromator an intrinsic function of the system, to be reflected in the efficiency curve and thereby facilitate the use of the efficiency calibration of the system in future experiments; and second, to average any localized change of the grating sensitivity over its entire surface. The area of the entrance slit of the monochromator was smaller than the image of the source and was centered on it. The height of the entrance slit was set at 2.5 mm and the width changed from 10 μ to 100 μ depending on the photon intensity of the lamp at a given wavelength.

3) Relations

How are the pulses counted in the scaler per unit time related to the output of the lamp, at a given voltage of the photo-

multiplier tube and setting of the discriminator bias? Define:

$I(\lambda)$ = Monochromatic photon intensity of the lamp
$$\frac{\text{photons}}{\text{sec cm}^2(\text{source}) \text{ str nm}}$$

$T(\lambda)$ = Transmission of the lenses.

e = Entrance slit width.

x = Exit slit width.

h = Limiting height, either of entrance or exit slit.

$\Omega(\lambda)$ = Solid angle subtended by the grating at the entrance slit.

$R(\lambda)$ = Product of reflectivity of mirrors and efficiency of the grating in the monochromator.

$P(\lambda)$ = Product of transmission of the light pipe at surface of PMT, sensitivity of the photomultiplier as a fn. of wavelength and losses in the electronics due to bias setting.

$d\lambda/dx$ = Reciprocal dispersion of the instrument.

C = Output in pulses/sec.

$I \times T$ = The monochromatic photon intensity of the image of the source at the entrance slit of the monochromator.

$e \times h$ = The area of the image source at the entrance slit.

$x \frac{d\lambda}{dx}$ is the spectral width seen by the photomultiplier at a given wavelength setting of the monochromator.

Then:

$$C = I \frac{d\lambda}{dx} (TR\Omega P) exh \quad (18)$$

As long as the system is used always overfilling the grating, then an absolute efficiency relation $S(\lambda)$ in units $\frac{\text{pulses/sec}}{\text{photon/sec} \times \text{str}}$

can be found:

$$S(\lambda) = \frac{C}{I \frac{d\lambda}{dx} e x h} \quad (19)$$

or a relative efficiency by:

$$\epsilon(\lambda) = k \frac{C}{I \frac{d\lambda}{dx}} \quad \text{in arbitrary units.} \quad (20)$$

$d\lambda/dx$, the reciprocal linear dispersion is obtained by differentiation with respect to β , the angle of diffraction, of

$$\lambda = \frac{d}{n} (\sin \alpha + \sin \beta) \quad (21)$$

where α = angle of incidence, n the order of the dispersion and d the space between lines in the grating. For this monochromator $\alpha - \beta$ obtained experimentally is $28^{\circ}52'$.

$$fd\beta = dx$$

$$\frac{d\lambda}{dx} = \frac{d\lambda}{fd\beta} = \frac{d}{nf} \cos \beta \quad (22)$$

In Fig. 19 a plot of $d\lambda/dx$ as a function of wavelength for this McPherson monochromator is shown using $d = 10^4/1.2 \text{ \AA}$ and $f = 3 \times 10^2 \text{ mm}$ with $n = 1$.

For this experiment the knowledge of $\epsilon(\lambda)$ was sufficient. For future reference, the constant to transform $\epsilon(\lambda)$ given in Fig. 20 into $S(\lambda)$ is

$$S(\lambda) = 7.56 \times 10^{-3} \epsilon(\lambda) \quad (23)$$

for a limiting slit height of 2.5 mm and the entrance and exit slit widths at 30μ each. Before applying relation 23, see word of caution on the next Section 4a.

4) Experimental procedure

Even when the experimental procedure for the calibration of the system is straightforward, several problems which arise from the same nature of the standard lamp emission spectrum had to be solved. The lamp emission is four orders of magnitude smaller at $\lambda 2800$ than what it is at $\lambda 5400$, adding an extra order at $\lambda 2500$. To get rid of stray light when it became of importance compared to the size of the signal, pre-calibrated filters had to be used. Besides, the counting losses in the system as a function of counting rate was determined and the linearity of slit width readings versus counting rates was measured.

(a) Linearity of the slits

By linearity of a slit, it is meant the relation between the amount of light going through the slit and its width read on its micrometer dial. The solution to this problem is not necessary in this experiment where only the relative efficiency $\epsilon(\lambda)$ is needed. Here the different wavelength sections where the efficiency was obtained using different slit widths can easily be renormalized if care was taken to measure some points at overlapping wavelengths, at both ends of the sections. But because of the possible future use of the instrument, perhaps involved in absolute measurements, some measurements were made to investigate the relation between the slit

widths and their micrometers. Keeping one slit fixed and plotting, for constant wavelength, the counting rate observed as a function of reading of the other slit width, it was found that the counting rate for both slits was linear with the dial reading down to 5μ . Below this width the counting rate remained constant while moving the micrometer to zero. So, indeed, the jaws stopped closing at 5μ as the instruction manual of the monochromator claims. However, when closing both slits at the same time, the counting rates did not follow a linear relation with the product of the read widths. The following equivalences were found between the slit width readings and the product of true slit widths as deduced by the changes in the counting rates: If the micrometers are set both at 100μ by definition the product of the widths $ex = 10^{-2} \text{ mm}^2$

if micrometers set at 30μ	$ex = 9 \times 10^{-4} \text{ mm}^2$
if micrometers set at 20μ	$ex = 4.569 \times 10^{-4} \text{ mm}^2$
if micrometers set at 10μ	$ex = 1.395 \times 10^{-4} \text{ mm}^2$.

Thus, expression 23 only holds when the slit widths used are $30\mu \times 30\mu$ and cannot be extended linearly to narrower slit widths. When going to narrower slits, expression 23 has to be modified using the values tabulated above.

(b) Calibrating the filters

When calibrating the system in the regions for $\lambda < 3800\text{\AA}$, and for $\lambda > 6000\text{\AA}$ because of the spectral response of the "S" cathode of the photomultiplier used, stray light became appreciable and to get rid of it precalibrated filters were used. The filters were

positioned in a holder between the lamp and the lenses. (See Fig. 18.) In order to obtain the transmission characteristics of the filters the same setup was used, but the standard lamp was substituted by a commercial Fe-Ne hollow-cathode source (Westinghouse, 20 ma max.). After setting the monochromator at the wavelength corresponding to the top of a strong transition, a reading was taken with the filter in position and out of position, the ratio giving then the transmission for the filter at that wavelength. Repeating the procedure for lines at different wavelengths, the transmission curve of the filter as a function of wavelength was obtained.

The filters calibrated came in standard size 5 cm x 5 cm and 3 mm thick. They were:

- a. A UV transmitting Corning 7-54 filter transmitting 85% at λ 3450 and 10% at λ 2350 and λ 4000. This filter would transmit again on the red for $\lambda > 6700\text{\AA}$.
- b. A series of clear-in-the-visible short wavelength-cutoff filters with sharp absorption edges, the transmission increasing from zero to a maximum of $90\% \pm 2\%$ in an average of 500\AA , remaining constant for longer wavelengths. These filters included:
 - a Corning 9-53 with λ cutoff at 2500\AA
 - a Schott WG-320 with λ cutoff at 2900\AA
 - a Corning 0-52 with λ cutoff at 3300\AA
 - a Kodak W-4 with λ cutoff at 4500\AA
 - a Kodak W-25 with λ cutoff at 5800\AA .

c. A neutral density filter Balzer ND2 with transmission of the order of one percent in the region $3500\text{\AA} < \lambda < 7600\text{\AA}$. It was found that some of the filters had transmission characteristics strongly position dependent. So, the filters were marked to use them always in the position they were calibrated.

The use of the filters was in many occasions direct; for instance, when using the 7-54 to get rid of stray radiation from region of $\lambda 5000$, or when calibrating in second order to get rid of radiation 2λ in first order, or when using the W-25 for radiation of $\lambda > 6000\text{\AA}$ to get rid of radiation from $\lambda 5000$. In other occasions their use was indirect, using them just to subtract stray light, i.e., in first order calibrating $\lambda 3000$, first a measurement was taken with no filter, then the Corning 0-52 was put in place and the measurement was repeated. This second measurement will be entirely due to the contribution of stray radiation from regions with $\lambda > 3300\text{\AA}$. Correcting this measurement by the transmission of the filter and subtracting it from the measurement with no filter gave an approximate measure of the real signal detected at $\lambda 3000$.

On several occasions more than one filter had to be used at a given time. No effect was noticed due to the increase in reflection surfaces so that the rule applied was: the transmission of a combination of filters equal to the pro-

duct of the transmission of the individual filters.

(c) Counting losses

The counting losses in the system due to saturation effects in the electronics were studied by two different methods. The first method was possible because a fast (50 Mc) counting system was made available to this laboratory by Douglas Advanced Research Labs. By direct comparison of the responses obtained by the 50 Mc electronics and the electronics incorporated in the McPherson system, the counting losses were determined as a function of counting rates. The other method, needing just a filter ND1 or ND2 as auxiliary equipment, consisted of the following: The instrument was set at a fixed wavelength and the lamp at low intensity. A reading with the system was taken with the filter in position and out of position, the ratio yielding the transmission of the filter at that wavelength. The intensity of the lamp was then increased by steps, and for each step a reading was taken with the filter in and out of position. When saturation occurred, the ratio of readings with filter in to out started to increase. The ratio of a reading with the filter in position to the transmission of the filter obtained at low counting rates gave the true counting rate. A plot of the ratio of the true counting rate to the apparent counting rate (reading obtained with filter out) versus the apparent counting rate gave the correction factor to correct for losses due to saturation. The results obtained by both methods agreed: The McPherson system was free of saturation up to 10 kHz. A 5% correction had to be applied at 35 kHz, 10% at 60 kHz, and 50% at 160 kHz. Because of the relatively slow

speed of the system, the Balzer ND2 filter was used in the calibration to attenuate the high counting rates obtained in some regions of the spectrum. (The ND2 filter was calibrated using the 50 Mc electronics.)

5) Results

After solving these problems the actual taking of the data for the calibration was simple. Before any calibration run the lamp was allowed to warm up at 35 amps for ~ half an hour. Points were taken 100\AA away from each other in the UV region and 200\AA away for $\lambda > 4400\text{\AA}$. Filters and saturation corrections were used, and slit widths changed when needed. Efficiency curves were obtained for the 2400 l/mm grating in first order from $\lambda 2800$ to $\lambda 5000$ and for the 1200 l/mm grating in first order from $\lambda 2800$ to $\lambda 7500$, and in second order from $\lambda 2800$ to $\lambda 5000$. The calibration measurements were obtained for different settings of geometry, slits and discriminator level. In all situations the results agreed within $\pm 2\%$ (for $\lambda > 3000\text{\AA}$). Another contributing source of uncertainty is the calibration of the filters. A 2% uncertainty was assigned to the sharp cutoffs and 4% to the 7-54 and ND2. A $\pm 4\%$ was then assigned to the relative efficiency curve for $\lambda > 3000\text{\AA}$, excluding systematic errors due to bad calibration of the lamp or error in the setting of the current. A plot of $\epsilon(\lambda)$ as a function of λ is shown in Fig. 20.

B. Calibration in the Middle UV.

1) Method and equipment

Because of the weakness of the radiation emission of the tungsten lamp for wavelengths below 2800\AA relative to the stray

radiation from longer wavelengths detected by the instrument, the efficiency of the system in this range was obtained following a different procedure. Here a two monochromators technique was used, the equipment shown in Fig. 21. As a source with a strong continuum in the middle ultraviolet, a high pressure Xenon lamp in a fused silica envelope (Osram XBO-162W/1) was used. It was run at a power of 150 watts A.C. using an Osram power supply. The additional monochromator used for this experiment was another f/5.3 0.3m McPherson monochromator loaned to us by Douglas Advanced Research Laboratories. (To avoid possible confusion, in what follows this monochromator will be referred to as the source monochromator). Light from the Xe arc was focused onto the entrance slit of the source monochromator by one of the achromatic lenses belonging to the McPherson system, which was left with only one. This arrangement, a source of monochromatic light of variable wavelength, will be referred to from now on as XeMS.

If the photon intensity of XeMS was known as a function of wavelength, then just by observing it with the McPherson system one could obtain the relative efficiency of the McPherson system. To measure the flux from XeMS, a calibrated detector had to be used. In this experiment a sodium-salicylate coated RCA 8575 photomultiplier tube was prepared for that effect. The sodium salicylate was not sprayed directly on the phototube face, but on a Kodak W-35 blue transmitting filter which was then sealed to the phototube face with Dow Corning #20057 grease. Sodium salicylate is a luminescent con-

verter with an emission spectrum peaked at 4200\AA and half width $\sim 800\text{\AA}$. This emission spectrum is similar to the spectral sensitivity of the bialkali photocathode of the RCA 8575 PMT. The blue filter with transmission characteristics matching the phosphor emission spectrum was used just as a precaution against unwanted radiation that would traverse the sodium salicylate without being converted and then be detected by the PMT. It was decided to use the sodium salicylate under the assumption that its excitation spectrum or relative quantum yield as a function of wavelength was flat in the region under consideration. Watanabe and Inn (1953) proved that in the region $800\text{\AA} < \lambda < 3000\text{\AA}$. However, Kristianpoller and Knapp (1964) have given evidence of the existence of a 20% dip on the sodium salicylate excitation spectrum at $\lambda 2000$, even when no other investigator has seen it (Hennes and Dunkelman, 1966). Experimentally it is important that the layer of sodium salicylate is thicker than 1.5 mg/cm^2 . Below this thickness irregularities in the efficiency spectrum are common (Hennes and Dunkelman, 1966; Samson, 1967). In preparing the coating of sodium salicylate for this experiment, the salicylate was dissolved in alcohol to saturation and sprayed on the blue filter in very uniform, fine grained layers. The final coating was around 6 mg/cm^2 thick, thick enough to be opaque to visible light.

2) Experimental setup

The experimental setup is shown in Fig. 21. The instruments were set on a heavy wooden table. The calibrated detector was located near the exit slit of the source monochromator and could

be moved in and out of the light path easily. The alignment was critical and difficult. The lenses were set on holders that would slide easily on a flat aluminum table with legs of adjustable height, one of the lenses laying between the Xe lamp and the source monochromator, and the other between the source monochromator and the McPherson monochromator. The aluminum table was made to be parallel to the plane defined by the source monochromator light path, and the Xe lamp and McPherson system were then brought to lie on that plane. The relative position of the different elements was chosen requiring: (1) that everything was set on the wooden table (limitation of space), and (2) that the grating of the McPherson monochromator was over-filled with light. The whole arrangement was very sensitive even to disturbances produced by persons walking around the table. For this reason the lenses had to be repositioned often for maximum counting rates.

The height of the entrance and exit slits of both monochromators were set to 1 mm. To avoid errors due to misalignment the exit slit of the McPherson was made wider than its entrance slit, which in turn was wider than the exit slit of source monochromator. The values used were:

Source monochromator	entrance = 25 μ	exit = 25 μ
McPherson monochromator	entrance = 50 μ	exit = 500 μ .

3) Experimental procedure

The high pressure Xe arc has an emission at $\lambda 2000$ smaller by orders of magnitude than its emission in the visible.

For this reason there is stray light that will be mixed with light from the right wavelength in the output of XeMS. This stray light will not reach the exit slit of the McPherson system, but will affect the measurement of the XeMS flux. To get rid of it in some occasions a set of narrow band interference filters from Optics Technology were used as part of XeMS (set at exit slit of source monochromator), a use that did not require the knowledge of the filter transmission characteristics. In other occasions, the subtraction of the stray light was preferred, using the Corning 9-53 and the Schott WG-320.

The procedure for calibration went as follows: The McPherson monochromator was set at a fixed wavelength, then the source monochromator was scanned in wavelength to get maximum signal in the McPherson system. On its final wavelength setting it read the same wavelength as the McPherson because both wavelength scales were calibrated right. Then the flux from the XeMS was measured by integrating the current from the PMT of the calibrated detector for a preset time, getting rid of stray light when present. The flux was then permitted to pass into the McPherson system and counted for a recorded time. This was repeated each 50\AA from 1900\AA to 3100\AA . The ratio of McPherson reading to flux measured gave the sought relative efficiency as a function of wavelength.

4) Results

Several complete sets of data were obtained for the $2400\ \ell/\text{mm}$ grating in first order and for the $1200\ \ell/\text{mm}$ grating in first and second order. The uncertainty assigned to the efficiency

curve in this range included the scattering in the different sets of data for the same curve due, in addition to statistical fluctuations, to changes of the alignment that occurred during one run or occurred in the interval between different runs. Other uncertainties taken into account are the uncertainty in the flatness of the excitation spectra of the phosphor used and the errors introduced with the subtraction of stray light. The estimated error is 12% for the region from $\lambda 2800$ to $\lambda 3000$ and 20% for region from $\lambda 2500$ to $\lambda 2800$.

C. Conclusions

The matching of the two efficiency curves was made in the wavelengths between $\lambda 2800$ and $\lambda 3100$. The value of the middle UV efficiency curve in this range was adjusted to the value of the visible efficiency curve in the same range. This gave the factor by which all the other points of the middle UV curve were multipliers. The final form of the curve is shown in Fig. 19. The shape of it could be roughly understood remembering that its main contributors are the photocathode ("S") spectral response and the efficiency curve of the grating (the 2400 ℓ /mm blazed at $\lambda 3000$ and the 1200 ℓ /mm blazed at $\lambda 5000\text{\AA}$). The fast drop of the efficiency curve at short wavelengths is probably due to atmospheric absorption.

The effects produced in the system by the use of polarized light were studied. Unfortunately, the prism polarizer used was not quartz, but glass so the short wavelength region ($\lambda < 3200\text{\AA}$) was not seen. In the region studied ($3200 < \lambda < 4500\text{\AA}$) no structural dif-

ferences were found in the response obtained from light polarized parallel to the grating grooves and light polarized perpendicular to them. On the average, the response of the former was 2.5 times stronger than the response of the latter.

10.3 Calibration of the Rowland System

By using exactly the same technique employed calibrating the McPherson system, the Rowland system was calibrated for the region with $\lambda > 2900\text{\AA}$ using the tungsten ribbon standard lamp. The Rowland system has already been described in Section 6.1-C. The experimental setup used during the calibration was identical to the one designed for the branch intensity measurements, with the tungsten ribbon lamp substituting the hollow-cathode source. Both the quartz window of the hollow cathode and the quartz beam splitter were left in the light path during the calibration, so that the efficiency curve includes any variations in their transmission as a function of wavelength. The geometry was set to give an image to source magnification of 3.5, overfilling the grating with light. The high magnification assured the use of just a small central region of the filament of the tungsten lamp, this then reducing uncertainties due to possible different temperatures in different regions of the filament. The spectrometer entrance slit width was fixed at 100μ and its height either .200" or .500", depending on the region of the spectrum under calibration. The readings corresponding to each of the height set-

tings were transformed to the same scale by determining a transformation factor measuring an identical section of the spectrum at the two height positions, the same way as when calibrating the McPherson system. In calibrating this system care was not taken at all to determine the absolute scale because these were plans of modifying the system at the conclusion of this experiment, and because it is not needed in the determination of the branching ratios. For a Rowland mounting the linear dispersion of the instrument is almost constant because the exit slit is always near the normal of the grating (Table 2), so the relative efficiency is given by

$$\epsilon(\lambda) = \frac{nC}{I(\lambda)} \quad (24)$$

where n is the order of the dispersion, C is the output in pulses/sec, and I is the monochromatic photon intensity of the standard lamp.

Filters were used in the same context as in the McPherson system calibration (Section 10.2-A.4). The same filters were needed and their transmission characteristics rechecked at different wavelengths. Agreement was found in all cases.

The counting losses for the system were determined using the neutral density filter method (Section 10.2A.4-c). No correction for saturation was needed for counting rates up to 60 kHz. A 4% correction had to be made at 100 kHz, 10% at 170 kHz, and 15% at 240 kHz. This system was then much faster than the McPherson system, and seldom were the counting rates high enough to require any saturation correction. When the counting rates were high, readings both

with the ND2 Balzer filter and with no filter were taken, and agreement between the two corrected readings was required.

For the calibration the exit slit assembly of the Rowland spectrometer was kept fixed at 1" reading on its micrometer, and the spectrometer was set at integer wavelengths. The readings were taken each 100Å from 2800Å to 4000Å, and each 200Å from 4000Å up.

The Rowland system was calibrated in first order in the range $3200 < \lambda < 7500$ and in second order in the range $2900 < \lambda < 4400$. The uncertainties assigned are mainly contributions from randomness originating from several sets of data, 4%. For the region below 3100Å the signal became weak and stray light contributed strongly. Here an uncertainty of 12% ($2800 < \lambda < 3000$) was assigned. The final efficiency curve for the Rowland system is shown in Fig. 22.

REFERENCES

1. C. W. Allen and C. H. Corliss, *MNRAS* 126, 37 (1963).
2. T. Andersen, private communication.
3. R. C. Ashenfelter, Ph.D. Thesis, CIT, p. 38 (1967).
4. S. Bashkin, *Nucl. Inst. and Methods* 28, 88 (1964).
5. S. Bashkin, *Beam-Foil Spectroscopy*, Chap. 4 of *New Uses for Low-Energy Accelerators* (Natl. Academy of Sciences, Washington D. C., 1968).
6. W. S. Bickel, *Appl. Opt.* 6, 1309 (1967).
7. J. M. Bridges and W. L. Wiese, *Astrophys. J.* 161, L71 (1970).
8. R. Cayrel and J. Jugaku, *Annales D'Astrophysique* 26 No. 6, 495 (1963).
9. C. H. Corliss, *J. Res. Natl. Bur. Std. (U.S.)* 66A, No. 1, 5 (1962).
10. C. H. Corliss and W. R. Bozman, *Natl. Bur. Std. Monograph No. 53* (1962).
11. C. H. Corliss and B. Warner, *Astrophys. J., Suppl.* 8, 395 No. 83 (1964).
12. C. H. Corliss and B. Warner, *J. Res. Natl. Bur. Std. (U.S.)* 70A, No. 4, 325 (1966).
13. C. H. Corliss and J. T. Tech, *Natl. Bur. Std. Monograph No. 108* (1968).
14. R. D. Cowan and G. H. Dieke, *Rev. of Mod. Phys.* 20, 418 (1948).
15. C. Cowley, *Astrophys. Letters* 5, 149 (1970).

16. H. M. Crosswhite, Johns Hopkins Spectroscopic Report No. 13 (Baltimore, 1958).
17. E. W. Foster, Rept. Progr. Phys. 27, 469 (1964).
18. Fused Quartz Catalog, Lamp Glass Dept., General Electric, p. 34.
19. T. Garz and M. Kock, Astron. and Astrophys. 2, 274 (1969a).
20. T. Garz, H. Holweger, M. Kock and J. Richter, Astron. and Astrophys. 2, 446 (1969b).
21. G. L. Grasdalen, M. Huber and W. H. Parkinson, Astrophys. J. 156, 1153 (1969).
22. L. Goldberg and A. K. Pierce, The Photosphere of the Sun, Handbuch der Physik, ed. S. Flügge, Vol. LII, 1 (Springer-Verlag, Berlin, 1959).
23. G. R. Harrison, MIT Wavelength Tables (Wiley and Sons Inc., New York, 1939).
24. J. Hennes and L. Dunkelmann, UV Technology, Chap. 15 of The Middle UV: Its Science and Technology, ed. by A. E. S. Green (Wiley and Sons Inc., New York, 1967).
25. M. Huber and F. L. Tobey, Astrophys. J. 152, 609 (1968).
26. K. Hunger, Zs. f. Ap. 39, 38 (1956).
27. C. C. Kiess, V. C. Rubin and C. E. Moore, J. Res. Natl. Bur. Std. (U.S.) 65A, No. 1, 1 (1961).
28. R. B. King and A. S. King, Astrophys. J. 87, 24 (1938).
29. N. Kristianpoller and R. A. Knapp, Appl. Opt. 3, 637 (1964).
30. M. Martinez, R. B. King and W. Whaling, Bull. Am. Phys. Soc. 13, 1674 (1968).

31. W. F. Meggers, C. H. Corliss and B. F. Scribner, Natl. Bur. Std. Monograph No. 32, (1961).
32. D. L. Mickey, P. Zucchini, J. Born and W. H. Smith, Rev. Sci. Instr. 41, 276 (1970).
33. B. M. Miles and W. L. Wiese, Natl. Bur. Std. Special Publication No. 320, (U.S. Dept. of Commerce, Washington D. C. 1970).
34. Ch. E. Moore, A Multiplet Table of Astrophysical Interest, Contributions from the Princeton University Observatory No. 20 (1945).
35. Ch. E. Moore, Atomic Energy Levels, Circular Natl. Bur. Std. 467, Vol. 2 (U. S. Dept. of Commerce, Washington D. C., 1958).
36. Ch. E. Moore, M. G. J. Minnaert and J. Houtgast, The Solar Spectrum 2935Å to 8770Å, Natl. Bur. Std. (Washington D. C., 1966).
37. J. E. Ross, Nature 225, 610 (1970).
38. J. A. R. Samson, Techniques of Vacuum UV Spectroscopy (Wiley and Sons Inc., New York, 1967).
39. P. L. Smith and W. Whaling, Phys. Rev. 188, 36 (1969).
40. R. Stair, R. G. Johnston and E. W. Halbach, J. Res. Natl. Bur. Std. (U.S.) 64A, No. 4, 291 (1960).
41. A. R. Striganov and N. S. Sventitskii, Tables of Spectral Lines of Neutral and Ionized Atoms (IFI/PLENIUM., New York and Washington, 1968).
42. R. J. Takens, Astron. and Astrophys. 5, 244 (1970).
43. S. Tolansky, High Resolution Spectroscopy (Methuen and Co. Ltd., London, 1947).

44. Utrecht Atlas of the Solar Spectrum, Revised Edition (1965).
45. G. L. Wares, private communication.
46. B. Warner, MNRAS 127, 413 (1964).
47. B. Warner and C. R. Crowley, J. Quant. Spectrosc. and Rad. Transf. 7, 751 (1967).
48. K. Watanabe and C. Y. Inn, J. Opt. Soc. Am. 43, 32 (1953).
49. W. Whaling, Atomic Lifetime Measurements, Chap. 5 of New Uses for Low Energy Accelerators (Natl. Academy of Sciences, Washington D. C., 1968).
50. G. L. Withbroe, Sci. Rept. No. 17, Shock Tube Spect. Lab., Harvard College Obs. (1967).
51. W. L. Wiese, Transition Probabilities for Allowed and Forbidden Lines: Lifetimes of Excited States; in Methods of Experimental Physics, B. Bederson and W. L. Fite, editors, 7A, 117 (Academic Press, New York, 1968a).
52. W. L. Wiese, Electric Arcs; in Methods of Experimental Physics, B. Bederson and W. L. Fite, editors, 7B, 341 (Academic Press, New York, 1968b).

TABLE 1

Lifetime measurements for Fe I. Column 1 lists the transition whose light decay curve was measured. Column 2 and 3 give the term and excitation energy of the level where the transition originates. Column 4 and 5 give the value for the lifetime of the level obtained in this experiment and by T. Andersen (1969) at Aarhus. (See page 18).

λ (Å)	Upper Level	E(kK)	τ_{exp} (nsec)	τ_{Aarhus} (nsec)
4199	$z^1H_5^0$	48383	13.8	11.0
4220	$y^3I_6^0$	52514	8.0	8.5
3765	$y^3I_7^0$	52655	9.7	9.0
4119	$z^1I_6^0$	53093	9.2	8.4
3233	$x^3I_7^0$	57027	11.4	12.1
3254	$x^3I_6^0$	57070	15.0	13.0

TABLE 2

Summary of the characteristics of the
Rowland Spectrometer

Type: Rowland Mounting

Spectral coverage: 2000Å → 7000Å

Aperture: f/48

Dispersion System: 600 grooves/mm Bausch and Lomb concave grating with
a radius of curvature of 6.65 m. Ruled area 55 mm by 138 mm.

Blaze wavelength: 3000Å in second order.

Resolving Power: 85% of theoretical (B. and L.)

$$\frac{\lambda}{\Delta\lambda} = Nm = 1.656 \times 10^5 \text{ in second order}$$

Exit slit: Fixed to a length of 25 mm and width of 21μ.

Reciprocal dispersion: $\frac{d\lambda}{dx} = \frac{d}{nR} \cos\beta = 1.253 \text{ Å/mm}$ in second
order ($\cos\beta = 1$)

Detector: Dry ice refrigerated EMI 9526B photomultiplier tube behind
the exit slit.

For more detail see page 25.

TABLE 3

Decay modes for the levels whose lifetime were measured, obtained from the Corliss and Tech (1968) compilation. The multiplet number and level designation are from Moore (1945), and the configuration and energy from Moore (1958). For further detail refer to page 27.

TABLE 3

Mult No.	Transition (Å)	Upper level			Lower level		
		Config.	Desig.	E(cm ⁻¹)	Config.	Desig.	E(cm ⁻¹)
	2411.558	3d ⁷ (a ² G)4p	z ¹ H ₅ ^o	48383	3d ⁷ (a ⁴ F)4s	a ⁵ F ₅	6928
186	3475.867				3d ⁶ 4s ²	a ³ H ₅	19621
186	3496.190				3d ⁶ 4s ²	a ³ H ₄	19788
	3603.673				3d ⁶ 4s ²	b ³ F ₄	20641
289	3789.178				3d ⁷ (a ² G)4s	a ³ G ₄	21999
423	4120.209				3d ⁶ 4s ²	b ³ G ₄	24119
522	4199.100				3d ⁷ (a ² G)4s	a ¹ G ₄	24575
594	4487.750				3d ⁷ (a ² H)4s	b ³ H ₆	26106
594	4537.680				3d ⁷ (a ² H)4s	b ³ H ₅	26351
594	4595.360				3d ⁷ (a ² H)4s	b ³ H ₄	26628
843	5242.500				3d ⁶ 4s ²	a ¹ I ₆	29313
928	5379.580				3d ⁶ 4s ²	b ¹ G ₄	29799

TABLE 3 (continued)

Mult	Transition	Upper level			Lower level		
		Config.	Desig.	E(cm ⁻¹)	Config.	Desig.	E(cm ⁻¹)
199	3018.134	3d ⁷ (a ² H)4p	y ³ I ₆ ⁰	52514	3d ⁶ 4s ²	a ³ H ₆	19390
199	3039.322				3d ⁶ 4s ²	a ³ H ₅	19621
443	3479.683				3d ⁶ 4s ²	b ³ G ₅	23784
608	3785.706				3d ⁷ (a ² H)4s	b ³ H ₆	26106
608	3821.181				3d ⁷ (a ² H)4s	b ³ H ₅	26351
800	4219.360				3d ⁷ (a ² H)4s	a ¹ H ₅	28820
849	4309.040				3d ⁶ 4s ²	a ¹ I ₆	29313
199	3005.302	3d ⁷ (a ² H)4p	y ³ I ₇ ⁰	52655	3d ⁶ 4s ²	a ³ H ₆	19390
608	3765.541				3d ⁷ (a ² H)4s	b ³ H ₆	26106

(continued)

TABLE 3 (continued)

Mult.	Transition (Å)	Upper level			Lower Level		
		Config.	Desig.	E(cm ⁻¹)	Config.	Desig.	E(cm ⁻¹)
200	2986.653	3d ⁷ (a ² H)4p	z ¹ I ₆ ^o	53094	3d ⁶ 4s ²	a ³ H ₅	19621
609	3738.308				3d ⁷ (a ² H)4s	b ³ H ₅	26351
801	4118.548				3d ⁷ (a ² H)4s	a ¹ H ₅	28820
850	4203.950				3d ⁶ 4s ²	a ¹ I ₆	29313
	2656.145	3d ⁶ 4s(b ² H)4p	x ³ I ₇ ^o	57028	3d ⁶ 4s ²	a ³ H ₆	19390
620	3233.053				3d ⁷ (a ² H)4s	b ³ H ₆	26106
	2669.492	3d ⁶ 4s(b ² H)4p	x ³ I ₆ ^o	57070	3d ⁶ 4s ²	a ³ H ₅	19621
620	3254.363				3d ⁷ (a ² H)4s	b ³ H ₅	26351
811	3538.790				3d ⁷ (a ² H)4s	a ¹ H ₅	28820

TABLE 4

Reduction of the data from the branching ratio measurements. For each transition λ_n , the corrected photon intensity M_c is obtained using equation 8 on page 37:

$$M_c = \frac{1}{F_c \epsilon_n} (M_p - M_B)$$

where M_p and M_B are the measurements at peak and background of the transition n , normalized to constant monitor counting rate. F_c stands for the discriminating filter transmission and ϵ_n is the detection efficiency of the instrument at the transition's wavelength. For more detail see page 37-38. The uncertainty in M_c is obtained on page 41.

TABLE 4

λ_n (Å)	M_p	M_B	F_c	ϵ_n	M_c	$\Delta M_c/M_c$ (%)
2411.56		0.0164	0.20	0.06	< 1.37 ^a	
3475.87	2.28	1.10		1.09	1.08	14
3496.19	0.366	0.282		1.08	0.0777	35
3603.67	1.03	0.44		0.99	0.595	15
3789.18	5.50	0.27	0.90	0.91	6.38	7
4120.21	14.71	0.31	0.90	2.20	7.27	7
4199.10	84.33	0.33	0.90	0.58	160.91	7
4487.75	0.432	0.202		2.58	0.0891	12
4537.68	0.137	0.107	0.90	2.58	0.131	33
4595.36	4.44	0.11	0.90	2.53	1.75 ^b	7
5242.50*	14.32	0.28	0.90	1.67	9.34	7
5379.58	3.00	0.10	0.90	1.33	2.42	7

-92-

(continued)

TABLE 4 (continued)

$\lambda_n(\text{\AA})$	M_p	M_B	F_c	ϵ_n	M_c	$\Delta M_c / M_c (\%)$
3018.13	0.412	0.092		0.97	0.330	14
3039.32	0.386	0.064	0.726	1.00	0.444	14
3479.68	0.241	0.107	0.90	1.09	0.137	11
3785.71	0.664	0.331	0.90	0.90	0.411	15
3821.18	18.66	0.66	0.90	0.89	22.47	7
4219.36*	5.881	0.054	0.90	0.57	11.36	7
4309.04	0.540	0.212		0.493	0.665	10
3005.30	0.217	0.015		0.96	0.21	13
3765.54*	7.94	0.050		0.91	8.67	6

(continued)

TABLE 4 (continued)

λ_n (Å)	M_p	M_B	F_c	ϵ_n	M_c	$\Delta M_c/M_c$ (%)
2986.65	0.262	0.091		0.95	0.180	15
3738.31	6.96	0.39	0.90	0.92	7.93	7
4118.55*	7.22	0.02	0.90	0.665	12.03	7
4203.95	1.69	0.031	0.90	0.58	2.64	7
2656.15	0.364	0.017	0.48	1.39	0.521 ^c	21
3233.05*	2.09	0.06		1.83	1.11	6
2669.49	2.56	0.18	0.49	1.37	3.54 ^d	21
3254.36*	11.43	0.03		1.14	10.00	6
3538.79	0.226	0.091	0.83	1.04	0.156	12

* Specifies the transition used to monitor the population of the upper level.

a) No transition was observed at $\lambda 2411.56$. The corrected photon intensity for this transition was obtained assuming a signal of the size of the background detected.

b) An 8% subtraction has been effected in the corrected photon intensity of $\lambda 4595.36$ to account for partial blending to $\lambda 4595.21$. See page 34.

(continued)

TABLE 4 (continued)

- c) These two transitions were measured with the McPherson monochromator. $\epsilon(\lambda)$ refers to the detection efficiency of this instrument.
- d) The intensity ratio of $\lambda 2669.49$ to $\lambda 3254.36$ was obtained using the McPherson monochromator, and the intensity ratio of $\lambda 3538.79$ to $\lambda 3254.36$ was obtained using the Rowland system. In both cases $\lambda 3254.36$ was used as monitor. The measurements have been scaled so that M_c for $\lambda 3254.36$ is equal to 10.00. The data for $\lambda 3254.36$ shown in the table corresponds to the measurement with the Rowland system.

TABLE 5

Branching ratios and transition probabilities with their respective uncertainties for the transitions studied in this experiment. For more detail refer to pages 38, 41 and 43-44. In the last column the $\log gf$ has been computed from equation 7 on page 13.

TABLE 5

λ Å	R_n (10^2)	$(\Delta R/R)$ (%)	A_n 10^6sec^{-1}	log gf
2411.56	<0.718		<0.520	<-2.30
3475.87	0.565	15	0.409 \pm 25%	-2.09
3496.19	0.0406	35	0.0294 \pm 41%	-3.22
3603.67	0.311	16	0.225 \pm 25%	-.232
3798.18	3.34	9	2.42 \pm 22%	-1.24
4120.21	3.80	9	2.75 \pm 22%	-1.11
4199.10	84.1	1	60.9 \pm 20%	0.25
4487.75	0.0465	14	0.0337 \pm 24%	-2.95
4537.68	0.0684	33	0.0496 \pm 39%	-2.77
4595.36	0.915	9	0.663 \pm 22%	-1.63
5242.50	4.89	9	3.54 \pm 22%	-0.79
5379.58	1.27	9	0.917 \pm 22%	-1.35
3018.13	0.921	14	1.15 \pm 25%	-1.69
3039.32	1.24	15	1.55 \pm 25%	-1.56
3479.68	0.382	12	0.477 \pm 23%	-1.95
3785.71	1.14	15	1.43 \pm 25%	-1.40
3821.18	62.8	3	78.4 \pm 20%	0.35
4219.36	31.7	6	39.6 \pm 21%	0.14
4309.04	1.86	11	2.32 \pm 23%	-1.08

(continued)

TABLE 5 (continued)

λ Å	R_n (10^2)	$(\Delta R/R)$ (%)	A_n 10^6sec^{-1}	log gf
3005.30	2.33	14	2.40 \pm 25%	-1.31
3765.54	97.7	0	100.6 \pm 20%	0.51
2986.65	0.790	16	0.854 \pm 25%	-1.83
3738.31	34.8	6	37.6 \pm 21%	0.01
4118.55	52.8	4	57.1 \pm 20%	0.28
4203.95	11.6	7	12.5 \pm 21%	-0.37
2656.15	31.9	15	28.0 \pm 25%	-0.35
3233.05	68.1	7	59.7 \pm 21%	0.15
2669.49	25.8	16	17.2 \pm 25%	-0.62
3254.36	73.1	6	48.7 \pm 21%	0.00
3538.79	1.14	13	0.759 \pm 24%	-1.73

TABLE 6

Comparison of the transition probabilities from this experiment with values from other measurements. For more details see pages 45-47.

TABLE 6
Fe I transition probabilities

Level (energy)	λ (Å)	Transition probabilities (10^6sec^{-1})			
		This exp.	NBS ^a	Other	Corliss ^e and Tech
$z^1H_5^0$	4199.1	60.9	52.0		236
(48383 cm^{-1})	5242.5	3.54	3.41		14.1
	4120.21	2.75	2.83		14.8
	3789.18	2.42	2.91		14.5
	5379.58	0.917	0.874		3.44
	4595.36	0.663	0.706		3.34
	2411.156	<0.52			8.59
	3475.87	0.409			22.2
	3603.67	0.225			2.85
	4537.68	0.0496			0.367
	4487.68	0.0337			0.441
	3496.19	0.0294			4.91

(continued)

TABLE 6 (continued)

Level (energy)	λ (Å)	Transition probabilities (10^6 sec^{-1})			
		This exp.	NBS ^a	Other	Corliss ^e and Tech
$y^3I_6^o$ (52514 cm^{-1})	3821.18	78.4	62.5		434
	4219.36	39.6	32.2	28.8 (AFCRL ^b)	296
	4309.04	2.32			27.7
	3039.32	1.55	1.37		15.7
	3785.71	1.43			15.0
	3018.13	1.15			13.9
	3479.68	0.477	0.614		6.44
$y^3I_7^o$ (52655 cm^{-1})	3765.54	100.6	88.3	87.1 (Kiel ^c)	641
	3005.3	2.40	3.58		44.0

(continued)

TABLE 6 (continued)

Level (energy)	λ (Å)	Transition probabilities (10^6 sec^{-1})			
		This exp.	NBS ^a	Other	Corliss ^e and Tech
$z^1I_6^o$ (53093 cm^{-1})	4118.55	57.1			437
	3738.31	37.6			441
	4203.95	12.5			54
	2986.65	0.854			13.5
$x^3I_7^o$ (57028 cm^{-1})	3233.05	59.7	51.2	32.4 (Grasdalen ^d)	1140
	2656.15	28.0	18.0		413
$x^3I_6^o$ (57070 cm^{-1})	3254.36	48.7	44.1	28.5 (Grasdalen ^d)	1140
	2669.49	17.2	11.7		268
	3538.79	0.759			19.6

a) J.M. Bridges and W.L. Wiese (1970)

b) G.L. Wares (1970)

c) T. Garz (1969)

d) G.L. Grasdalen et al (1969)

e) C.H. Corliss and J.L. Tech (1968)

TABLE 7

Comparison of the branching ratios obtained in this experiment
with the branching ratios computed from the CT transition probabilities.
For further detail see page 47.

TABLE 7
 Comparison of Branching Ratios
 $A_{ij} / \sum_j A_{ij}$

λ (Å)	$R_{\text{this exp.}}$ (10^2)	R_{CT} (10^2)	$R_{\text{CT}}/R_{\text{this exp.}}$
2411.56	<0.718	2.64	>3.68
3475.87	0.565	6.82	12.1
3496.19	0.0406	1.51	37.2
3603.67	0.311	0.875	2.82
3789.18	3.34	4.45	1.33
4120.21	3.80	4.55	1.20
4199.10	84.0	72.5	0.86
4487.75	0.0465	0.135	2.91
4537.68	0.0684	0.113	1.65
4595.36	0.915	1.03	1.12
5242.50	4.89	4.33	0.89
5379.58	1.27	1.06	0.84
3018.13	0.921	1.72	1.87
3039.32	1.24	1.94	1.56
3479.68	0.382	0.796	2.09
3785.71	1.14	1.85	1.62
3821.18	62.8	53.7	0.86
4219.36	31.7	36.6	1.15
4309.04	1.86	3.43	1.84

TABLE 7 (continued)

λ (Å)	$R_{\text{this exp.}}$ (10^2)	R_{CT} (10^2)	$R_{\text{CT}}/R_{\text{this exp.}}$
3005.30	2.33	6.42	2.76
3765.54	97.7	93.6	0.96
2986.65	0.790	1.43	1.81
3738.31	34.8	46.6	1.34
4118.55	52.8	46.2	0.88
4203.95	11.6	5.71	0.49
2656.15	31.9	26.6	0.83
3233.05	68.1	73.4	1.08
2669.49	25.8	18.8	0.73
3254.36	73.1	79.9	1.09
3538.79	1.14	1.37	1.21

TABLE 8

Data for Curve of Growth *

$\lambda(\text{\AA})$	$\chi_i(\text{ev})$	log gf	$W_\lambda(\text{m\AA})$	$\log \frac{W}{\lambda} + 6$	log Γ
4118.55	3.57	0.28	154	1.57	1.69
4120.21	2.99	-1.11	97	1.37	2.21
4199.10	3.05	0.25	183	1.64	2.15
4487.75	3.24	-2.95	15	0.52	1.98
4537.68	3.27	-2.77	13	0.46	1.95
4595.36	3.30	-1.63	61	1.12	1.93
5242.5	3.63	-0.79	80	1.20	1.61
5379.58	3.69	-1.35	56	1.02	1.56
3233.05	3.24	0.15	93	1.67	2.01
3254.36	3.27	0.00	80	1.52	1.94
3479.68	2.95	-1.95	48	1.14	2.22
3538.79	3.57	-1.73	29	0.91	1.70
3738.31	3.27	0.01	155	1.62	1.97
3765.54	3.24	0.51	174	1.75	1.95
3789.18	2.73	-1.24	110	1.55	2.46
3821.18	3.27	0.35	93	1.69	1.98

* χ_i from Moore (1945); log gf from this work; W_λ from the second revision of Rowland's table by Moore, Minnaert and Houtgast (1969); log Γ from Cayrel and Jugaku (1963). For more details see page 57.

FIGURE 1

Experimental arrangement used in the lifetime measurements. The magnetic analyzer passband is $M/20$, the electrostatic analyzer passband is $\pm E/500$. The lethe bed mounting allows the monochromator to be moved parallel to the beam. The double delay-line amplifier and single-channel analyzer permit fast counting of single photon pulses from the refrigerated photomultiplier tube. To equalize counting periods, the total beam current is integrated. For further details see pag. 151

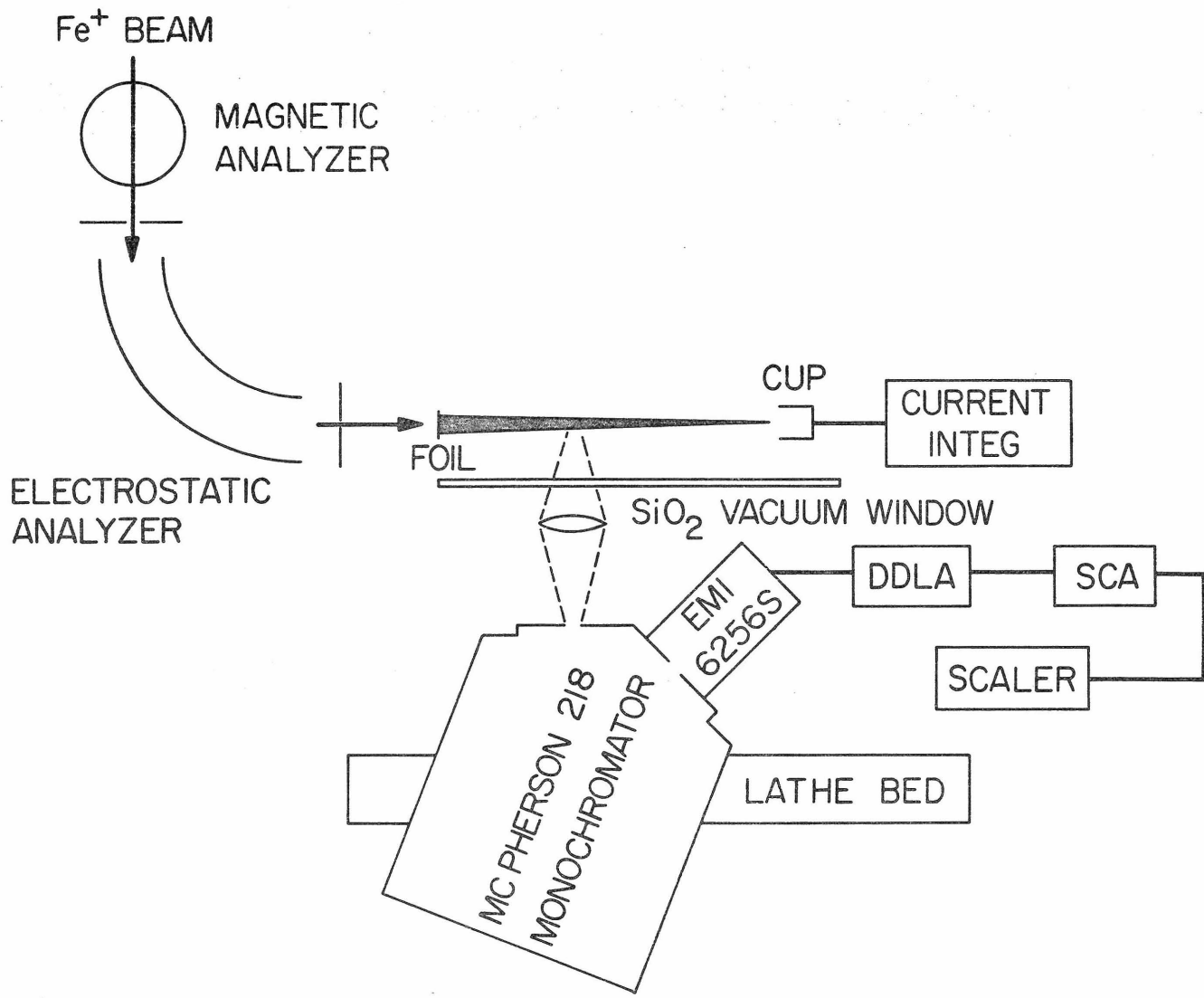
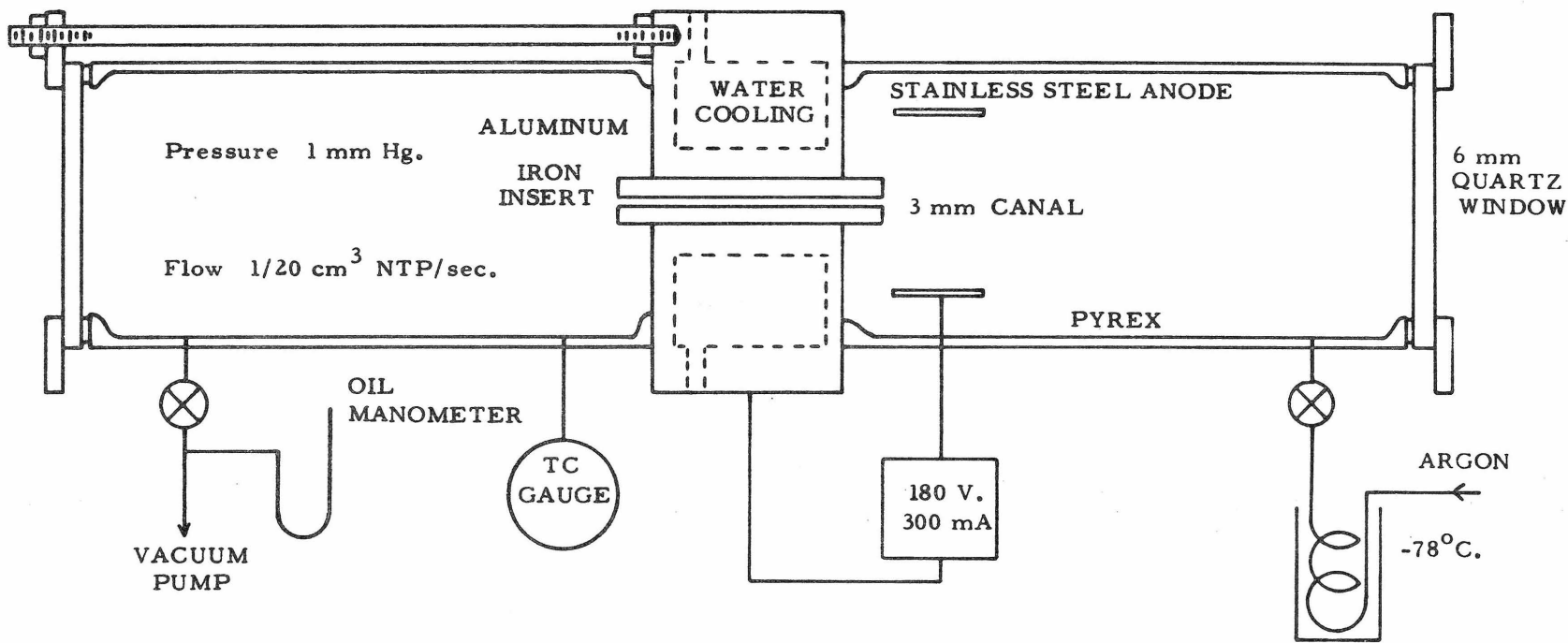


Fig. 1

FIGURE 2

Hollow-cathode source used to excite the levels of Fe I. For details
see page 21.



-110-

Fig. 2

FIGURE 3

Arrangement of source and spectrometers used in the measurement of the branches. An image of the hollow-cathode source is made at the entrance slit of a 6.65 m Rowland spectrometer. The quartz plate in the light path sends a fraction of the light into a McPherson monochromator which records the intensity of a line and hence monitors the population of the upper level. The McPherson instrument has been stopped to match the aperture of the 6.65 m spectrometer. For further details see page 23.

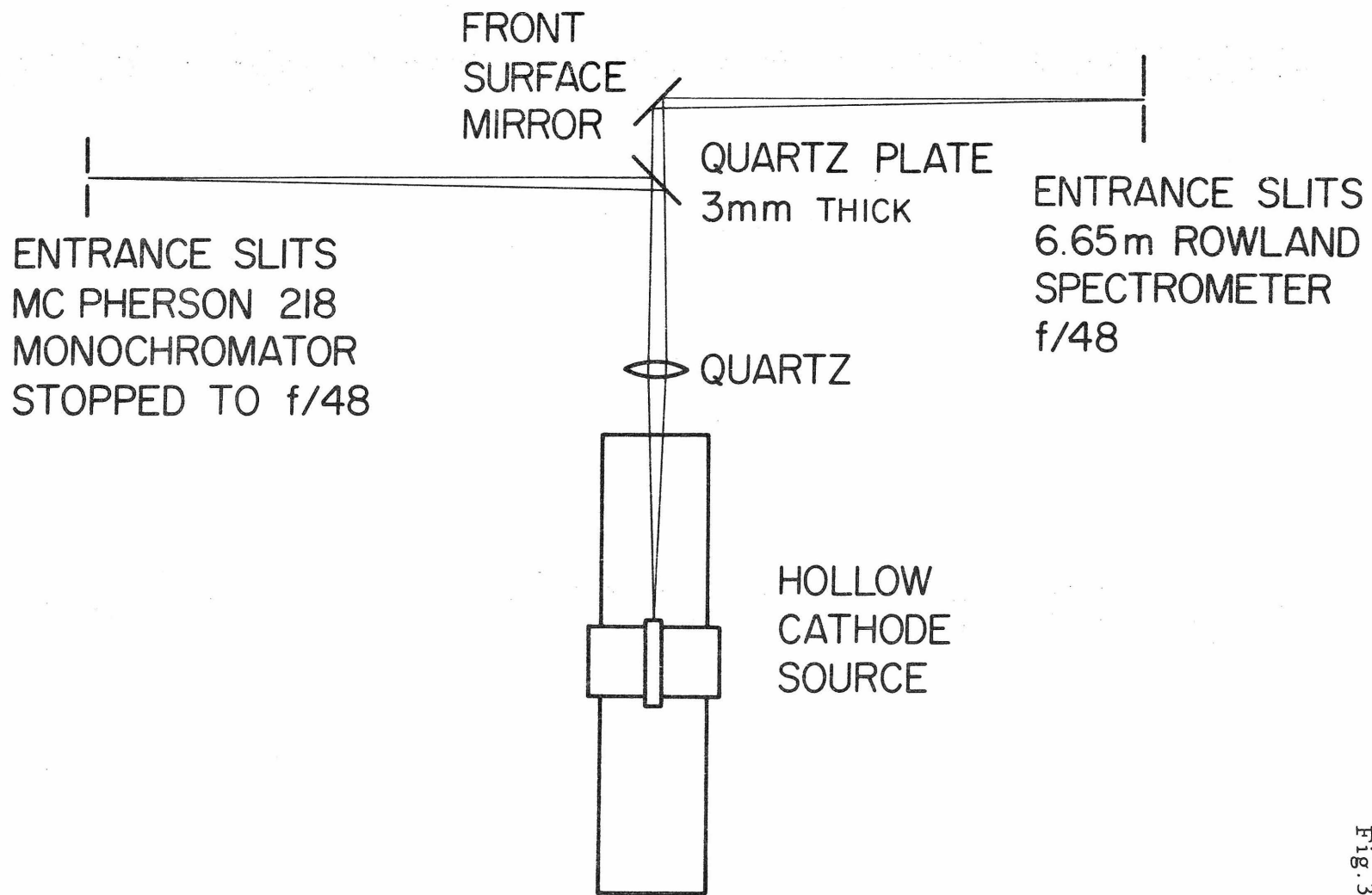


Fig. 3

FIGURE 4

Block diagram of the electronic circuitry used in the branching ratio measurements. The commercially available instruments symbolized by the boxes are:

For the monitor:

- 1) Dry ice refrigerated EMI 6256S PMT.
- 2) Fluke model 402M power supply (1200V).
- 3) Charge sensitive preamplifier: Tennenlac #438.
- 4) Preamp. power supply: Tennenlac model 901RM.
- 5) Double delay-line amplifier and single-channel analyzer: Hamner #388.
- 6) Scaler: Ortec model 430.

For the Rowland detector:

- 1) Dry ice refrigerated EMI 9526B PMT.
- 2) Fluke model 412B power supply (1100V).
- 3) Solid state preamplifier-discriminator described by Mickey et al (1970).
- 4) Preamp. power supply (12V).
- 5) Count. Rate meter: Mechtronics Nuclear #775.
- 6) Chart recorder: Moseley
- 7) Scaler: Ortec model 430.

Both scalers were gated by an Ortec model 431 timer/scaler. For more details see pages 25-26.

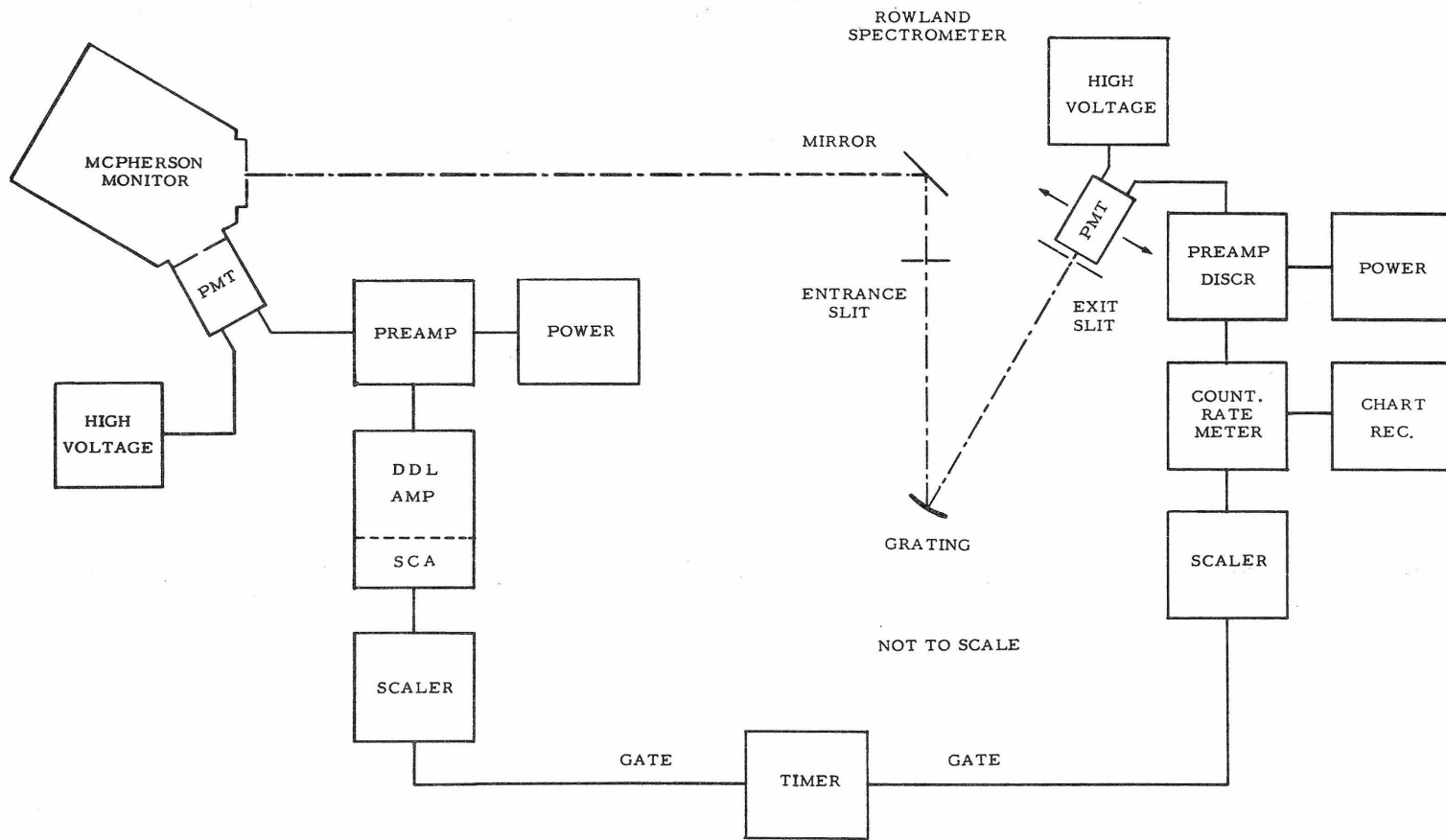


Fig. 4

FIGURE 5

Spectrum obtained for the region of $\lambda 2411.56$. Ar at 0.5 mm Hg pressure was used as the carrier gas. The discharge current was 400 ma. The spectrometer was used in second order, with the Corning 7-54 filter in to eliminate contributions from first order. The labelled transitions are Fe I unless otherwise specified. For the line identification procedure refer to page 27. For more detail concerning this figure refer to page 29 or 48.

Fig. 5

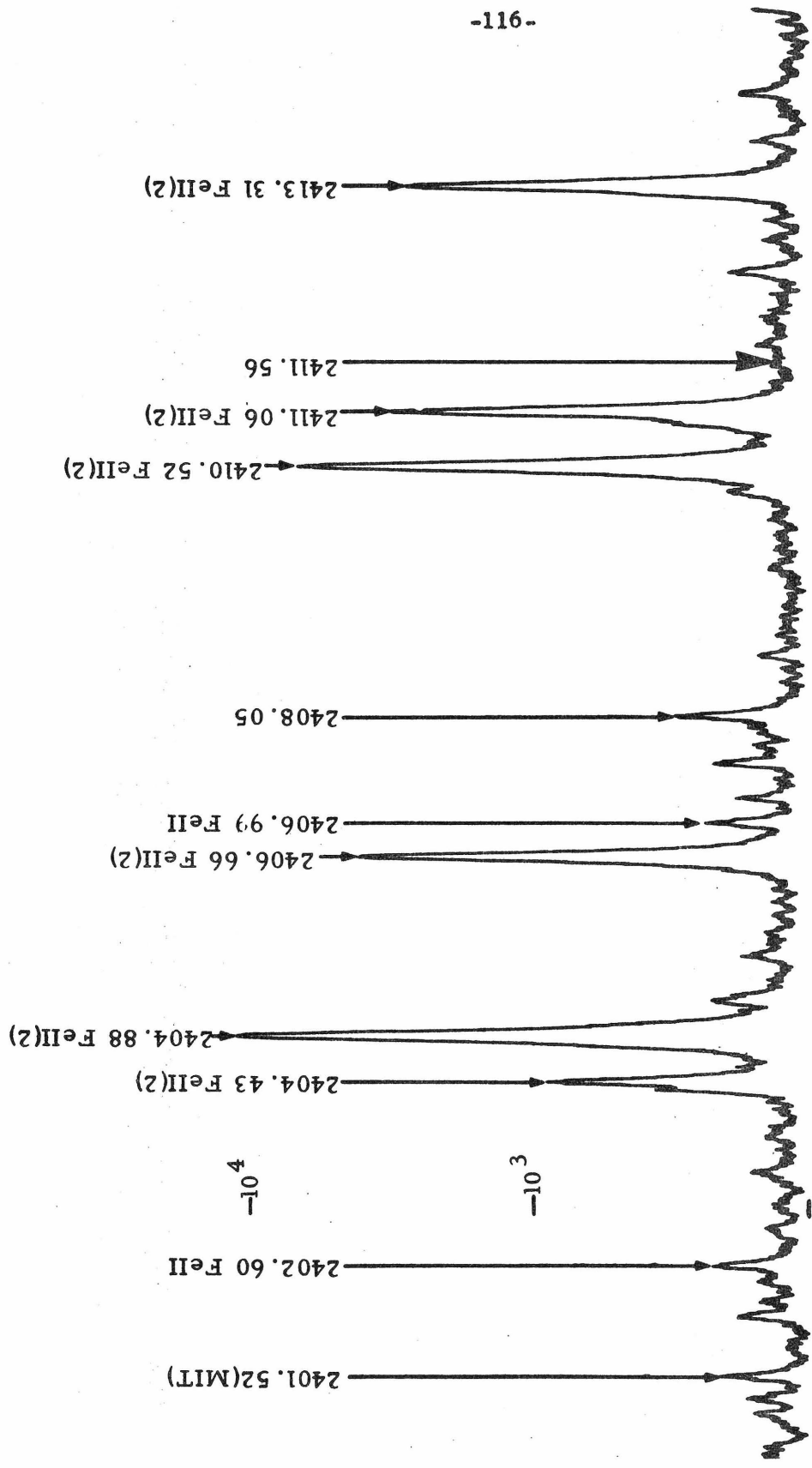


FIGURE 6

Spectrum obtained for the region of $\lambda 4219.36$. He at 2 mm Hg pressure was used as the carrier gas. The discharge current was 300 ma. The labelled transitions belong to FeI unless otherwise specified. For the line identification procedure refer to page 27. For more detail concerning this figure refer to page 32.

Fig. 6

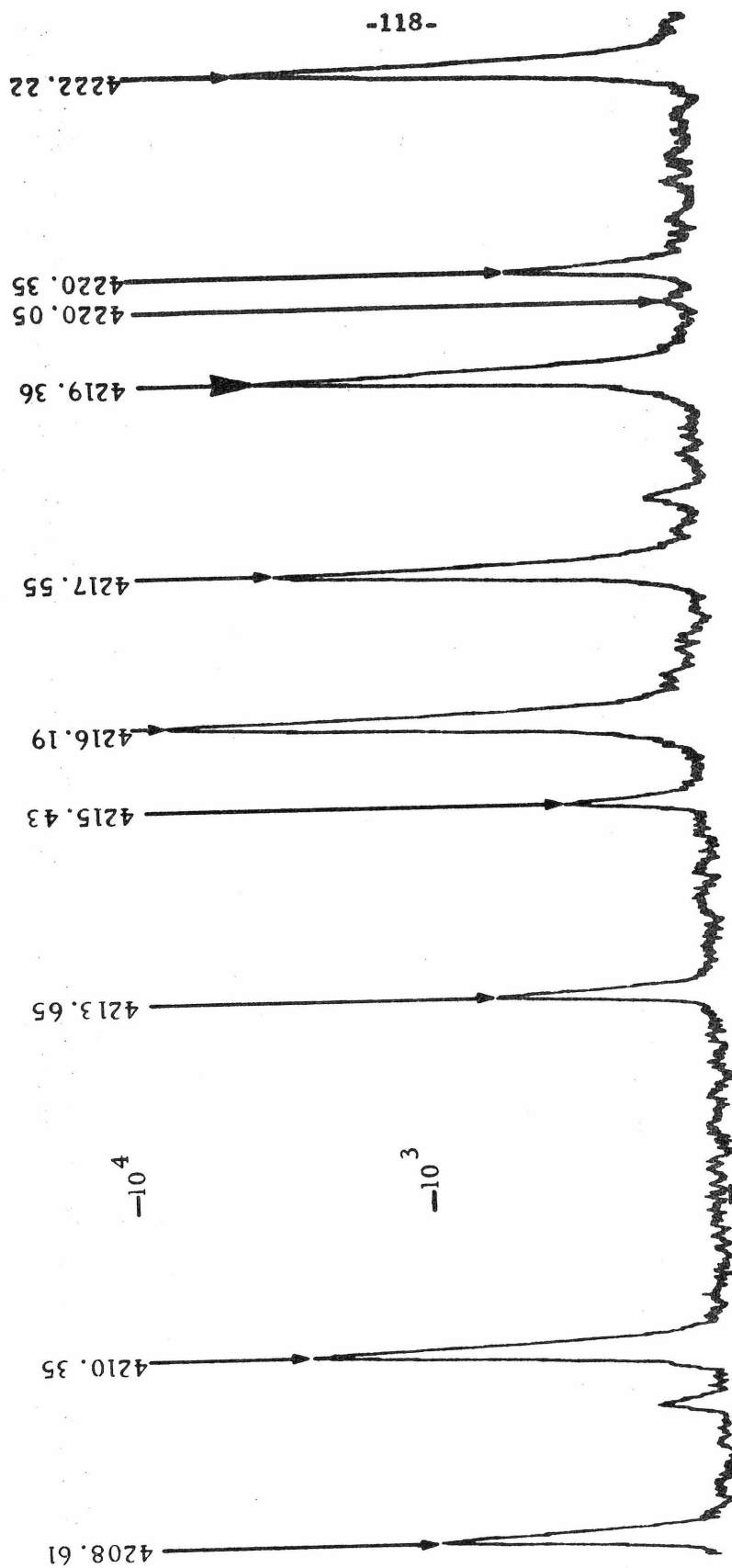


FIGURE 7

Part A of this figure depicts a diagram of level $\gamma^3 I_7^0$ at 52655 cm^{-1} with its two decay modes. Part B shows the spectrum of the two transitions. Each spectrum was obtained with different conditions in the discharge and different entrance slit widths in the spectrometer. This figure is used in part 6.2-C (page 33) to explain the experimental procedure.

Fig.7

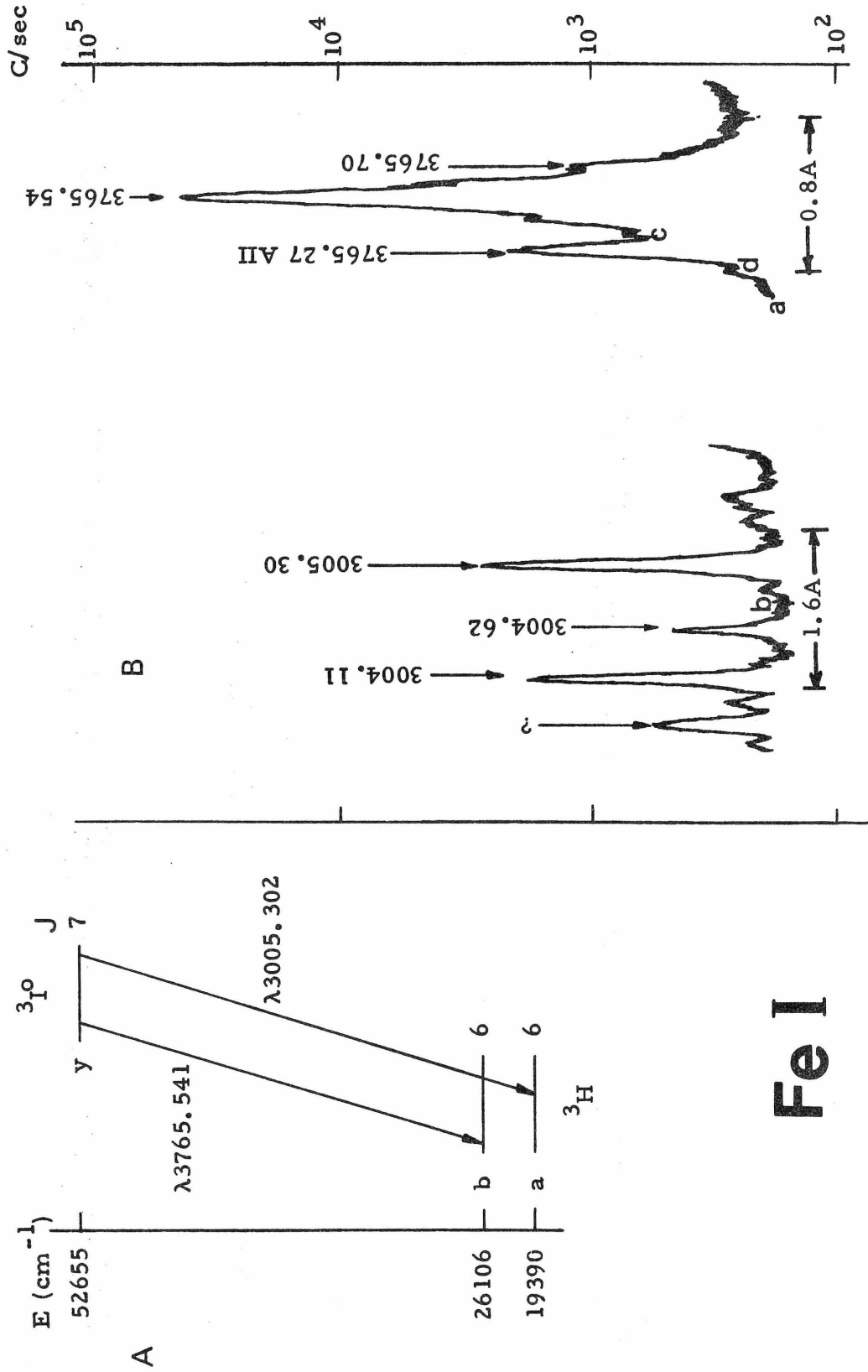


FIGURE 8

The log of the ratio of the transition probabilities obtained by Bridges and Wiese (1970) to the transition probabilities obtained in this experiment for overlapping lines, is plotted against the wavelength of the lines. For further details see page 47.

Fig.8

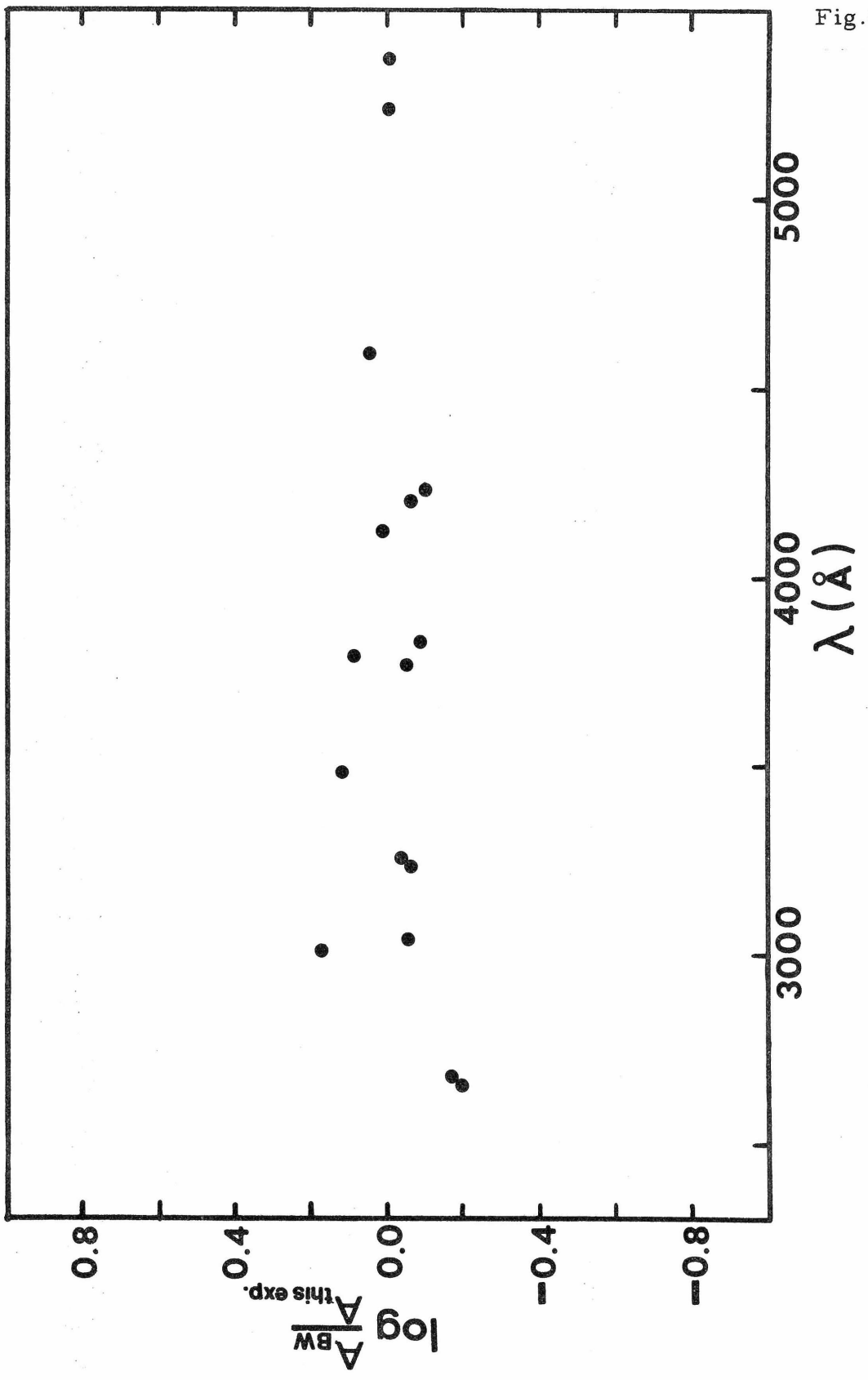


FIGURE 9

A) Spectrum obtained for the region of $\lambda 3496.19$. Ar at 0.5 mm Hg pressure was used as the carrier gas. The discharge current was 300 ma. The labelled transitions are from FeI unless otherwise specified. For more details see page 48.

B) Section of FeI spectrum published by Crosswhite (1958). The position of the transitions $\lambda 3475.87$ and 3496.19 and of the scale at $\lambda 3495-98$ has been obtained by interpolating the transitions labelled near the regions of interest. For discussion of this spectrum see page 48.

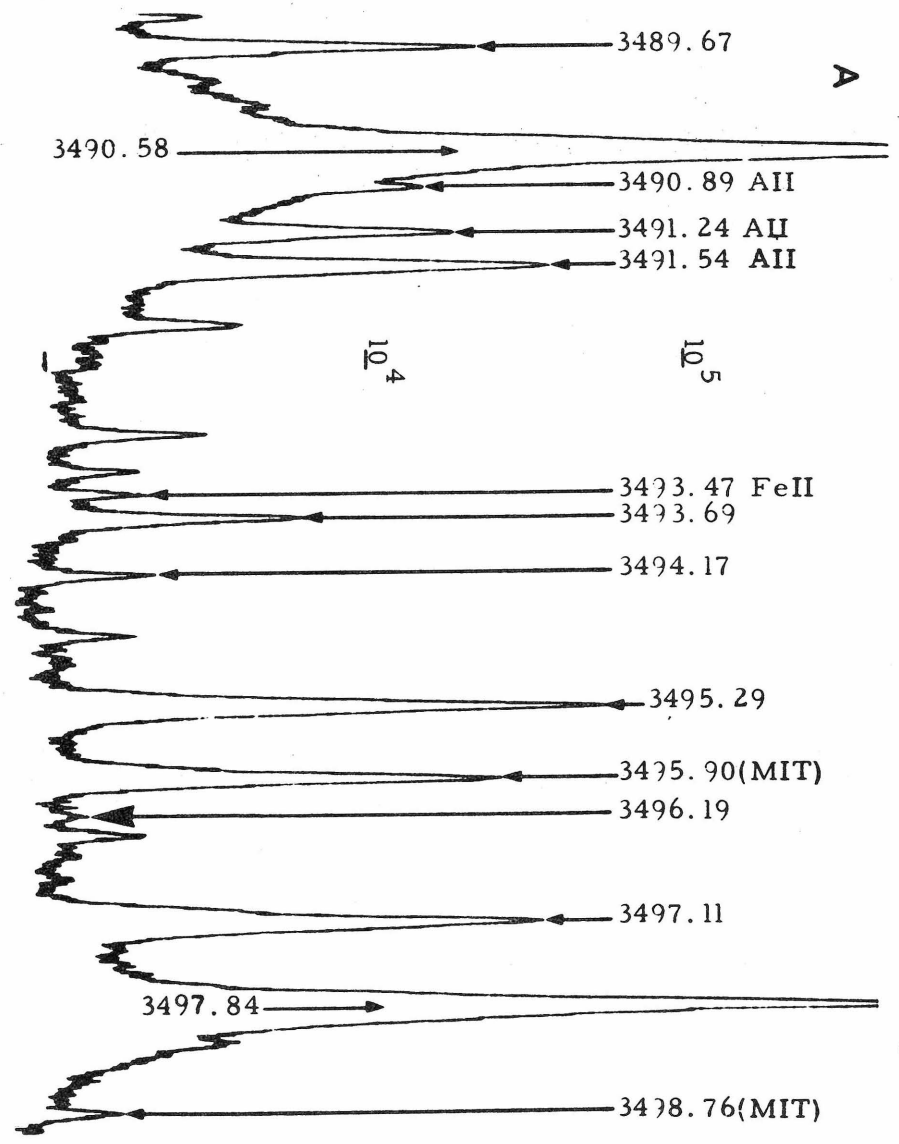
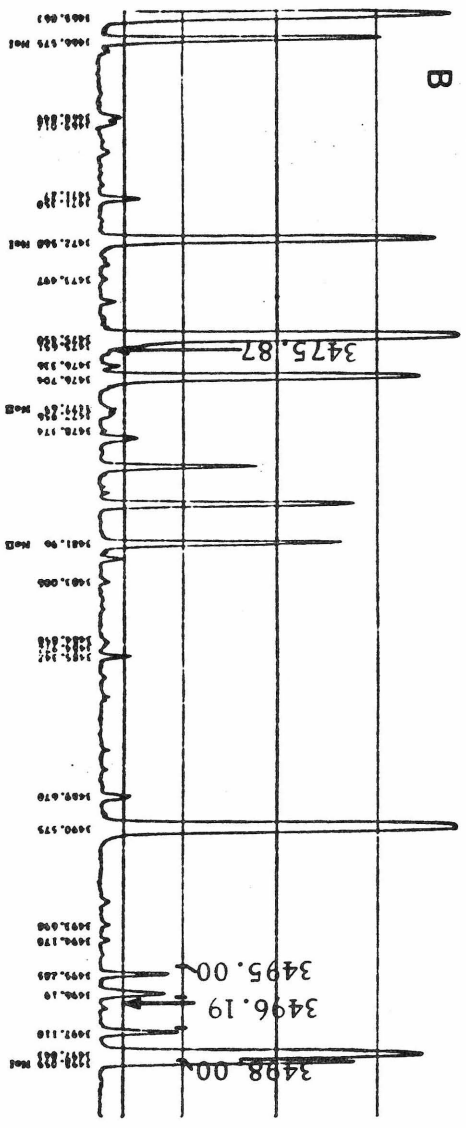


Fig. 9

FIGURE 10

Spectrum obtained for the region of $\lambda 3475.87$. Ar at 0.5 mm Hg pressure was used as the carrier gas. The discharge current was 300 ma. The labelled transitions belong to FeI unless otherwise specified. For the line identification procedure refer to page 27. For further detail concerning this figure see page 48.

Fig. 10

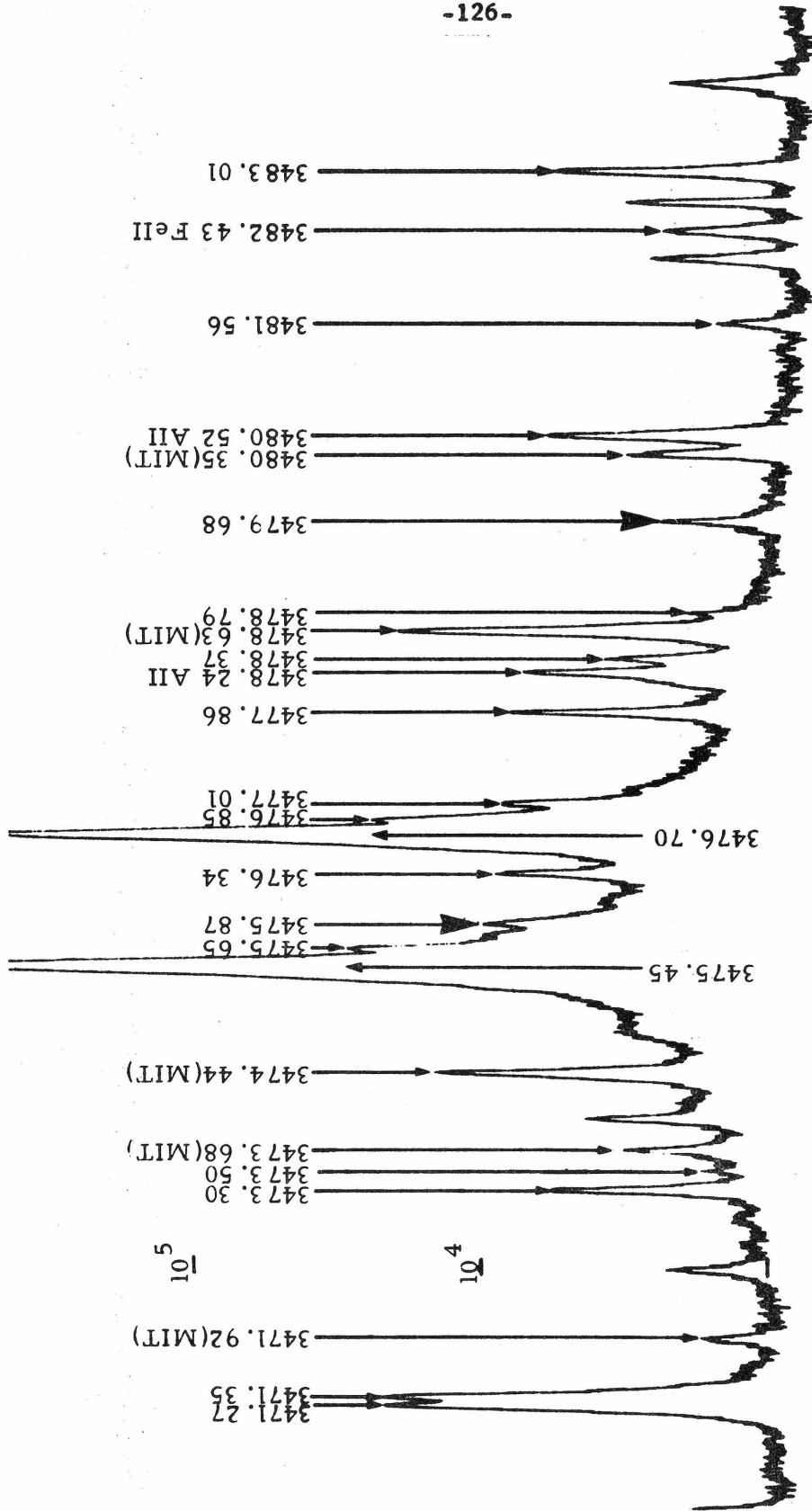


FIGURE 11

Ratio of the Corliss and Tech (CT) branching ratios to the branching ratios obtained in this experiment, plotted against the wavelength of the transitions. For further detail refer to page 49.

Fig.11

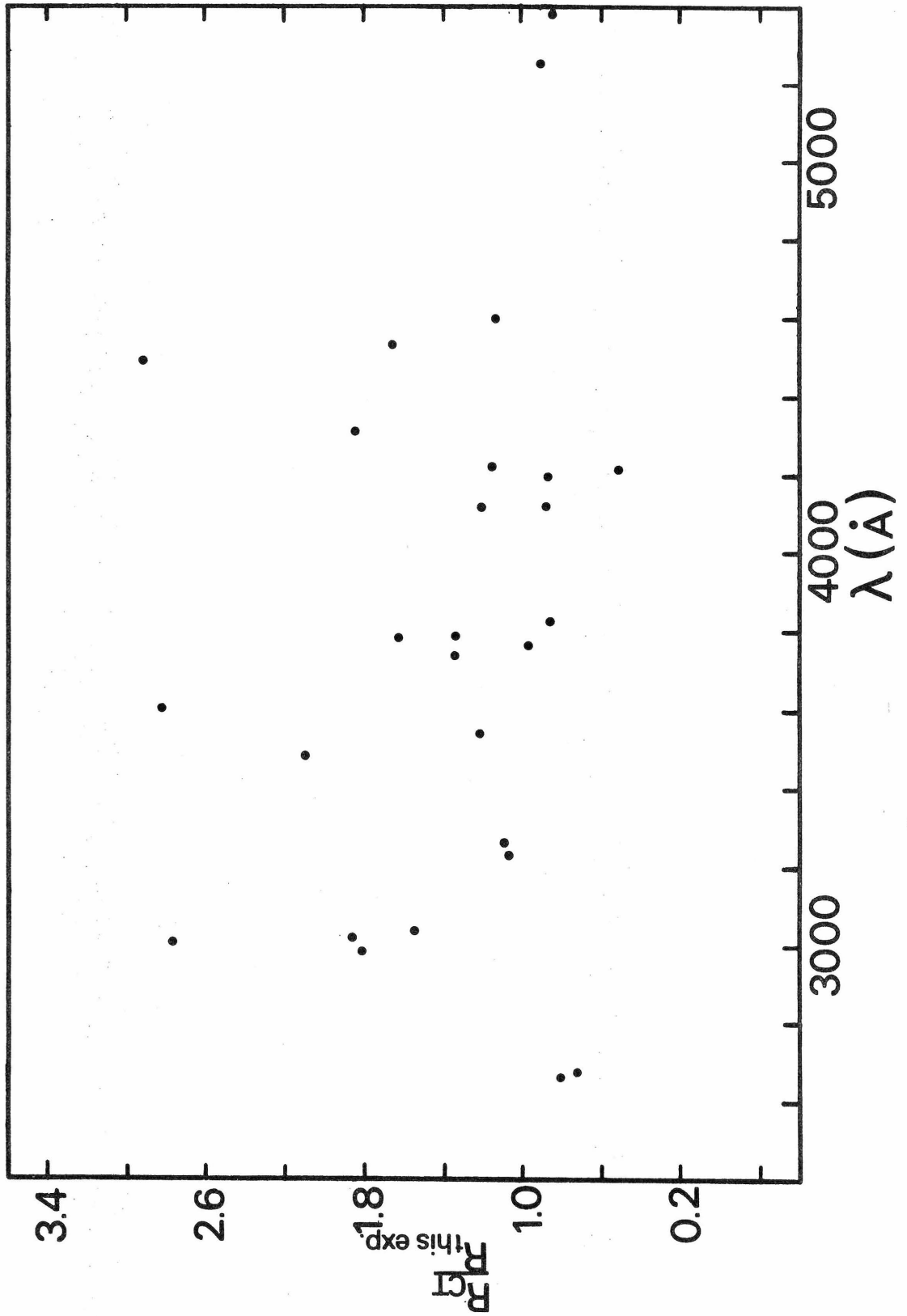


FIGURE 12

Ratio of the CT branching ratios to the branching ratios obtained
in this experiment plotted against the branching ratios from this experiment.
For further detail see page 49.

Fig. 12

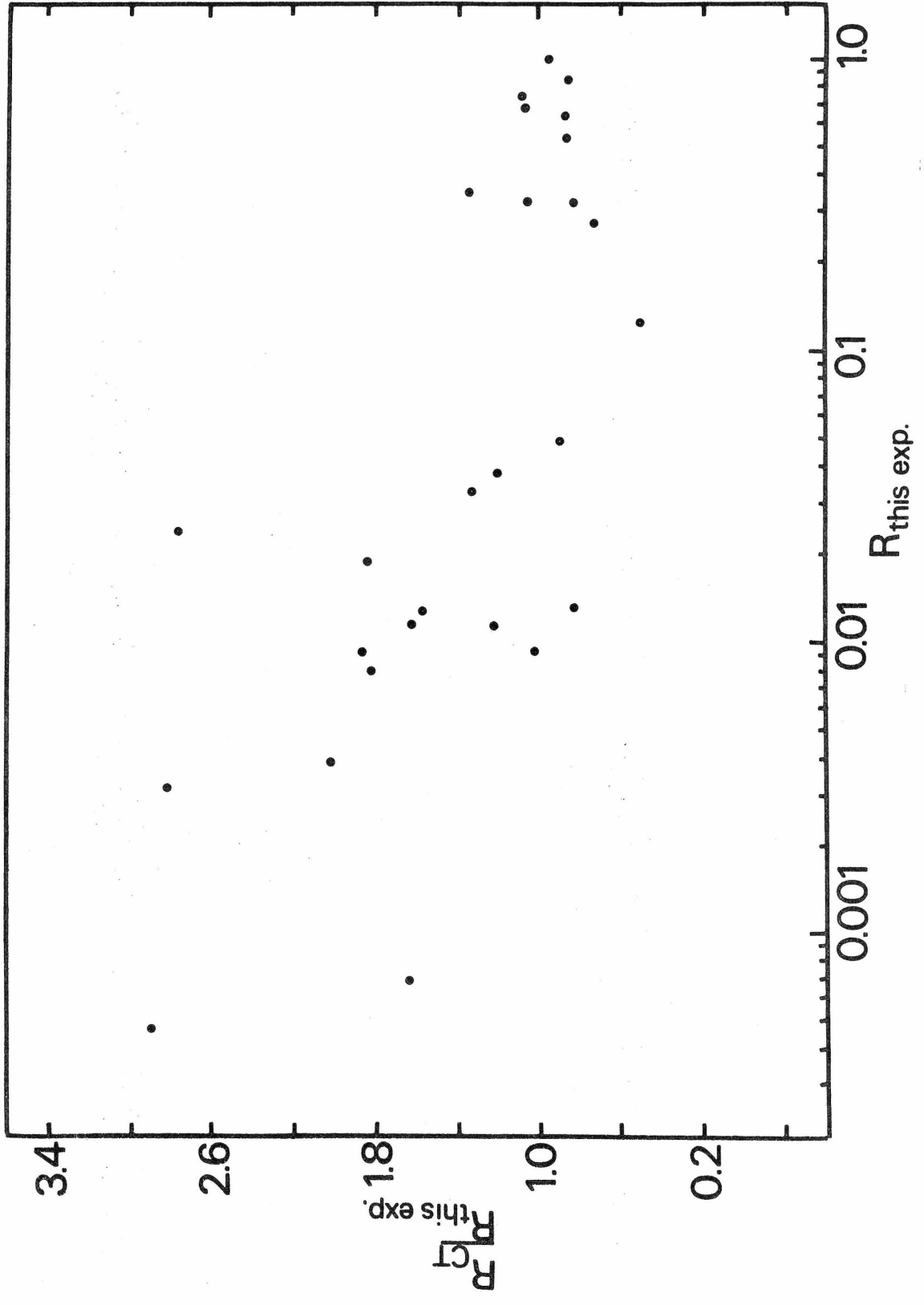


FIGURE 13

The log of the ratio of the CT transition probabilities to the transition probabilities obtained in this experiment is plotted against the wavelength of the transitions. For a detailed discussion of this figure, refer to page 49.

Fig.13

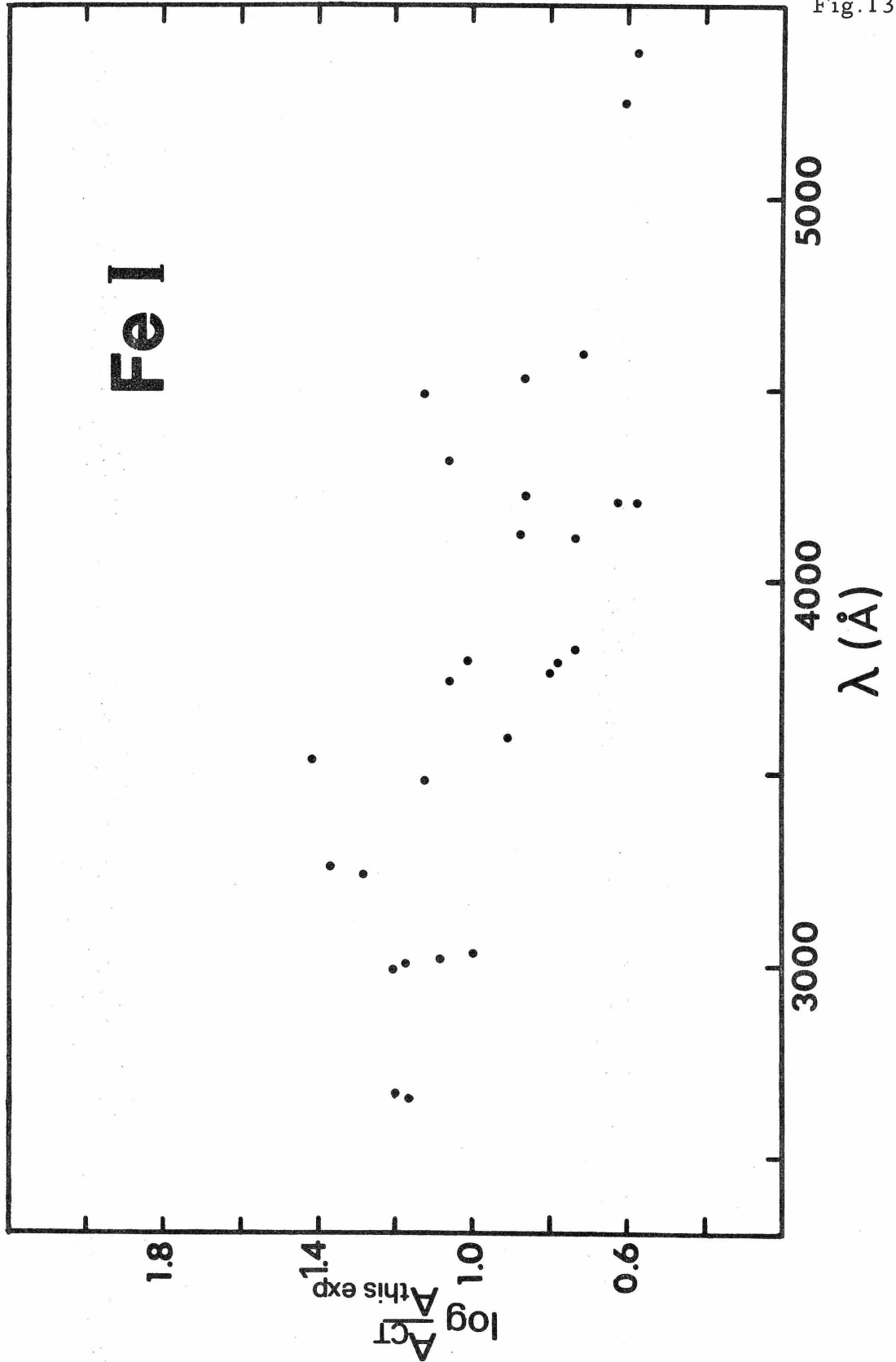


FIGURE 14

The log of the ratio of the transition probabilities listed by CT to the values obtained by Garz and Kock (1969), Bridges and Wiese (1970) and in the present experiment, have been plotted as a function of the energy of the upper level. The meaning of this plot and of the lines drawn on it is given on pages 51-55.

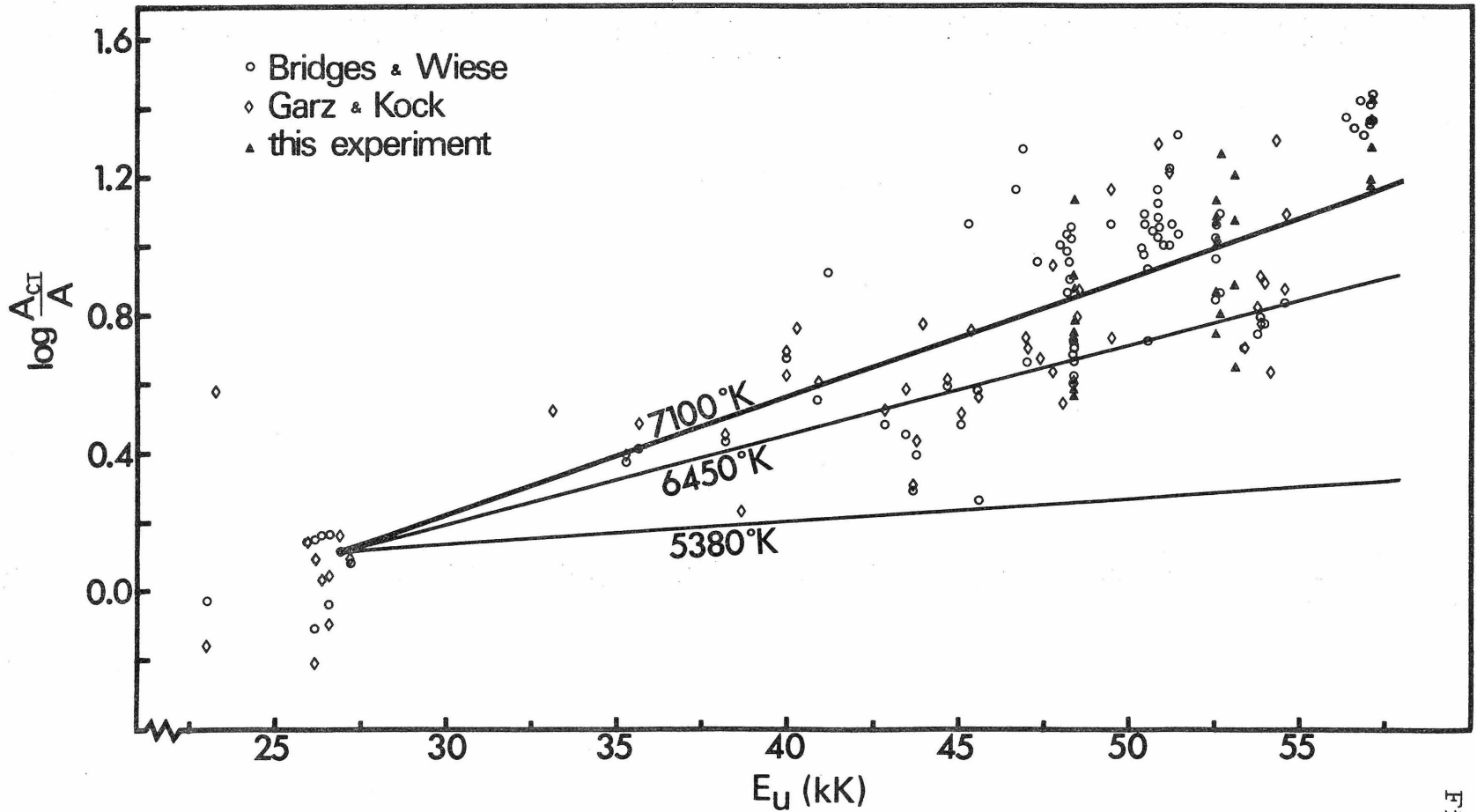


Fig. 14

FIGURE 15

A curve of growth for the center of the solar disk. The experimental curve has been obtained using the data on table 8 and the model of Cayrel and Jugaku (1963). The curve fitted through the points is a theoretical curve calculated by Hunger (1956) for pure absorption using the Milne-Eddington model. Note that the fit depends strongly in the two weakest points. From the curve one obtains an iron abundance $\log \frac{N_{Fe}}{N_H} + 12.0 = 7.40$. For more detail see page 59.

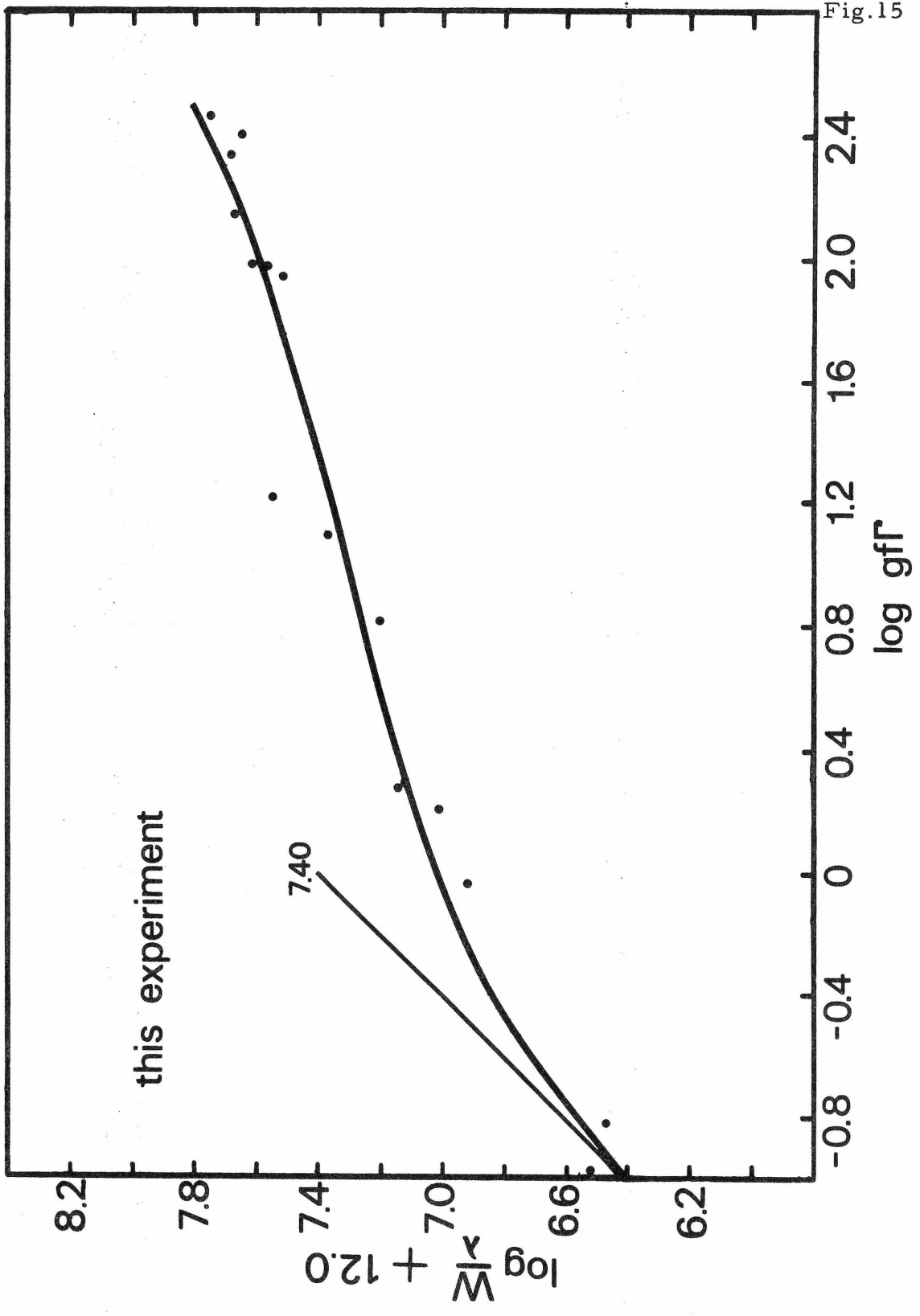


Fig.15

FIGURE 16

A curve of growth for the center of the solar disk. The experimental curve was obtained using the data in table 1 of the Garz et al (1969b) paper. All other details are the same as on figure 15. From the fit an iron abundance $\log \frac{N_{\text{Fe}}}{N_{\text{H}}} + 12.0 = 7.60$. For more details see page 59.

Fig.16

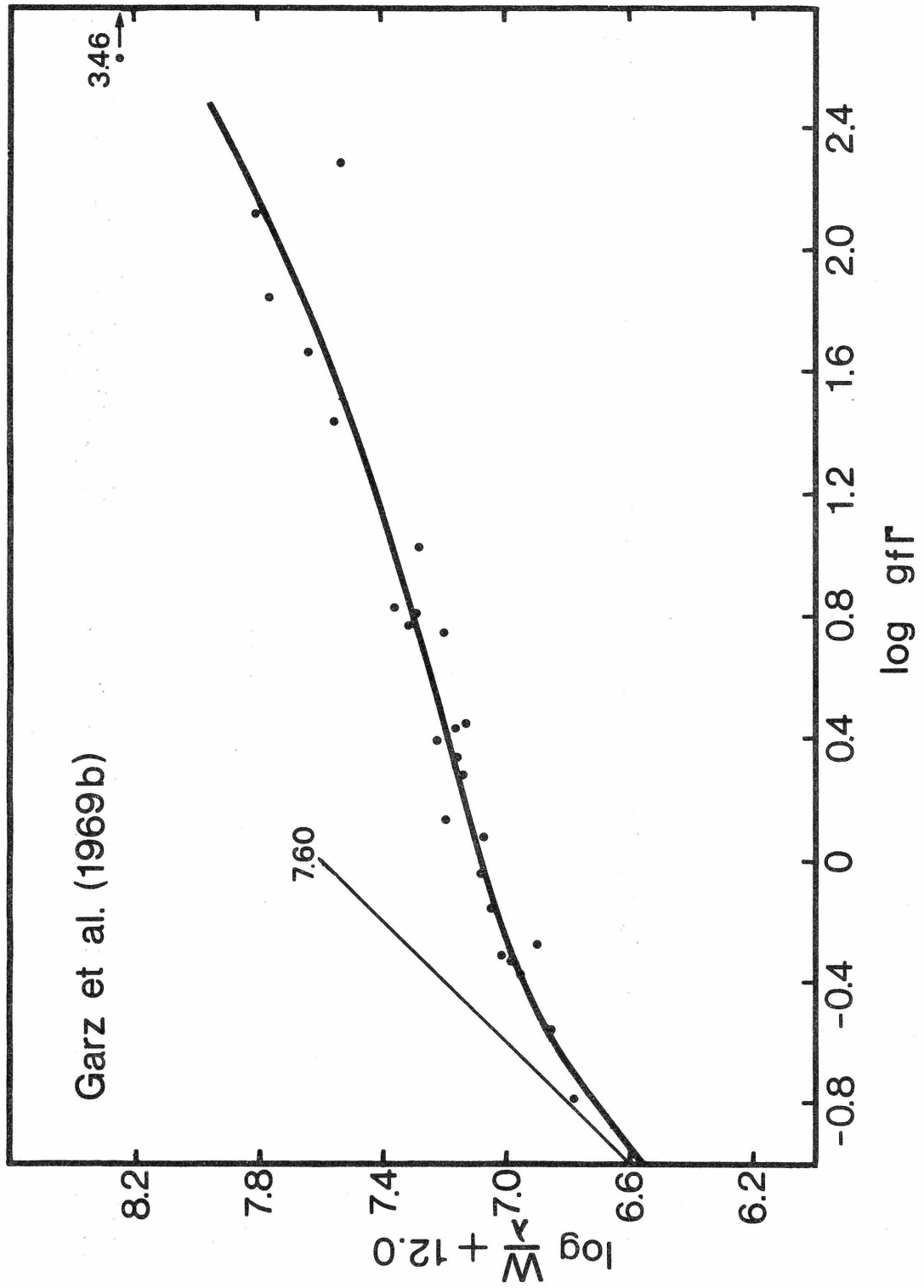


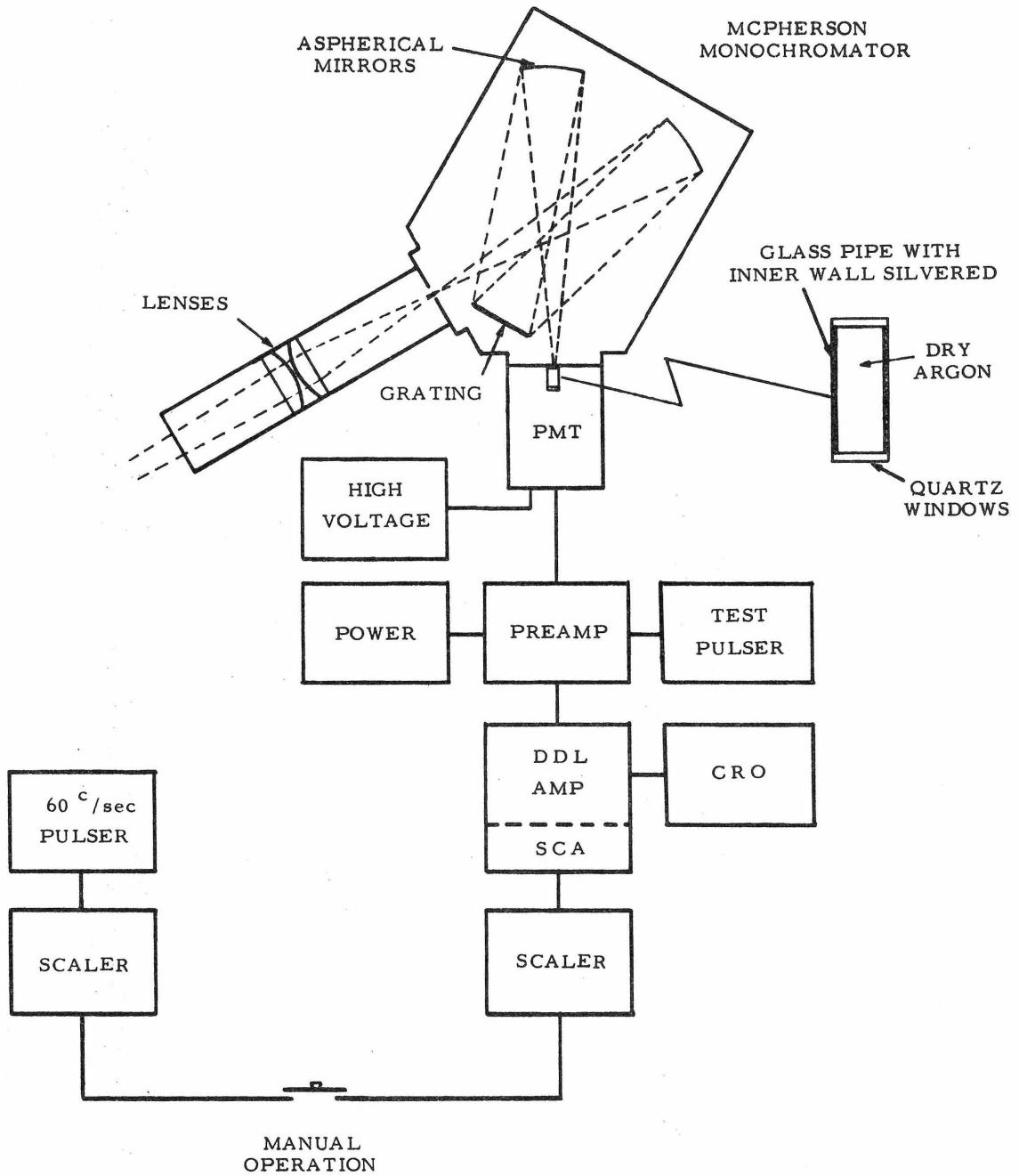
FIGURE 17

The McPherson system consisted of a 0.3 m, $f/5.3$ Czerny-Turner McPherson monochromator and two achromatic LiF-SiO₂ lenses 4.8 cm diameter and 9.0 ± 0.3 cm combined focal length. Photons at the exit slit travel through a light pipe to the photocathode of an EMI 6256S PMT cooled with dry ice. The light pipe was designed to avoid condensation on the cooled windows. The commercially available instruments symbolized by the boxes are:

- 1) Fluke model 412B power supply (1000V).
- 2) Charge sensitive preamplifier: Tennenlac 100C.
- 3) Preamp. power supply: Tennenlac 900.
- 4) Double delay-line amplifier and single-channel analyzer: Hamner #388.
- 5) Scaler: RIDL model 49-28 (6 electronic decades).

As a clock a scaler counting $60^c/\text{sec.}$ was used. Clock and photon scalers were turned on and off manually. For more details see pages 62-63.

Fig.17



MCPHERSON SYSTEM

FIGURE 18

Experimental arrangement for the calibration of the McPherson system
in the region $\lambda > 2900\text{\AA}$. For more details see page 64.

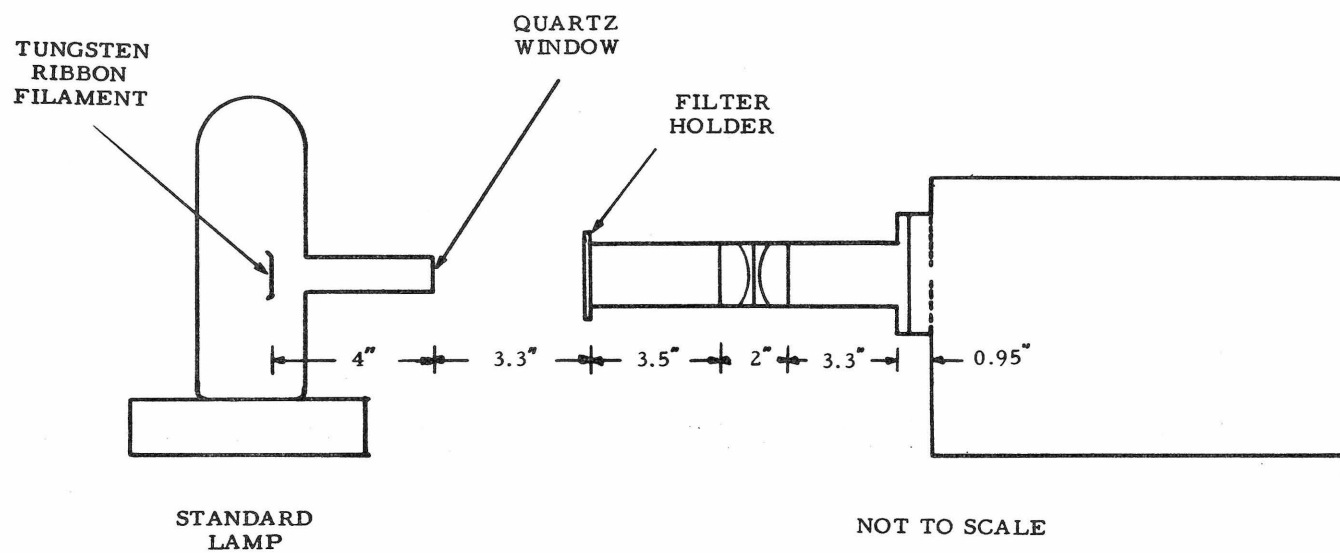


Fig. 18

FIGURE 19

The reciprocal linear dispersion has been calculated for the McPherson model 213 monochromator. The curve applies for the 1200 ¹/mm grating in first order. Experimentally $\beta - \alpha = 28^{\circ}52'$. The curve was obtained by solving:

$$\lambda n = d(\sin \alpha + \sin \beta) \quad \text{and}$$

$$\frac{d\lambda}{dx} = \frac{d}{nf} \cos \beta$$

For more details see page 66.

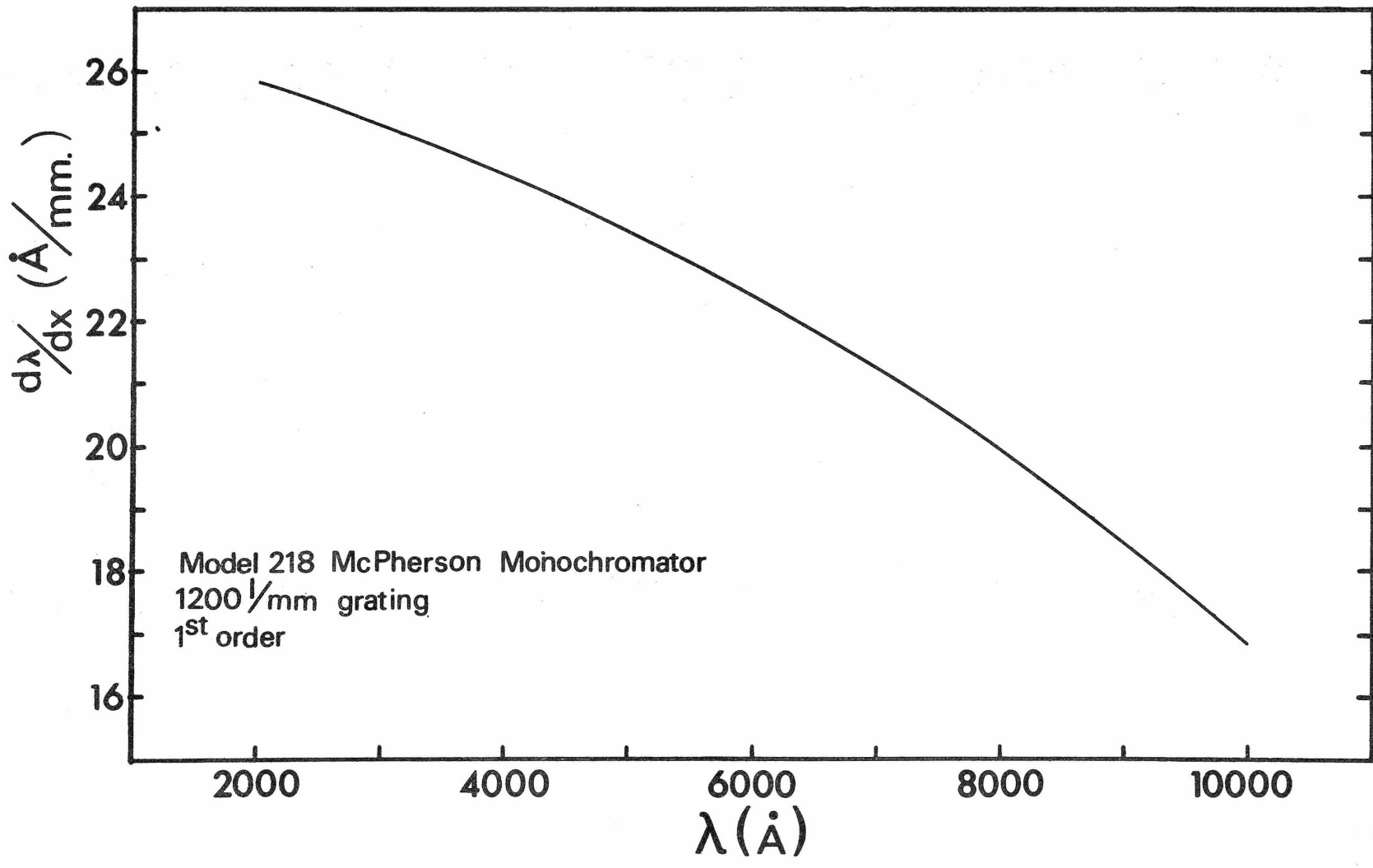


Fig. 19

FIGURE 20

Relative detection efficiency of the McPherson system as a function of wavelength. The region above 2800Å was obtained using the tungsten ribbon standard lamp (figure 18). The region below 3000Å was obtained using a Xe lamp plus a dispersor as a source (figure 21). The two sections were matched in the overlapping region. For details about the calibration see part 10.2. The conclusions are on page 77.

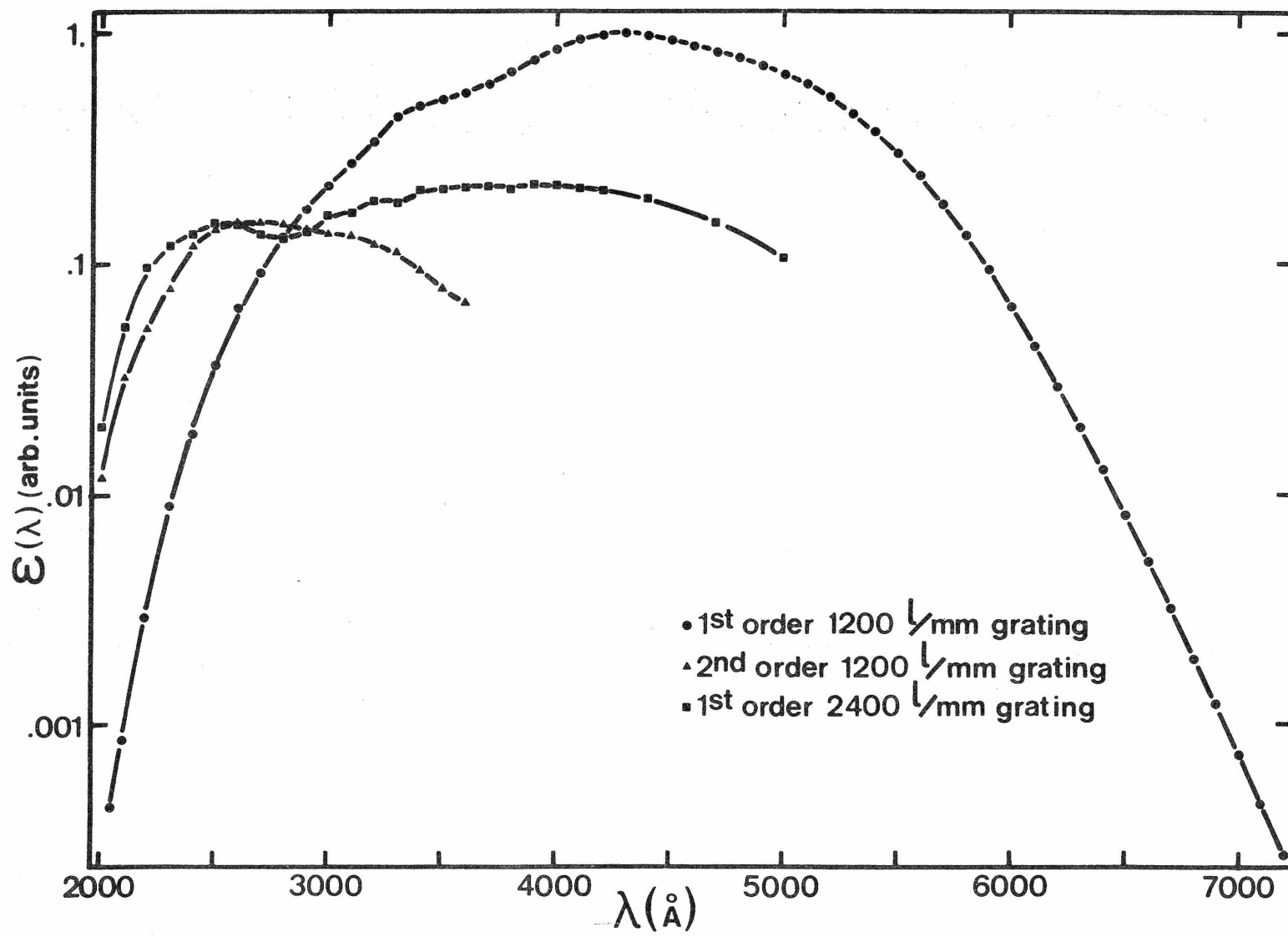


Fig. 20

FIGURE 21

Experimental arrangement for the calibration of the McPherson system in the middle ultraviolet. The combination of Xe arc, source monochromator and the lens between them is referred in the text, page 73, as XeMS.

The intermediate detector consisted of a GE 8575 PMT with a sodium salicylate coated blue filter in front of its photocathode. A negative potential of 2000V was applied to the phototube and its negative current output was fed into an Elcor Integrator model A308C. See pages 72-76 for more details.

Fig.21

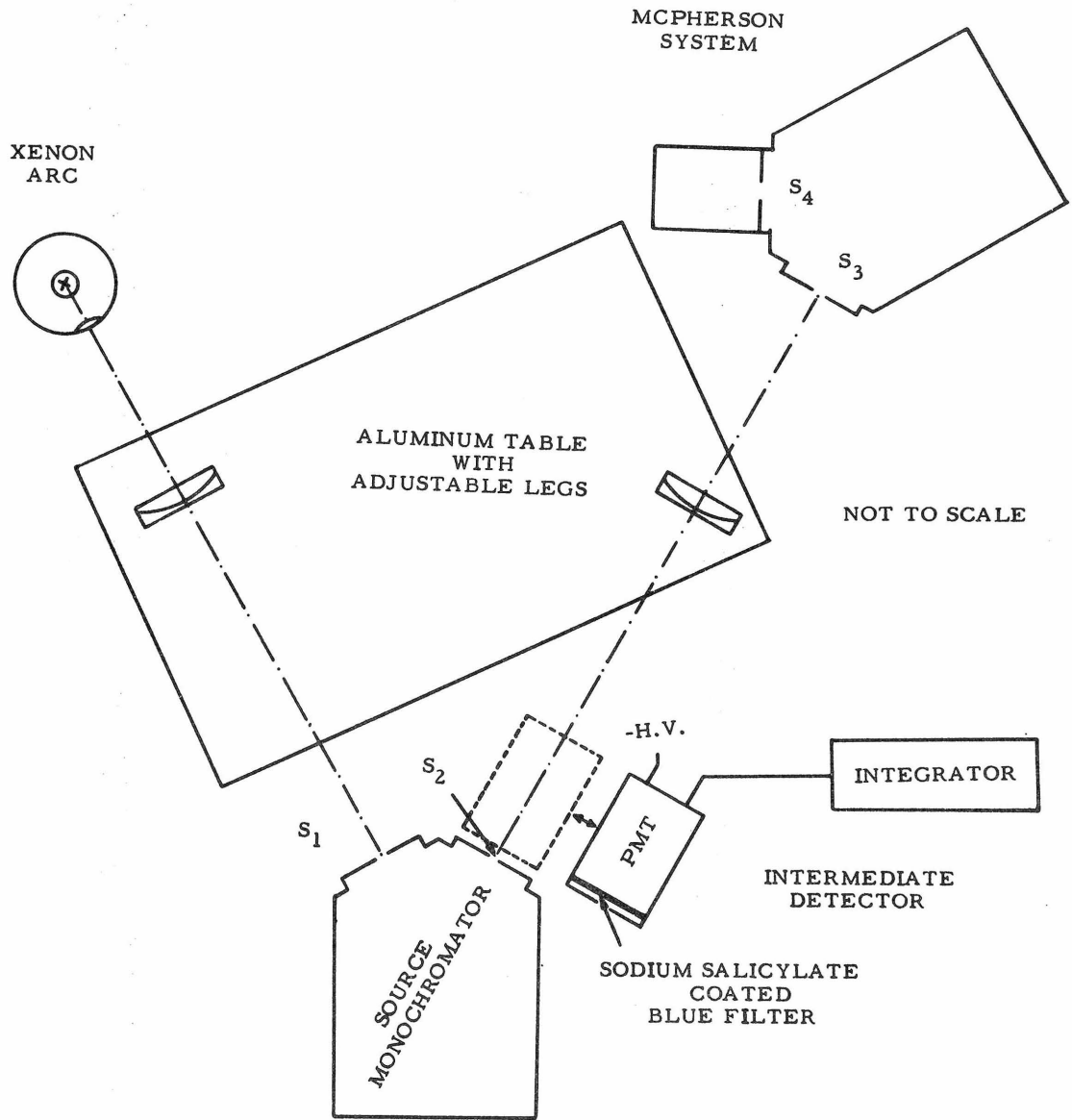
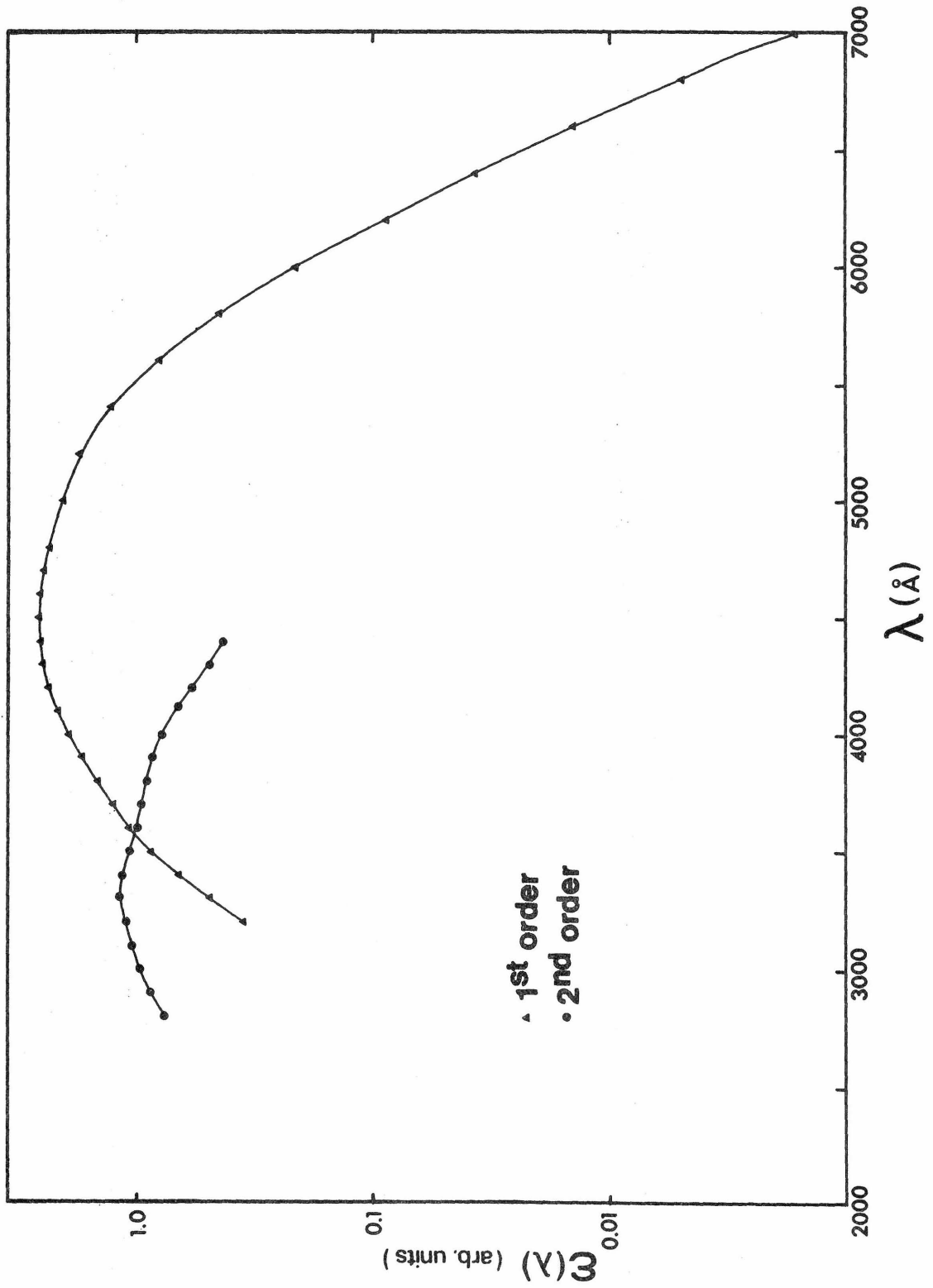


FIGURE 22

Relative detection efficiency of the Rowland system as a function of wavelength. The tungsten ribbon standard lamp was used as the source. For more detail about the calibration procedure and the efficiency curve refer to pages 78-80.

Fig.22



11.

THE ASTROPHYSICAL JOURNAL, Vol. 158, October 1969

© 1969. The University of Chicago. All rights reserved. Printed in U.S.A.

LIFETIMES OF SOME Fe I STATES BY BEAM-FOIL SPECTROSCOPY*

WARD WHALING, ROBERT B. KING, AND MARIO MARTINEZ-GARCIA†

California Institute of Technology

Received 1969 February 13

ABSTRACT

The light emitted by 500-keV Fe atoms excited by passage through a thin carbon foil has been analyzed spectroscopically to identify fifty known transitions in Fe I. The light decay downstream from the foil has been measured to find the lifetime of six levels in Fe I between 48 and 57 kK. Our lifetimes are longer than those computed by summing the transition probabilities of Corliss and Tech by a factor that increases from 4.5 at 48 kK to 21 at 57 kK. The dependence of this factor on excitation energy raises doubt about the level population assumed by Corliss and Tech in interpreting the relative line intensities from the arc source.

I. INTRODUCTION

The lifetime of an atomic energy level is equal to the reciprocal of the sum of the transition probabilities of all transitions from the excited level to lower levels. Therefore, if the relative values of these transition probabilities are known, measurement of the lifetime of the excited level determines the absolute scale of the transition probabilities. Unlike other methods of measuring absolute transition probabilities, the lifetime method does not require a determination of the absolute concentration of absorbing or emitting atoms, the greatest source of uncertainty and systematic error in other methods of measurement.

Beam-foil spectroscopy, developed by Bashkin (1964), permits direct measurement of the lifetimes of highly excited states of neutral atoms and ions. This paper describes measurements of the lifetimes of several states in Fe I, and discusses the corrections these measurements imply for the published tables of absolute transition probabilities (or *gf*-values) for Fe I lines.

II. EXPERIMENTAL METHOD

Fe⁺ ions were produced in a thermal source (Magnuson *et al.* 1965) mounted in the high-voltage terminal of an electrostatic accelerator. The ion beam was deflected electrostatically through 80° to measure and control the ion energy. The electrostatic analyzer, calibrated against the ¹⁸F(*p,αγ*)¹⁸O resonance at 340.45 keV, fixed the incident beam energy in the experiment at 505 ± 1 keV.

The beam then passed through a defining aperture 1 mm × 3 mm and into a self-supporting carbon foil of nominal thickness 10 ± 4 μg cm⁻². This foil thickness is that quoted by the supplier; our own measurements of the energy of the ions emerging from the foil, again by electrostatic deflection, are consistent with the energy loss in a foil of 10 ± 2 μg cm⁻².

The Fe beam emerging from the foil was composed of 12 percent neutral Fe I (Smith and Whaling 1968). A higher percentage of Fe I could be produced at a lower beam energy, but our accelerator operates more stably at higher energies, and the choice of 505 keV was a compromise. After emerging from the foil, the beam traveled 30 cm in a vacuum of ≤ 5 × 10⁻⁶ torr and then entered a shielded Faraday cup and current integrator

* Supported in part by the National Science Foundation [GP-9114] and the Office of Naval Research [Nonr-220(47), Nonr-220(49)].

† Fellow of Instituto Nacional de la Investigación Científica.

which measured the total charge carried by the beam. We assume that this integrated current is proportional to the number of neutral iron atoms in the beam since the fractions in various charge states should be constant if the incident beam energy is held constant and the foil thickness varies only over $\pm 4 \mu\text{g cm}^{-2}$, corresponding to $\pm 16 \text{ keV}$ in the degraded beam energy of 467 keV. The energy loss in the foil is computed from Lindhard's $k\epsilon^{1/2}$ (Lindhard, Scharff, and Schiott 1963).

Ions emerging from the foil in excited electronic states decay in the 30-cm flight path between the foil and the collector, and indeed the beam is visible, glowing with a blue-green light that is strongest in the immediate vicinity of the foil and decays rapidly downstream as the excited states decay. We have made a spectral analysis of this radiation with two different instruments. We have photographed the glowing beam with an astronomical spectrograph¹ containing two glass prisms, an $f/3$ Schmitt camera with dispersion 75 \AA mm^{-1} at $\lambda 3950$ and 120 \AA mm^{-1} at $\lambda 4400$. Although we have used fast Kodak Ia-E plates, exposures of 4 hours were required because of the low brightness of the source. With a typical Fe^+ beam current of 0.2–0.3 μA , the carbon foils are punctured after about 5 minutes of bombardment, and as many as thirty-four foils were used in some exposures. An iron-arc reference spectrum was photographed alongside the Fe beam spectrum, and the two spectra were compared in a Grant comparator to establish the wavelengths of the Fe beam lines.

The glass prisms limit our spectrographic measurements to $\lambda \geq 3400 \text{ \AA}$. We have also analyzed the spectrum between 2000 and 4000 \AA with a McPherson 0.3-m monochromator² containing a grating of 2400 lines mm^{-1} and a refrigerated EMI 6256S photomultiplier. Single-photon pulses were detected with conventional pulse-counting electronics. An image of the glowing beam was focused by a quartz lens on the entrance slits of the spectrometer. The aperture of the quartz lens introduces a Doppler line width of 4 \AA (full or base-line width) at 4000 \AA . The slits of the spectrometer were set to match this line width, and the observed line width (FWHM) was 5 \AA . The spectrum was measured point by point every 2 \AA between 2000 and 4200 \AA , counting at each wavelength for the time required for the Faraday cup to collect 9 μC of Fe ions.

III. LINE IDENTIFICATION

The identification of an observed line with a known transition in Fe I is not trivial because of the high density of lines in the iron spectrum—the average interval between adjacent lines is less than 1 \AA in the wavelength region of our experiment. Because of the low intensity of the source we are not able to use high resolution, and the line width on our best spectrograms is never less than 2 \AA . In view of these difficulties, it is gratifying that we have been able to identify thirty-four of the forty-two lines in our 500-keV spectrograms, $\lambda \geq 3400 \text{ \AA}$, with known transitions in Fe I, using the relative intensity within multiplets as the criterion for identification.

After the identifications had been completed, we observed a regularity in the results that supports our identifications. The lines that we observe usually have large gf -values as tabulated in Corliss and Tech (1968). In the region $3000 \geq \lambda \geq 5000 \text{ \AA}$ which contains more than 2000 classified lines of Fe I, Corliss and Tech list ninety-three lines with $gf \geq 5$. In this same region, we observe only fifty lines, but we see twenty-five of the lines with $gf \geq 5$. Though we see only ~ 2 percent of the total known lines, we see more than one-quarter of the lines with $gf \geq 5$. Our experimental method appears to favor large gf -values, and we might well expect to see, for example, $\lambda 3586$ which has $gf = 10$. We therefore identify observed $\lambda 3585.4$ with multiplet 611 even though it is the only

¹ We are indebted to Dr. A. J. Deutsch of the Mount Wilson and Palomar observatories for making this instrument available to us.

² We are indebted to Dr. G. M. Lawrence and the Douglas Advanced Research Laboratories for making this instrument available.

member of multiplet 611 that we see, and a similar justification applies to the other multiplets (522, 800, 801) that contain only a single line.

We have not yet succeeded in identifying the charges of the ions responsible for individual lines appearing in our spectrograms. However, comparing spectrograms taken at 0.5, 0.75, 1.0, and 1.5 MeV shows that the intensity of the lines we have attributed to Fe I decrease with increasing beam energy, behavior consistent with the reduced fraction of Fe I at higher beam energy.³

Table 1 indicates the electron configurations between which the observed transitions take place. It is interesting to note that of the fifty Fe I transitions identified, forty-six are of the form $3d^7 4s \leftarrow 3d^7 4p$, with the parent ion configuration unchanged. In only two instances (611 and 620) is the upper term configuration of the form $3d^6 4s 4p$, and in neither case is the parent ion in the ground state of the Fe⁺ ion: $3d^6 4s$ ($a^6 D$).

IV. LIFETIME MEASUREMENTS

For six of the stronger lines in Table 1 we have been able to measure the decay in the line intensity as a function of the distance downstream from the foil. For these measurements the monochromator and the lens which imaged the glowing beam on the monochromator entrance slit were mounted on a lathe bed aligned parallel to the ion beam. The position of the detector along the beam could be read ± 0.05 mm with a dial indicator fastened to the lathe bed. The long dimension (1 cm) of the spectrometer slit was perpendicular to the glowing beam, so that any divergence caused by small angle scattering in the foil would scatter an insignificant fraction of the beam out of the field of view of the detection system.

The entrance and exit slits of the monochromator were set at 260μ , each equivalent to 3.4 \AA , to match approximately the Doppler width introduced by the $\pm 6^\circ$ aperture of the entrance lens. The entrance lens produced an image at the entrance slits reduced by a factor of $2/3$, so that the beam segment observed was only 0.17 mm long. At each position, the number of photons counted was corrected for a time-dependent background, typically from five to fifteen counts in a 10–30-sec counting period while $3 \mu\text{C}$ of Fe ions were collected in the Faraday cup. The resulting decay curve is shown in Figure 1 for measurements at 3766 \AA . The spectrum in the inset shows the line profile observed with the monochromator settings used in the decay-curve measurements. The monochromator slits are the principal source of line width, but a reduction in entrance slit width would reduce the beam segment observed and the counting rate.

The experimental points have been fitted to a single exponential by the method of least squares. The straight lines through the points show this fit and the standard deviation of the exponent found in the least-squares solution. The beam energy incident on the foil was 505 keV; energy loss in the carbon foil of thickness $10 \pm 4 \mu\text{g cm}^{-2}$ is 38 ± 15 keV, so that the ion velocity is $1.26 \times 10^8 \text{ cm sec}^{-1} \pm 1.6$ percent. The decay period of the curve in Figure 1 is $1.23 \text{ cm} \pm 4.4$ percent, so that the mean life of the state from which this radiation comes is $9.7 \pm 0.6 \times 10^{-9}$ sec. Similar measurements have been made for all the lines listed in Table 2.

The decay curve for $\lambda 4119$ shown in Figure 2 illustrates a phenomenon found in several of our measurements. The spectrum in the inset shows that this line lies over a continuous background, and our decay curve measured at the peak at $\lambda = 4119$ must be corrected for the contribution from this background which varies with position in a way which we can estimate only by making measurements at a nearby wavelength, $\lambda 4127$ in this case. The dashed curve in Figure 2 is obtained by subtracting the curve through the $\lambda 4127$ measurements from the curve through the $\lambda 4119$ measurements. The dotted curve, which should represent the decay of the line radiation alone, has a shape different

³ The variation of the intensity of these lines, and a list of unidentified lines will be found in Whaling, King, and Smith (1968).

TABLE 1
Fe I LINES IDENTIFIED IN THE 500-KEV BEAM-FOIL SPECTRA

Mult. No.* Configurations	λ^\dagger	Identification Terms [†]	gf [‡]	Observed	
				λ^\S	Int.
(21)	3734.81	$a^5F_5 - y^5F_5^o$	3.72	3735.9	10
$3d^7(a^4F)4s-$	3749.49	4-4	2.75	3749.8	20
$3d^7(a^4F)4p$	3758.24	3-3	2.04	3758.2	10
(23)	3581.20	$a^5F_5 - z^5G_6^o$	3.98	3781.9	20
$3d^7(a^4F)4s-$	3647.84	4-5	1.38	3649.8	1
$3d^7(a^4F)4p$	3631.46	3-4	1.66	3632.2	30
(24)	3570.10	$a^5F_4 - z^3G_5^o$	2.45	3570.4	10
$3d^7(a^4F)4s-$	3565.38	3-4	1.29	3564*	
$3d^7(a^4F)4p$					
(41)	4383.55	$a^3F_4 - z^5G_5^o$	3.24	4383.5	40
$3d^7(a^4F)4s-$	4404.75	3-4	1.78	4405.1	
$3d^7(a^4F)4p$					
(42)	4271.76	$a^3F_4 - z^3G_5^o$	1.58	4272.6	20
$3d^7(a^4F)4s-$	4307.91	3-4	2.09	4308.5	30
$3d^7(a^4F)4p$	4325.77	2-3	2.29	4325.5	50
	4250.79	3-3	0.53	4250.0	10
(43)	4045.82	$a^3F_4 - y^3F_4^o$	4.57	4045.3	80
$3d^7(a^4F)4s-$	4063.60	3-3	2.75	4063.7	50
$3d^7(a^4F)4p$	4071.74	2-2	2.63	4027.1	40
	3969.26	4-3	0.96	3969.0	20
	4005.25	3-2	0.81	4006.0	20
	4143.87	3-4	0.76	4145.4	20
(45)	3815.84	$a^3F_4 - y^3D_3^o$	3.98	3816.0	40
$3d^7(a^4F)4s-$	3827.83	3-2	3.55	3827.5	20
$3d^7(a^4F)4p$	3841.05	2-1	2.95	3841.5	30
	3902.95	3-3	1.02	3903*	
	3888.52	2-2	0.85	3888*	

TABLE 1 -- Continued

Mult. No.* Configurations	λ^\dagger	Identification		Observed	
		Terms [†]	gf^\ddagger	λ^\S	Int.
(81) 3d ⁷ (a ⁴ P)4s- 3d ⁷ (a ⁴ P)4p	3445.15	a ⁵ P ₃ -u ⁵ D ₄ ^o	3.65	3446*	
(294) 3d ⁷ (a ² G)4s- 3d ⁷ (a ² G)4p	3606.68 3605.45 3621.46 3638.30	a ³ G ₅ -y ³ H ₆ ^o 4-4 4-5 3-4	15.9 13.3 10.9 5.17	3606.1 3621.4 3640*	10 10
(295) 3d ⁷ (a ² G)4s- 3d ⁷ (a ² G)4p	3622.00 3640.39 3651.47	a ³ G ₃ -v ³ G ₃ ^o 4-5 3-4	7.93 8.97 11.7	3622.0 3640.0 3650.6	20 10 10
(304) 3d ⁷ (a ² G)4s- 3d ⁷ (a ² H)4p	3370.79 3369.55 3380.11	a ³ G ₅ -u ³ G ₅ ^o 4-4 3-3	8.02 5.02 3.47	3370* 3380*	
(496) 3d ⁷ (a ² P)4s- 3d ⁷ (a ² P)4p	3617.79 3632.04	c ³ P ₂ -u ³ D ₃ ^o 1-2	12.0 9.29	3618.2 3632.2	30 30
(522) 3d ⁷ (a ² G)4s- 3d ⁷ (a ² G)4p	4199.10	a ¹ G ₄ -z ¹ H ₅ ^o	6.85	4199.1	50
(607) 3d ⁷ (a ² H)4s- 3d ⁷ (a ² H)4p	3797.52 3806.70	b ³ H ₆ -w ³ H ₆ ^o 5-5	9.05 7.55	3797.7 3806.2	30 50
(608) 3d ⁷ (a ² H)4s- 3d ⁷ (a ² H)4p	3765.54 3765.70 3821.18 3805.35	b ³ H ₆ -y ³ I ₇ ^o 5-5 5-6 4-5	20.5 0.53 12.4 16.1	3765.7 3821.4 3806.2	60 30 50

TABLE 1 -- Continued

Mult. No.* Configurations	Identification			Observed	
	λ^\dagger	Terms [†]	gf [‡]	λ^\S	Int.
(611) 3d ⁷ (a ² H)4s- 3d ⁶ 4s(a ⁴ G)4p	3586.11	b ³ H ₆ -t ³ G ₅ ^o	24.6	3585.4	20
(620)	3233.05	b ³ H ₆ -x ³ I ₇ ^o	26.7	3233*	
3d ⁷ (a ² H)4s-	3254.36	5-6	23.5	3254*	
3d ⁶ 4s(b ³ H)4p	3280.26	4-5	22.6	3280*	
(680)	3292.02	a ³ D ₃ -u ³ F ₄ ^o	15.5	3292*	
3d ⁷ (a ² D)4s-	3314.74	2-3	18.1	3314*	
3d ⁷ (a ² D)4p					
(800)	4219.36	a ¹ H ₅ -y ³ I ₆ ^o	10.3	4219.6	30
3d ⁷ (a ² H)4s-					
3d ⁷ (a ² H)4p					
(801)	4118.55	a ¹ H ₅ -z ¹ I ₆ ^o	14.4	4119.2	60
3d ⁷ (a ² H)4s-					
3d ⁷ (a ² H)4p					

*The first column contains the multiplet number used in the Revised Multiplet Table (Moore 1945) and the electron configurations of the lower and higher terms from Atomic Energy Levels (Moore 1952).

†The wavelength and term designations in the second and third columns are from the Revised Multiplet Table.

‡gf-values from the tabulation of Corliss and Tech (1968).

§Wavelength observed in the 500-keV beam-foil spectra. Those given to the nearest 0.1 Å are usually the mean measurements on two or more plates. Those given to the nearest 1 Å were measured with the spectrometer and are identified by an asterisk.

||Eye estimates, on an arbitrary scale, of the relative intensity of the lines as they appeared close to the foil. No intensity is listed for lines measured only with the spectrometer.

from either of the two solid curves, and one would like to understand this behavior, or at least make certain that it does not cast doubt on our measured lifetimes.

The concave downward decay curve is characteristic of the decay of a state which is itself repopulated by the decay of one or more higher states when the upper state has a lifetime $\tau_{\text{upper}} < \tau_{\text{obs}}$. If $\tau_{\text{upper}} \ll \tau_{\text{obs}}$, the decay curve may even rise initially in the neighborhood of the foil (Denis *et al.* 1967). The upper states from which $\lambda 4119$ originates, $z^1I_6^o$, is 53093 cm^{-1} above the ground state, and there are no known singlet even states lying at higher energy. Even allowing for intersystem transitions, the highest known even states in Fe I are quintet states that lie only 6000 cm^{-1} above the z^1I^o state. Because of this small energy difference and the necessity for a spin change, significant cascading transitions into z^1I^o seem unlikely. The shape of the dotted line is therefore

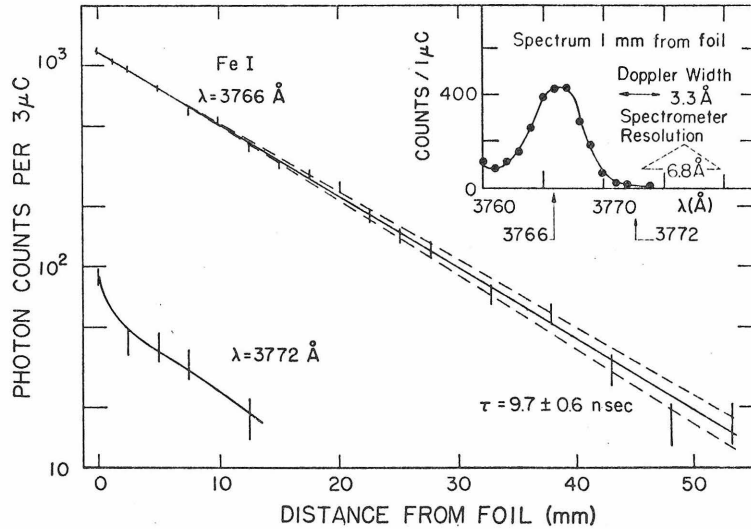


FIG. 1.—Light-decay curve for $\lambda 3765$, showing photons counted as a function of distance from the foil. Vertical bars indicate the statistical uncertainty in the individual points. Solid line is least-squares fit to the experimental points; dashed lines show standard deviation of this fit. Spectrum scan in inset was taken with the same resolution used in the light-decay measurements. All measurements have been corrected for time-dependent, dark-current counts of five to fifteen counts.

TABLE 2
LIFETIMES OF Fe I LEVELS*

Multiplet (1)	λ (Å) (2)	Upper Level (3)	E (kK) (4)	τ_{exp} (nsec) (5)	τ_{CT} (nsec) (6)	$\tau_{\text{exp}}/\tau_{\text{CT}}$ (7)
522....	4199	$z^1H_6^o$	48382	13.8	3.07	4.5
800....	4220	$y^3I_6^o$	52513	8.0	1.24	6.4
608....	3765	$y^3I_7^o$	52655	9.7	1.46	6.6
801....	4119	$z^1I_6^o$	53093	9.25	1.06	8.7
620....	3233	$x^3I_7^o$	57027	11.4	0.65	17.5
620....	3254	$x^3I_6^o$	57070	15	0.70	21.4

* Listed in order of increasing excitation energy of the upper level (col. [4]). Column (2) lists the wavelength of the decay channel observed. Column (6) lists the lifetime computed by Corliss and Tech (1967). Column (7) lists the ratio of the measured and computed lifetimes.

difficult to explain unless one assumes that transitions into $z^1I_6^o$ come from unknown auto-ionizing states whose lifetimes are very much shorter than our measured values. If $\tau_{\text{upper}} \ll \tau_{\text{obs}}$, the decay curve approaches the slope of τ_{obs} asymptotically for large t (or z). In Figure 2 the slope of the dotted line for large z corresponds to $\tau = 9.25$ nsec. Values of τ corrected for a continuous background in this way are listed in column (5) of Table 2. This background correction forces us to determine the slope from observations far from the foil where the statistical uncertainty is larger. Consequently, the precision of our lifetime measurements is roughly proportional to the (line intensity)/(background) ratio: we estimate that for the worst case ($\lambda 3254$) the uncertainty in τ is no more than 20 percent. We have altered experimental conditions by: (1) increasing the pressure in the region in which the atoms decay by a factor of 20; (2) increasing the field of view of the monochromator by a factor of 2; (3) biasing the target, normally grounded, at +300 V to suppress electron emission; and (4) increasing the beam energy from 500 to 600 keV.

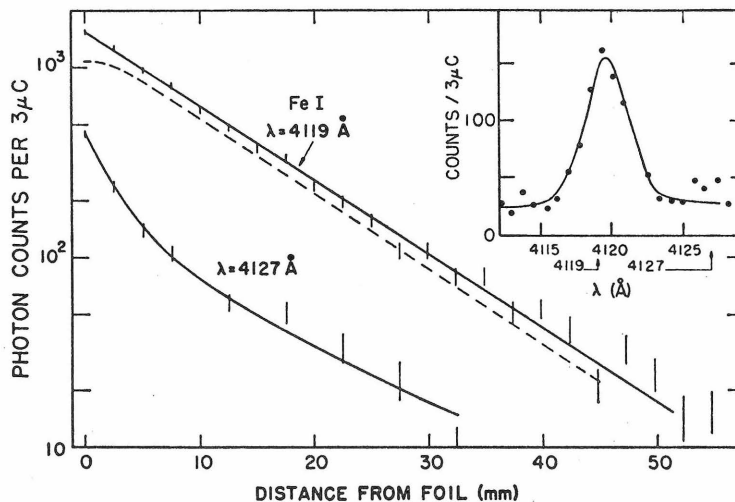


FIG. 2.—Light-decay curve for $\lambda 4119$. Inset shows the spectrum scan taken with the spectrometer resolution used in the decay-curve measurements. Arrows indicate wavelengths at which the line-plus-continuum decay curve and the continuum decay curve were measured. Dashed line is the line decay curve obtained by subtraction.

None of these changes altered the measured lifetime by as much as 10 percent. None of the decay curves for the levels in Table 2 shows evidence of cascading from longer-lived states, and indeed, no transitions are known from higher levels into any of these levels. A few transitions in the far-infrared are possible from higher terms which belong to electron configurations that include a $4d$ or $5s$ electron, but we have seen no lines in our beam-foil spectra from levels of these configurations.

The strongest line in our 500-keV beam-foil spectra, $\lambda 4045$, is of interest since its upper level, at 36.6 kK, lies far below the lowest upper level in Table 2. The light-decay curve for $\lambda 4045$ is complex, indicating that this level is repopulated by transitions from higher levels. The line $\lambda 4383$ exhibits a similar complex decay. We have not been able to decompose these complex decay curves into a sum of exponential terms to yield lifetimes that are independent of the bombarding energy.

V. COMPARISON WITH OTHER MEASUREMENTS

In Table 2, column (6), we list the lifetimes for the levels we have measured as computed by Corliss and Tech (1967) from the tabulation of atomic-transition probabilities

by Corliss and Tech (1968). The ratio $\tau_{\text{exp}}/\tau_{\text{CT}}$ in column (7) varies from 4.5 to 21, the discrepancy increasing with the excitation energy of the level. We have not been able to find a reasonable explanation for this discrepancy. Corliss and Tech neglect weak and unobserved transitions in computing lifetimes, but the addition of these weak-decay channels would further reduce their lifetimes which are already shorter than τ_{exp} . The errors one might suspect in the experiment, such as nonradiative de-excitation, or scattering of atoms out of the field of view of the monochromator, would make our measured lifetime too short. Cascading from long-lived states can flatten out the light-decay curve, but such decay curves do not follow the simple exponential dependence that we observe, and furthermore, we know of no states from which such cascading might take place. The fact that $\tau_{\text{exp}}/\tau_{\text{CT}}$ varies with excitation energy of the radiating state is especially troubling since it raises doubt about the internal consistency of the CT tables. It is interesting to note that our measured lifetimes are in much better agreement with an earlier tabulation of transition probabilities by Corliss and Warner (1966): the ratio $\tau_{\text{exp}}/\tau_{\text{CW}}$ is 4.7 ± 1.1 , and the ratio is independent of excitation energy.

There are recent direct measurements of transition probabilities for many levels in Fe I between 48 and 58 kK by absorption in a shock tube, but only two of the transitions studied by the shock-tube method involve levels for which we have measured τ . However, one can compare our lifetime measurements with the shock-tube measurements of oscillator strengths by comparing both with the summary of Corliss and Tech, since the CT values should be internally consistent at a particular excitation energy, based as they are on relative line intensities.

Byard (1967) has measured gf -values for eight lines in Fe I from upper levels between 49 and 55 kK. His transition probabilities are lower than those of CT by a factor of 2. At corresponding excitation energies, we would find transition probabilities lower than CT by a factor of 6, hence lower than Byard by a factor of 3.

Huber and Tobey (1968) have measured gf -values of many lines from upper levels between 48 and 58 kK. On the average, the values are a factor of 9 lower than those of Corliss and Tech. This ratio agrees with the average value of the ratio $\tau_{\text{exp}}/\tau_{\text{CT}}$ listed in column (7) of Table 2, but this agreement conceals the fact that we find a discrepancy that increases with increasing excitation energy, whereas Huber and Tobey find no such energy dependence.

Grasdalen, Huber, and Parkinson (1968) have measured gf -values for thirty-three transitions in Fe I with upper levels between 48 and 58 kK. Their transition probabilities are lower than those of Corliss and Tech by a factor that ranges between 8 and 65, hence lower than the transition probabilities that we would compute by a factor of 2, on the average.

Grasdalen *et al.* have measured gf for $\lambda 3233.05$, one of the lines on which we made lifetime measurements. If the branching ratio from Corliss and Tech for the two transitions ($\lambda = 2656.14$ and 3233.05 Å) out of the upper level ($x^3I_1^o$) is used, our lifetime value in Table 2 yields $A(\lambda 3233.05) = 6.5 \times 10^7 \text{ sec}^{-1}$, whereas Grasdalen *et al.* find $3.2 \times 10^7 \text{ sec}^{-1}$. A similar comparison can be made for $\lambda 3254.36$: the Harvard result is $A(\lambda 3254.36) = 2.85 \times 10^7 \text{ sec}^{-1}$; the Caltech lifetime and the CT branching ratio give $A(\lambda 3254.36) = 5.3 \times 10^7 \text{ sec}^{-1}$. These two transitions at 3233.05 and 3254.36 Å for which the Harvard absorption measurements and the Caltech emission measurements differ by a nearly constant factor, 2.0 and 1.9, are just those for which our discrepancy with the Corliss and Tech values is most serious, nearly a factor of 20. This discrepancy leads us to question the relative level populations used by Corliss and Tech in computing their transition probabilities.

VI. CONCLUSION

The beam-foil method of lifetime measurement is applicable to Fe I levels of high excitation energy; lower levels are fed by cascading transitions which obscure the life-

398 W. WHALING, R. B. KING, AND M. MARTINEZ-GARCIA

time of the level observed. Our measured lifetimes indicate that the transition probabilities of Corliss and Tech (1967) for levels above 48 kK are too large by a factor of ~ 9 , in qualitative agreement with recent shock-tube measurements. However, the lifetime measurements suggest that the values of Corliss and Tech should be corrected by a factor that increases with increasing excitation energy.

REFERENCES

- Bashkin, S. 1964, *Phys. Lett.*, **10**, 63.
———. 1968, in *Beam Foil Spectroscopy*, ed. S. Bashkin (New York: Gordon & Breach).
Byard, P. L. 1967, *J. Quant. Spectrosc. and Rad. Transf.*, **7**, 559.
Corliss, C. H., and Tech, J. L. 1967, *J. Res. N.B.S.*, Vol. **71A**, No. 6.
———. 1968, *N.B.S. Monog.*, No. 108.
Corliss, C. H., and Warner, B. 1966, *J. Res. N.B.S.*, Vol. **70A**, 325.
Denis, A., Desesquelles, J., Dufay, M., and Poulizac, M. C. 1967, *CR*, **265**, 471.
Grasdalen, G. L., Huber, M., and Parkinson, W. H. 1968, *Harvard College Obs. Sci. Rept.*, No. 27 (unpublished).
Huber, M., and Tobey, F. L. 1968, *A p. J.*, **152**, 609.
Lindhard, J., Scharff, M., and Schiott, H. E. 1963, *Mat. Fys. Medd. Dan. Vid. Sels.*, Vol. **33**, No. 14.
Magnuson, G. D., Carlston, C. E., Mahadevan, P., and Comeaux, A. R. 1965, *Rev. Sci. Instr.*, **36**, 136.
Moore, C. E. 1945, *Contr. Princeton Univ. Obs.*, No. 20.
Smith, P. L., and Whaling, W. 1968, *Bull. Am. Phys. Soc.*, **13**, 1656.
Whaling, W., King, R. B., and Smith, P. L. 1968, in *Beam Foil Spectroscopy*, ed. S. Bashkin (New York: Gordon & Breach).